# THEORETICAL STUDIES ON ORGANOMETALLIC COMPLEXES AND TRANSITION METAL CLUSTERS

A Thesis

Submitted for the Degree of

**DOCTOR OF PHILOSOPHY**

By

**Susmita De**

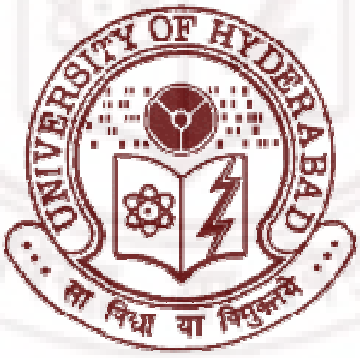


School of Chemistry

**University of Hyderabad**

Hyderabad 500 046

INDIA

July 2009

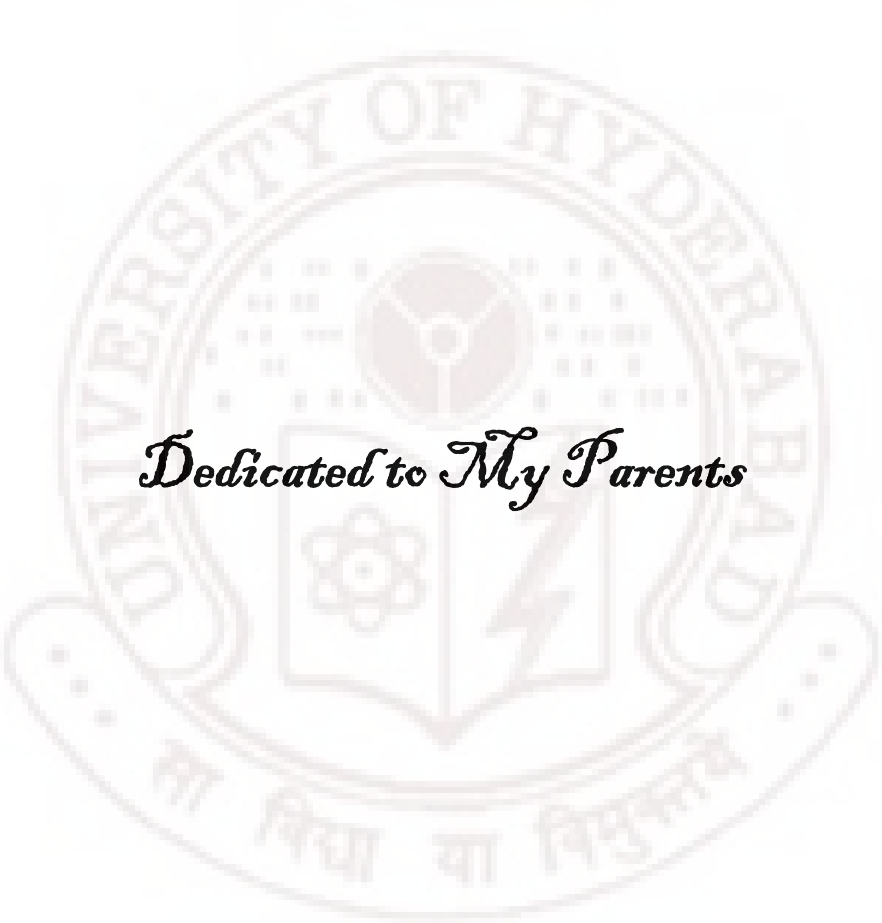

*Dedicated to My Parents*

# *CONTENTS*

## *STATEMENT*

I do hereby declare that the work embodied in this thesis is the result of investigations carried out by me in the **School of Chemistry, University of Hyderabad, Hyderabad, India,** under the supervision of **Prof. Eluvathingal D. Jemmis**.

In keeping with the general practice of reporting scientific observations, due acknowledgements have been made whenever the work described is based on the findings of other investigators.

***Susmita De***

## *CERTIFICATE*

Certified that the work embodied in the thesis entitled "**Theoretical Studies on Organometallic Complexes and Transition Metal Clusters"** has been carried out by **Mrs. Susmita De** under my supervision and the same has not been submitted elsewhere for any degree.

**Eluvathingal D. Jemmis**
Thesis Supervisor

**S. Mahapatra**
Co-supervisor

**Dean**
School of Chemistry

## *ACKNOWLEDGEMENTS*

I would like to express my gratitude to all those who have been accompanied and supported to complete this doctoral thesis. First, I would like to express profound gratitude to my supervisor, Prof. E. D. Jemmis, for his invaluable support, encouragement, supervision and useful suggestions throughout this research work. His moral support and continuous guidance enabled me to complete my work successfully.

I am also highly thankful to my thesis co-supervisor Prof. Susanta Mahapatra for his valuable support. I am deeply indebted to Dr. Chandan Kumar Pal whose continuous stimulating encouragement helped me to join for Ph. D.

I express my sincere thanks to our collaborators Prof. Simon Aldridge, Prof. A. G. Samuelson and Prof. S. Bhattacharya. I am very grateful to Prof. G. Frenking, University of Marburg for providing me a work place in his group to complete this thesis work.

I thank CSIR, New Delhi for the financial assistance. Computational facilities of the Centre for Modeling and Simulation and Design (CMSD), University of Hyderabad and Supercomputer and Education and Research Centre (SERC), Indian Institute of Science are greatly acknowledged.

I express my sincere thanks to Dean and all the faculty members of the School of Chemistry, University of Hyderabad; Chairman and all the faculty

members in Department of Inorganic and Physical Chemistry, Indian Institute of Science. Special thanks to Prof. Umapathy.

I sincerely thank all non-teaching staff of the School of Chemistry as well as Department of Inorganic and Physical Chemistry for providing their valuable services whenever needed.

I thank all my former and present lab members for their help. Special thanks to Usha, Shameema, Dr. Biswarup, Dibyendu and Subhendu for their valuable support. I would like to thank all my friends at School of Chemistry and Ladies hostel, especially Bhaswatidi, Anindita, Suparna, Rumpa, Wazida, Abhijitda, Rajesh, Subhasda, group members of Prof. S. Mahapatra and 'the Bengali group' who made my stay enjoyable in Hyderabad. I also thank my friends from IPC and other friends Paromita, Neenu, Linta, Nicky, Ashik, Rogers, Mathew, Thomas, Shijo, Pradeep, Anshita, mausumidi, Nima, Sanjukta, ramkumar, sangeeta, akshai and 'chitrangada dance team' for making my stay memorable at the IISc campus. Special thanks to members of Prof. Frenking's group.

Finally, I take this opportunity to express my profound gratitude to my beloved parents for their love, encouragement and moral support. Very special thanks to my husband Param, not only for his immense love, affection and constant support but also for valuable scientific suggestions and assistance in every step of my thesis.

***Susmita***

## CONTENTS OF THE CD

The main folder “Susmita_Thesis” in the CD contains a ‘.pdf’ file with the table of contents of the thesis (TOC.pdf) having pages i-xiv (see the table of contents). The sub-folder “Chapters” contains five files corresponding to the five chapters comprised in the thesis. The files are given appropriate names “Chapter*.pdf” where * is 1, 2, 3, 4 and 5 respectively. The List of Publications of the candidate is put in the file Publications.pdf in the same folder.

# CHAPTER 1

# INTRODUCTION TO COMPUTATIONAL CHEMISTRY AND OVERVIEW OF THE THESIS

$$H\Psi=E\Psi$$

## [1.1] Introduction

"……*The underlying physical laws necessary for the mathematical theory of a large part of physics and the whole of chemistry are thus completely known, and the difficulty is only that the exact application of these laws leads to equations much too complicated to be solvable*....." – P. A. M. Dirac

This famous statement by Dirac in the year 1929[1] regarding the laws of chemistry and physics referred mainly to the postulation of the Schrödinger equation.[2] Over the years, several approximations have been emerged to solve the Schrödinger equation.[3,4] Subsequently the application of quantum mechanics to solve problems in chemistry has been incorporated into efficient computer programs. These computational efforts received a critical boost when Hohenberg and Kohn[5], and Kohn and Sham[6], reformulated the Schrödinger equation into density functional theory (DFT),[7] a theory based on the electron density. The increase in the applications of quantum chemistry has been facilitated by the development of faster computers and quantum chemistry softwares. This branch of chemistry that uses computers to assist in solving chemical problems is called computational chemistry.

In the begining, the application of computational chemistry was limited to small molecules and for computing organic reaction mechanisms. The computational studies on transition-metal chemistry have lagged behind organic chemistry due to the requirement of more complicated quantitative wave functions. Currently, computational studies to predict the structure, bonding, reactivity and reaction mechanism of organometallic complexes have been proved to be an essential tool to complement the experimental research. This thesis deals with the

computational study of the structure, bonding and reactivity of transition metal organometallic complexes and clusters. Brief descriptions of the basis of the electronic structure methods used in this thesis are given in the following sections, followed by an overview of the remaining chapters.

## [1.2] Electronic Structure Methods

Electronic structure methods are based upon the principles of quantum mechanics and employ a variety of mathematical techniques to solve the fundamental equations.[3,4] This can usually be classified as *ab initio,* semi-empirical and density functional methods. The first method, *ab initio*, means "from the beginning" and uses only the fundamental constants to solve the Schrödinger equation. Semiempirical methods on the other hand simplify the computation either by approximating the different integrals using parameters derived from the experimental data of atoms and molecules or by neglecting some of them. In contrast to these wavefunction based methods, the density functional methods calculate the molecular electron probability density and calculate molecular electronic energy from density. The following sections provide an overview of the theory underlying *ab initio* and density functional theory methods.

### [1.2.1] *Ab initio* Methods

*Ab initio* methods are based on the Schrödinger equation.[2] The solution to Schrödinger equation gives the energy and wavefunction of atoms and molecules.[3,4]

The wavefunction can be used to calculate the electronic distribution that can be further used to find the physical properties of the system.

### [1.2.1.1] Schrödinger Equation and Hamiltonian

The Schrödinger equation describes the behaviour of electrons in atoms and molecules.[2] The time-independent Schrödinger equation, in its succinct form, can be expressed as,

$$\hat{\mathrm{H}}\Psi = \mathrm{E}\Psi \tag{1.1}$$

where $\hat{\mathrm{H}}$ is the Hamiltonian operator for a system of nuclei and electrons, E is the total energy and $\Psi$ is the wave function which defines the system. The non-relativistic Hamiltonian operator $\hat{\mathrm{H}}$ for any molecule having $M$ nuclei and $N$ electrons, assuming the nuclei and electrons to be point masses, is

$$\hat{\mathrm{H}} = -\frac{\hbar^2}{2m_A}\sum_{A=1}^{M}\nabla_A^2 - \frac{\hbar^2}{2m_i}\sum_{i=1}^{N}\nabla_i^2 - \sum_{A=1}^{M}\sum_{i=1}^{N}\frac{Z_A e^2}{r_{iA}} + \sum_{A=1}^{M}\sum_{B>A}^{M}\frac{Z_A Z_B e^2}{r_{AB}} + \sum_{i=1}^{N}\sum_{j>i}^{N}\frac{e^2}{r_{ij}} \tag{1.2}$$

where $A$ and $B$ refer to the nuclei and $i$ and $j$ to the electrons. Here, $m$ is the mass and $r$ is the position vector of the particles, $e$ is the electronic charge, $Z$ is the atomic number, $\hbar$ is represented by the Planck's constant divided by $2\pi$ and $\nabla^2$ is the Laplacian Operator. The first and second terms are the nuclear and electronic kinetic energy operators. The third, fourth and fifth terms represent the potential energy for the nuclear-electron attraction, nuclear-nuclear repulsion and electron-electron repulsion respectively.

The energy and wave function of a molecule can be obtained by solving the Schrödinger equation.[3,4] However, it is very difficult to solve the Schrödinger equation exactly for any system with more than one electron. Thus, various degrees of approximations using a finite wave function are used for solving the chemical problems. Some of the main approximations are briefly outlined here.

### [1.2.1.2] Born-Oppenheimer Approximation

The Born-Oppenheimer approximation,[8] which was introduced by Max Born and J. Robert Oppenheimer in 1927, separates the motion of the electrons in a molecule from the motion of the nuclei. The separation is based on the fact that the nuclei are much heavier than the electrons and move more slowly. Hence, to a good approximation, the electrons in a molecule can be considered moving in a field of fixed nuclei. Thus, the nuclear kinetic energy term can be neglected and the potential for the nuclear-nuclear repulsion can be considered to be a constant. This gives rise to the electronic Hamiltonian $\hat{\mathrm{H}}_{elec}$, which describes the motion of $N$ electrons in the field of $M$ point charges.

$$\hat{\mathrm{H}}_{elec} = -\frac{\hbar^2}{2m_i}\sum_{i=1}^{N}\nabla_i^2 - \sum_{A=1}^{M}\sum_{i=1}^{N}\frac{Z_A e^2}{r_{iA}} + \sum_{i=1}^{N}\sum_{j<i}^{N}\frac{e^2}{r_{ij}} \tag{1.3}$$

Hence, Schrödinger equation for the electronic motion can be written in a compact form as,

$$\hat{\mathrm{H}}_{elec}\Psi_{elec} = \mathrm{E}_{elec}\Psi_{elec} \tag{1.4}$$

The electronic energy $E_{elec}$ and the electronic wave function $\Psi_{elec}$ depend parametrically on the nuclear coordinates and explicitly on the electronic coordinates. The total energy of the system including the internuclear repulsion is

$$E_{tot} = E_{elec} + \sum_{A=1}^{M} \sum_{B>A}^{M} \frac{Z_A Z_B e^2}{r_{AB}} \tag{1.5}$$

The spectral studies support the Born-Oppenheimer approximation but it fails when nontrivial coupling of electronic and nuclear motion occurs in cases such as Jahn-Teller and Renner effects.[3,4] Further approximations are required to get reliable information on the electronic structure for large molecules.

**[1.2.1.3] LCAO-MO Approximation**

The linear combination of atomic orbital (LCAO) approximation is commonly used to construct the trial wave function for a molecule.[3,4] In this approximation, it is considered that near one nucleus the potential exerted by the other nuclei is negligible. Hence, the nature of the wave function near the nucleus must be analogous to the wave function of a hydrogen atom centered at that point. Thus, the molecular orbital ($\Psi$) can be considered as a combination of atomic orbitals ($\phi$) centered at each nucleus forming an orthonormal basis.

$$\Psi = \sum_{i=1}^{n} c_i \phi_i \tag{1.6}$$

where $c_i$ is the coefficient of each atomic orbitals $\phi_i$.

### [1.2.1.4] Variation Theorem

The set of molecular orbital (MO) expansion coefficients $c_i$ in LCAO approximation can be solved using the principles of variational theorem. According to variation theorem for a given system, the exact ground state wave function has the lowest expectation value for $\hat{H}$ and thus lowest energy $E_0$. In other words the energy calculated using a trial wave function is always greater than or equal to the exact ground state energy $E_0$.[3,4]

$$E_\Psi = \frac{\int \Psi^* \hat{H} \Psi d\tau}{\int \Psi^* \Psi d\tau} \geq E_0 \qquad (1.7)$$

The wave function and ground state energy can be obtained by minimizing $E_\Psi$ with respect to parameters that define the trial wave function $\Psi$. For getting good approximate ground state energy and wave function, many trial functions have to be tried and the lowest value of the variational integral gives the closest approximation to $E_0$ and ground state wave function.

### [1.2.1.5] Hartree-Fock Self Consistent Field Theory

In the Hartree-Fock theory,[3,4,9] each electron is assumed to be moving in the field of the nuclei and in the average field of other electrons. As a result, the motion of a given electron is considered independent of the actual position of the other electrons. It is to be noted that the Hamiltonian operator considering Born-Oppenheimer approximation (Eq. 1.3) is a sum of three terms. The first two terms depends only on the coordinates of one electron. This is nothing but a sum of one-

electron Hamiltonian operators $\sum_{i=1}^{N} \hat{h}_{elec}^{i}$. The one-electron operator $\hat{h}_{elec}^{i}$ includes kinetic energy of the electrons and the potential energy due to the attractive coulombic interaction between the nuclei and electrons.

$$\hat{h}_{elec}^{i} = -\frac{\hbar^2}{2m_i}\nabla_i^2 - \sum_{A=1}^{M}\frac{Z_A e^2}{r_{iA}} \tag{1.8}$$

The third term in the Hamiltonian is the sum of electron-electron repulsions, which depends upon the coordinates of two electrons. The Hamiltonian can thus be written as the sum of one- and two- electron terms.

$$\hat{\mathrm{H}}_{elec} = \sum_{i=1}^{N}\hat{h}_{elec}^{i} + \sum_{i=1}^{N}\sum_{j>i}^{N}\frac{e^2}{r_{ij}} \tag{1.9}$$

The best approximate solution to the electronic Schrödinger equation is given by the variational principle (Eq. 1.7). It will try to find the wavefunction $\Psi_{elec}$ that give the lowest possible energy. Thus, the electronic energy of an approximate wave function $\Psi_{elec}$ is given by

$$\mathrm{E}_{elec} = \frac{\int \Psi_{elec}^{*}\hat{\mathrm{H}}_{elec}\Psi_{elec}\,d\tau}{\int \Psi_{elec}^{*}\Psi_{elec}\,d\tau} \tag{1.10}$$

Now, considering the normalization of the electronic wavefunction, the equation 1.10 becomes

$$\mathrm{E}_{elec} = \int \Psi_{elec}^{*}\hat{\mathrm{H}}_{elec}\Psi_{elec}\,d\tau \tag{1.11}$$

Substitution of the electronic Hamiltonian from equation 1.9 leads to

$$E_{elec} = \int \Psi^*_{elec} \left\{ \sum_{i=1}^{N} \hat{h}^i_{elec} \right\} \Psi_{elec} d\tau + \int \Psi^*_{elec} \left\{ \sum_{i=1}^{N} \sum_{j>i}^{N} \frac{e^2}{r_{ij}} \right\} \Psi_{elec} d\tau \qquad (1.12)$$

Integration of the first term leads to sum of the one-electron energies $\varepsilon_i$ and is represented by $2\sum_{i=1}^{N/2} \varepsilon_i$. The second integral can be expressed in terms of coulomb integral ($J_{ij}$) and exchange integral ($K_{ij}$) as $\sum_{i=1}^{N/2} \sum_{j=1}^{N/2} 2J_{ij} - K_{ij}$

where,

$$J_{ij} = \int \Psi^*_i(1) \Psi_i(1) \left( \frac{1}{r_{12}} \right) \Psi^*_j(2) \Psi_j(2) d\upsilon_1 d\upsilon_2 \qquad (1.13)$$

$$K_{ij} = \int \Psi_i(1) \Psi_j(2) \left( \frac{1}{r_{12}} \right) \Psi^*_i(2) \Psi^*_j(1) d\upsilon_1 d\upsilon_2 \qquad (1.14)$$

The coulomb integral $J_{ij}$ represents the energy of the coulombic interaction between an electron in orbital $\Psi_i$ with an electron in orbital $\Psi_j$. This is a destabilization interaction between the electrons and always positive. The term exchange integral $K_{ij}$ arises from the consideration of the electron spin in the antisymetric wavefunction. Hence, the total energy can be represented as

$$E_{elec} = 2\sum_{i=1}^{N/2} \varepsilon_i + \sum_{i=1}^{N/2} \sum_{j=1}^{N/2} 2J_{ij} - K_{ij} \qquad (1.15)$$

The corresponding operator for this energy expression is called the Fock operator ($\hat{F}$). The energy and wave function are determined by solving the following Hartree-Fock equation,

$$\hat{F}\Psi_i = \varepsilon_i \Psi_i \qquad i = 1, 2, 3, ....., N \qquad (1.16)$$

The simple approximate form for molecular wavefunction can be represented as linear combination of atomic orbital (LCAO).

$$\Psi_i = \sum_{\upsilon=1}^{K} c_{\upsilon i}\phi_\upsilon \tag{1.17}$$

Now, introducing the LCAO approximation into the Hartree-Fock equation (1.16) we get,

$$\widehat{F}\sum_{\upsilon=1}^{K} c_{\upsilon i}\phi_\upsilon = \varepsilon_i \sum_{\upsilon=1}^{K} c_{\upsilon i}\phi_\upsilon \tag{1.18}$$

Multiplication of equation 1.18 by $\phi_\nu^*$ and then integrating over all space leads to

$$\sum_{\upsilon=1}^{K} c_{\upsilon i}\left(\mathrm{F}_{\nu\upsilon} - \varepsilon_i \mathrm{S}_{\nu\upsilon}\right) = 0 \tag{1.19}$$

Here, $\mathrm{F}_{\nu\upsilon}$ and $\mathrm{S}_{\nu\upsilon}$ are defined as the following integrals

$$\mathrm{F}_{\nu\upsilon} = \int \phi_\nu^* \widehat{F}\ \phi_\upsilon d\tau \tag{1.20}$$

$$\mathrm{S}_{\nu\upsilon} = \int \phi_\nu^* \phi_\upsilon d\tau \tag{1.21}$$

To obtain a nontrivial solution to equation 1.19 i.e. a solution for which the values of the coefficients $c_{\upsilon i}$ are non zero, the term $\sum_{\upsilon=1}^{K}\left(\mathrm{F}_{\nu\upsilon} - \varepsilon_i \mathrm{S}_{\nu\upsilon}\right)$ must be equal to zero. This leads to *K* equations known as Secular equations and the corresponding determinant is called Secular Determinant.

$$\begin{vmatrix} F_{11}-\varepsilon_1 S_{11} & F_{12}-\varepsilon_1 S_{12} & \ldots & F_{1K}-\varepsilon_1 S_{1K} \\ F_{21}-\varepsilon_2 S_{21} & F_{22}-\varepsilon_2 S_{22} & \ldots & F_{2K}-\varepsilon_2 S_{2K} \\ \ldots & & & \\ F_{K1}-\varepsilon_K S_{K1} & F_{K2}-\varepsilon_K S_{K2} & \ldots & F_{KK}-\varepsilon_K S_{KK} \end{vmatrix} = 0 \qquad (1.22)$$

The solution of equation 1.22 gives a set of *K* energy values, $\varepsilon_1, \varepsilon_2, \varepsilon_3, \ldots, \varepsilon_K$ and a set of *K* wave functions, $\Psi_1, \Psi_2, \ldots, \Psi_K$. The equation is not linear and must be solved iteratively. The solution to the equation begins with the initial guess for the molecular wave function $\Psi_i$ (Eq. 1.17). This requires selection of a set of basis functions $\phi_\upsilon$ and a set of guesses for the initial values of the coefficients $c_{\upsilon i}$. These are used to obtain a set of values for the $\varepsilon_i$. These values for the $\varepsilon_i$ are then substituted into the secular equation 1.22 and a new set of values for the coefficients $c_{\upsilon i}$ are obtained. This iterative process is continued until the variations in the values of the $\varepsilon_i$ and the $c_{\upsilon i}$ from one cycle to the next fall below a threshold. The resulting values for the $c_{\upsilon i}$ are used to obtain the wave function $\Psi_i$ that minimize the value of energy $\varepsilon_i$. The procedure is called Self Consistent Field (SCF) method.

**[1.2.1.6] Electron Correlation**

The Hartree-Fock (HF) theory takes into account an average effect of electron repulsion, but not the explicit electron-electron interactions. This indicates that the probability of finding an electron at some location around an atom is determined by the distance from the nucleus but not the distance from the other electrons. However, in reality, the movement of electrons is influenced by the repulsion from individual electrons and it will affect the probability of finding one

electron at a particular region near other electrons. If we consider the effect of explicit electron-electron repulsions into the calculation, we can improve the energy and the wavefunction of a system. This is known as electron correlation.[10] The HF energy can be improve with larger and more complete set of basis functions. However, the larger and complete basis sets can lower the HF energy to a limit called Hartree-Fock limit.[3,4] The difference between the exact non-relativistic ground state energy $E_{nonrel}$ and the Hartree-Fock limit energy $E_{HF}$ is called the correlation energy ($E_{corr}$).

$$E_{corr} = E_{nonrel} - E_{HF} \tag{1.23}$$

The three common methods which incorporate electron correlation viz. Møller-Plesset Perturbation theory,[11] Configuration Interaction,[12] and Coupled Cluster Theory[13] are discussed in the following sections. These calculations begin with a HF calculation and then correct for the correlation.

**[1.2.1.6.1] Møller-Plesset Perturbation Theory**

The electron correlation in Møller-Plesset Perturbation (MP) theory can be accounted for by treating the real molecule as a perturbed system. This method takes the sum of the one electron HF operator as the zeroth order unperturbed Hamiltonian $\hat{H}^{(0)}$ and is very close to the exact Hamiltonian $\hat{H}$. The energy and the wave functions of the Hamiltonian $\hat{H}^{(0)}$ can be systematically improved by a parameter $\lambda$ associated with the perturbating operator ($\hat{H}^{(1)}$). Within the limit of

perturbation theory the perturbation $\hat{H}^{(1)}$ is presumed to be relatively small compared to the unperturbed Hamiltonian.

$$\hat{H} = \hat{H}^{(0)} + \lambda \hat{H}^{(1)} \tag{1.24}$$

In this method, the perturbed wave function and perturbed energy are expressed as a power series in $\lambda$

$$\Psi = \Psi^{(0)} + \lambda\Psi^{(1)} + \lambda^2\Psi^{(2)} + \cdots\cdots \tag{1.25}$$

$$E = E^{(0)} + \lambda E^{(1)} + \lambda^2 E^{(2)} + \cdots\cdots \tag{1.26}$$

The energy correction in MP theory can be taken as various orders like 1st order (MP1), 2nd order (MP2), 3rd order (MP3) and so on. The 1st order energy correction is nothing but HF energy.[11]

**[1.2.1.6.2] Configuration Interaction Method**

A configuration interaction (CI) wave function is constructed from the HF wave function and adding new determinants that represent promotion of electrons from the occupied to virtual orbitals. The actual wave function of the system is a linear combination of these Slater determinants that corresponds to different electronic configurations.

Configuration interaction methods are classified by the number of excitations used to create each determinant. If only one electron has been excited for each determinant, it is called a configuration interaction single-excitation (CIS) calculation. CIS calculations give an approximation to the excited states of the

molecule, but do not change the ground state energy. Single and double excitation (CISD) calculations yield a ground state energy that has been corrected for correlation. The configuration interaction calculation with all possible excitations is called full CI. The full CI calculation using an infinitely large basis set will give an exact quantum mechanical energy.[12] However, full CI calculations are possible only for small molecules.

**[1.2.1.6.3] Coupled Cluster Theory**

Here, the correlated wave function is expressed as a sum of the HF ground state determinant and determinants representing the promotion of electrons from this state to the virtual MOs. However, unlike CI, this sum of the determinant is constructed by operating a series of excitation operators ($\hat{T}$) on the HF wave function.

$$\Psi = e^{\hat{T}}\Psi_{HF} \tag{1.27}$$

where $\hat{T} = \hat{T}_1 + \hat{T}_2 + \cdots\cdots$

The operators $\hat{T}_1, \hat{T}_2, \cdots\cdots$ represent promotion of one, two,… number of electrons into virtual orbitals. The different coupled cluster methods are named as coupled cluster doubles (CCD), coupled cluster singles and doubles (CCSD), etc depending upon how many terms are included in constructing the excitation operator.[13]

**[1.2.2] Basis Set**

For performing any quantum mechanical calculation the molecular orbitals $\psi_i$ are considered as the linear combination of a given set of functions $\phi_i$, called basis sets.[3,4]

$$\psi_i = \sum_{i=1}^{N} C_i \phi_i \tag{1.28}$$

These basis functions $\phi_i$ contain a radial $\mathrm{R}_{nl}(r)$ and angular part $\mathrm{Y}_{lm}(\theta\varphi)$. The angular function $\mathrm{Y}_{lm}(\theta\varphi)$ commonly known as the spherical harmonics, which contains all the angular information needed to describe the wave function. The different types of basis functions differ in the radial function $\mathrm{R}_{nl}(r)$.

One such basis functions is the Slater Type Orbitals (STO).[14] The atomic orbitals (AO) can be always represented by Slater type functions which have exponential radial parts. The radial part of a STO with principal quantum number $n$ can be represented in the form

$$\mathrm{R}_{nl}(r) \propto r^{n-1} e^{(-\xi r)} \tag{1.29}$$

where, $\xi$ is the orbital exponent. STOs can be used as basis functions for more accurate solutions for small atoms and molecules. Sometimes two or more numbers of STOs are used to improve the accuracy. The many-centre two-electron integrals involving STOs are rather difficult to evaluate which require numerical integration techniques and are very computational time consuming. This problem can be overcome to some extent by the use of Gaussian type functions introduced by

Boys.[15] These gives easily integrable poly electronic functions. The very commonly used Gaussian Type Orbital (GTO) has the radial function in the form

$$R_{nl}(r) \propto r^{n-1} e^{(-\alpha r^2)} \tag{1.30}$$

The main disadvantage of the Gaussian function is that it does not adequately describe the form of real atomic orbitals. In particular, the Gaussian function lacks a cusp at the nucleus and hence the region near the nucleus is described rather poorly. In practice, more number of GTOs with different orbital exponents are used to fit the atomic orbitals. Depending upon the number of Gaussian functions used to describe an orbital, the basis set can be termed as minimal basis set, double zeta (DZ), triple zeta (TZ) basis set and so on. Since mainly valence orbitals are involved in chemical bonding, the efficiency can be enhanced without excessive computing time by increasing the number of GTOs only for the valence orbitals. This results in split valence basis sets.

However, to maintain the same degree of accuracy with less computational cost the Gaussian functions can be contracted to form contracted Gaussian type orbitals. In this procedure, the number of GTOs remains the same but the number of variational coefficients reduces drastically. These GTOs are then referred as primitives and the resulting functions as the contracted Gaussians functions. The contraction can be expressed as follows

$$\phi_i = \sum_{p=1}^{Q} D_{ip} g_p \tag{1.31}$$

where, $D_{ip}$ are the coefficients within a given basis set and $g_p$ are the primitive GTOs.

Further improvement of the basis set could be made by including polarization and diffusion functions. The basis sets, which add basis functions whose angular quantum number is greater than the maximum angular quantum number of the valence shell of the ground state atom is called polarized basis set. For anions, compounds with lone pairs and H-bonded dimers where electron density has a significant value at a large distance from nuclei, highly diffuse function with very small orbital exponent are used for better agreement with experiment.

Computations involving heavier atoms are relatively difficult than those involving first and second row atoms of the periodic table. This is because of the increasing number of two electron integrals to be evaluated. This can be overcome by the use of pseudo potentials. Since the core orbitals are not affected by the changes in chemical bonding, one can treat them by an average potential. The valence electrons can be described by appropriate basis functions. A commonly used pseudo potential is the Effective Core Potential (ECP)[16] and is of the general form,

$$\mathrm{ECP}(r)=\sum_{i}^{k} C_i r^{n_i} e^{(-\alpha_i r^2)} \tag{1.32}$$

where, $k$ is the number of terms in the expansion, $C_i$ is a coefficient of each term, $r$ is the distance from the nucleus $n_i$ and $\alpha_i$ is an exponent for $i^{\text{th}}$ term. The use of ECP is found to be computationally very efficient, particularly for transition metals,

because it reduces the number of basis functions. ECP also makes room for the incorporation of relativistic effects.

### [1.2.3] Density Functional Theory

Density Functional Theory (DFT)[7] simplifies the many body problem in wavefunction based methods by using with the electronic charge density $\rho$ as fundamental variable rather than the wavefunction. Thus, for N electrons system the basic variable $\rho$ depends only on the three spatial coordinates rather than the intractable 3*N* spatial coordinates and *N* spin coordinates required to describe the many-body electronic wave function. Here, the many-body problem of calculating electron-electron interaction energy is transformed into single-body problem, without explicitly calculating the electron-electron interaction energy. This is done by using ground state density $\rho_0$ and the single particle wave function.

Hohenberg and Kohn established the connection between the electron density and the many-electron Schrödinger equation. They (HK-I theorem)[5] showed that all the properties of a molecular system can in principle be deduced from the electronic density function of the system. The ground state energy is thus a functional of ground state electron probability density $\rho_0$.

$$E_0 = \varepsilon\left[\rho_0(r)\right] \tag{1.33}$$

Similarly, the ground-state wave function ($\Psi_0$) for a system is a functional of the ground state electron density $\rho_0$.

$$\Psi_0 = \psi\left[\rho_0(r)\right] \tag{1.34}$$

Thus, the number of electrons, (N) can be determined from the ground state electron density $\rho_0$ as

$$N = \int \rho_0(r) d^3r \tag{1.35}$$

The HK-II theorem[5] states that for every trial density function $\rho(r)$ that satisfies the equation 1.35 for total number of electrons and $\rho(r) \geq 0$ for all *r*, the following inequality holds.

$$E_0 \leq E\left[\rho(r)\right] \tag{1.36}$$

In other words, if some density represents the correct number of electrons of the system, the total energy calculated from this density cannot be lower than the true energy of the ground state.

Kohn and Sham proposed a method for minimization of energy functional, $E\left[\rho(r)\right]$ known as Kohn-Sham (KS) method.[6] According to this, the total-energy functional can be written in terms of electron density as

$$E\left[\rho(r)\right] = T\left[\rho(r)\right] + U\left[\rho(r)\right] + V\left[\rho(r)\right] \tag{1.37}$$

where T[$\rho(r)$], U[$\rho(r)$] and V[$\rho(r)$] are the functionals for the electronic kinetic energy, electron-electron interaction energy and potential energy for interaction between electron and nuclei, called as external potential $\upsilon(r)$. The potential energy in the given potential $\upsilon(r)$ is given by,

$$\mathrm{V}\left[\rho(r)\right] = \int \upsilon(r)\rho(r)d^3r \tag{1.38}$$

The minimization of the energy functional $\mathrm{E}\left[\rho(r)\right]$ with respect to $\rho(r)$ in principle will lead to the ground state energy of the system.

The KS method considers a reference system of non-interacting electrons to approximate the kinetic energy T[$\rho(r)$] and electron-electron interaction U[$\rho(r)$] functionals. According to this assumption, the kinetic energy $T_s[\rho(r)]$ and electron-electron interaction $U_s[\rho(r)]$ for the reference system are exactly known. Therefore, the kinetic energy T[$\rho(r)$] and electron-electron interaction U[$\rho(r)$] functionals can be expressed as,

$$\mathrm{T}\left[\rho(r)\right] = T_s[\rho(r)] + \Delta T[\rho(r)] \tag{1.39}$$

$$\mathrm{U}\left[\rho(r)\right] = U_s[\rho(r)] + \Delta U[\rho(r)] \tag{1.40}$$

where $\Delta$T[$\rho(r)$] and $\Delta$U[$\rho(r)$] are the difference in average electronic kinetic energy and electron-electron repulsion terms in comparison to the non-interacting reference system. Thus, substituting V[$\rho(r)$], T[$\rho(r)$] and U[$\rho(r)$] from Eq. 1.38, 1.39 and 1.40, to the total-energy functional in Eq. 1.37 gives

$$\mathrm{E}\left[\rho(r)\right] = T_s[\rho(r)] + \Delta T[\rho(r)] + U_s[\rho(r)] + \Delta U[\rho(r)] + \int \upsilon(r)\rho(r)d^3r \tag{1.41}$$

Here, the unknown terms are $\Delta T[\rho(r)]$ and $\Delta U[\rho(r)]$ and the sum of these terms is called the exchange-correlation functional, $E_{xc}[\rho(r)]$.

$$\mathrm{E}_{xc}\left[\rho(r)\right] = \Delta T[\rho(r)] + \Delta U[\rho(r)] \tag{1.42}$$

It can also be written as sum of the exchange and correlation functionals.

$$\mathrm{E}_{xc}\left[\rho(r)\right]=\mathrm{E}_{x}\left[\rho(r)\right]+\mathrm{E}_{c}\left[\rho(r)\right] \tag{1.43}$$

where $\mathrm{E}_x[\rho(r)]$ is due to the Pauli principle (exchange energy) and $\mathrm{E}_c[\rho(r)]$ is due to correlations. The accuracy of Kohn-Sham (KS) method depends on the quality of this exchange-correlation functional, $\mathrm{E}_{xc}\left[\rho(r)\right]$.

DFT in principle gives a good description of ground state properties but the practical applications are based on approximations for the exchange-correlation functional, $\mathrm{E}_{xc}\left[\rho(r)\right]$. Solving the exact exchange-correlation would solve the many-body problem exactly, which is not feasible in practice and thus require approximation. Some of the popular approximations are described below.

**[1.2.3.1] Local Density Approximation (LDA)**

In LDA, the contribution of each volume element to the total exchange correlation energy is taken to be that of the homogenous electron gas density at that point. When the density $\rho$ varies with position extremely slowly then the energy functional $\mathrm{E}_{xc}^{LDA}\left[\rho(r)\right]$ can be expressed as,

$$\mathrm{E}_{xc}^{LDA}\left[\rho(r)\right]=\int \varepsilon_{xc}^{LDA}[\rho(r)]d^{3}r \tag{1.44}$$

$\varepsilon_{xc}^{LDA}[\rho(r)]$ is the exchange-correlation energy density of homogenous electron gas with electron density $\rho$.

**[1.2.3.2] Local Spin-Density Approximation (LSDA)**

Unlike LDA, LSDA allows electrons with different spins to occupy different spatial orbitals. Hence, for open-shell molecules and molecular geometries near dissociation LSDA works better than LDA. Here, the exchange correlation energy is given by

$$E_{xc}^{LSDA}\left[\rho^{\alpha}(r),\rho^{\beta}(r)\right]=\int \varepsilon_{xc}^{LSDA}\left[\rho^{\alpha}(r),\rho^{\beta}(r)\right]d^{3}r \qquad (1.45)$$

**[1.2.3.3] Generalized Gradient Approximation (GGA)**

The LDA and LSDA use the exchange-correlation energy for the uniform electron gas at every point in the system regardless of the real charge density. For a system of non-uniform charge density the exchange-correlation energy can deviate significantly from the uniform result. This deviation can be expressed in terms of the gradient and higher spatial derivatives of the total charge density. The GGA estimates the contribution of each volume element based on the magnitude and gradient of the electron density within that element. This can be achieved by expressing the energy functional with more general functions of $\rho(r)$ and $\nabla\rho(r)$. Such energy functionals are of the general form

$$E_{xc}^{GGA}\left[\rho^{\alpha}(r),\rho^{\beta}(r)\right]=\int \varepsilon_{xc}^{GGA}\left[\rho^{\alpha}(r),\rho^{\beta}(r),\nabla\rho^{\alpha}(r),\nabla\rho^{\alpha}(r)\right]d^{3}r \qquad (1.46)$$

Different GGAs differ in the choice of the functions $\rho$ and $\nabla\rho$.

### [1.2.3.4] Hybrid Functional

The hybrids functional are constructed by mixing the certain percentage of Hartree-Fock exchange with exchange and correlation from DFT exchange-correlation functional. Different hybrid functionals are available based on the approximations to the exchange and correlation functionals. The commonly used functional in this thesis is the hybrid functional B3LYP.[17a-c] This is a combination of the Lee-Yang-Parr GGA for correlation and Becke's three-parameter hybrid functional B3 for exchange. The hybrid functional B3 is a linear combination of a fraction of Hartree-Fock exchange and the DFT exchange functional.

$$E_{xc}^{B3LYP} = E_{xc}^{LDA} + a_0(E_x^{HF} - E_x^{LDA}) + a_x(E_x^{GGA} - E_x^{LDA}) + a_c(E_c^{GGA} - E_c^{LDA}) \qquad (1.47)$$

where $a_0$ = 0.20, $a_x$ = 0.72 and $a_c$ = 0.81 are the three empirical parameters determined by fitting the predicted values to a set of atomization energies, ionization potentials, proton affinities and total atomic energies.

## [1.3] Theoretical Methods Used in the Thesis

The level of theory used in this thesis for computations is the hybrid HF-DFT method, B3LYP[17a-c] and LANL2DZ[17d-f] basis set with the effective core potentials of Hay and Wadt. Frequency calculations were carried out at the same level of theory to characterize the nature of the optimized structures. Gaussian 03 program package is used for the calculations.[18] In some cases, single point energy calculation at higher level is performed for verification. These cases are mentioned in detail in the appropriate chapters.

## [1.4] Overview of the Thesis

The remaining four chapters of the thesis are organized as follows. In the second and third chapters of thesis, the reactivity of the cationic Fe-borylene complex toward metathesis, β-hydride transfer and insertion reactions are described. The structure and bonding of mono and dinuclear metallacycles of $Cp_2Ti$ and $Cp_2Zr$ with C2-cumulenes (HNCCNH and OCCO) are studied in the fourth chapter. In the last chapter, a total valence electron count for the condensed transition metal clusters has been proposed which establishes the missing link between the electron count for condensed boranes (*mno* rule), and transition metal clusters (Mingos' rule).

### [1.4.1] Chapter 2: Reactivity of Cationic Terminal Fe-Borylene Complex: Mechanism for Boron Metathesis

Transition metal borylene complexes have received significant attention in the recent years, which is partially attributed to the similarities with classical organometallic ligand systems such as Fischer carbenes and vinylidenes. Recently metathesis reactions of the transition metal aminoborylene complex $[Cp(CO)_2FeBN(i\text{-}Pr)_2]^+(BAr^f_4)^-$ ($Ar^f$ = 3,5-$(CF_3)_2C_6H_3$) (**1a**) with AX (**2**), where A = $Ph_3P$, $Ph_3As$; X = O, S, were reported by Aldridge and co-workers (Scheme 1.1a).[19] It led to the isolation of $[Cp(CO)_2Fe(A)]^+(BAr^f_4)^-$ (**3**) and $(i\text{-}Pr)_2NBX$ (**4**). The reaction of $Ph_2CO$ with **1a**, however, does not follow the metathesis pathway; the ligand transformation process, Meerwein−Ponndorf β-hydride transfer from an isopropyl substituent of the aminoborylene ligand to the coordinated ketone, takes place instead (Scheme 1.1b).[20]

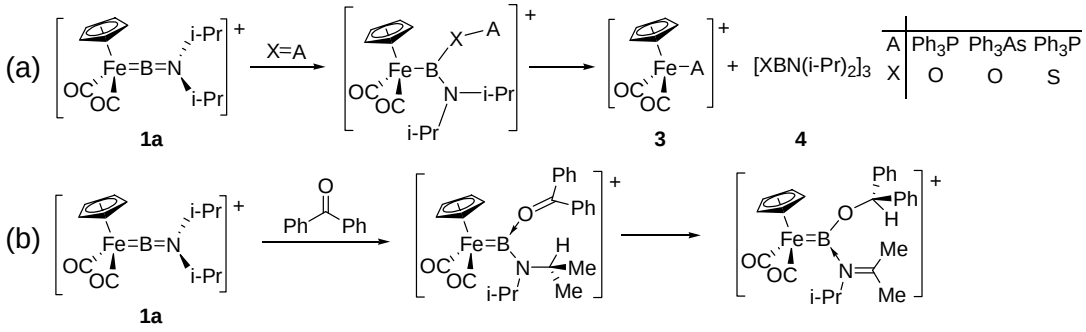


**Scheme 1.1:** Schematic Representation of the Reactions of **1a** (a) Metathesis Reaction with AX (b) β-Hydride-Transfer Reaction with $Ph_2CO$.

Obviously, not all unsaturated substrates are suitable to undergo metathesis with the borylene complex. This raises many interesting questions about the details of the reaction, the characteristics of the metal-borylene complex, and the unsaturated substrates likely to undergo boron metathesis. The analysis[21] shows that boron metathesis proceeds via the initial attack of the substrates at the positively charged boron atom of the metal-borylene complex and forms the more preferable acyclic intermediate. On the contrary, the attack of the olefin takes place at the metal end of the M=C bond of the metal-carbene complex in olefin metathesis and proceeds via [2+2] cyclo-addition. The energetics of boron metathesis and olefin metathesis reactions are comparable. Substrates which are polar and have low-lying σ*-MO (weak σ-bond) prefer boron metathesis reaction. The relative stability of the metathesis products is controlled by the strength of the M-E and B-X bonds of the products (Scheme 1.1a). The β-hydride transfer (Scheme 1.1b) is a competitive reaction to boron metathesis for the substrates having low-lying π*-MO. The metathesis reactions of the Fe-borylene complex with various substrates indicate the role of polarity in tuning the reaction in a preferred direction.

### [1.4.2] Chapter 3: Reactivity of Cationic Terminal Fe-Borylene Complex toward Carbodiimide and Isocyanate: Insertion versus Metathesis Reactions

In contrast to boron metathesis, the reaction of the borylene complex **1a**, or its dicyclohexylamino counterpart $[CpFe(CO)_2(BNCy_2)]^+$ (**1b**) with dicyclohexylcarbodiimide (CyNCNCy) gives an insertion product, in which two equivalents of carbodiimide are assimilated, one into each of the Fe=B and B=N double bonds to form the spirocyclic complexes **5a,b** (Scheme 1.2a).[22] On the other hand, the reaction of isocyanates (R'NCO; R' = Ph, 2,6-Xyl, Cy) with **1b** gives an entirely different type of product i.e. $[CpFe(CO)_2(CNR')]^+$ (**6**) via a net oxygen abstraction process from the heteroallene precursor (Scheme 1.2b).[23] To rationalize the difference in the reactivity of **1a** and **1b** toward carbodiimide and isocyanates, mechanistic study has been carried out.

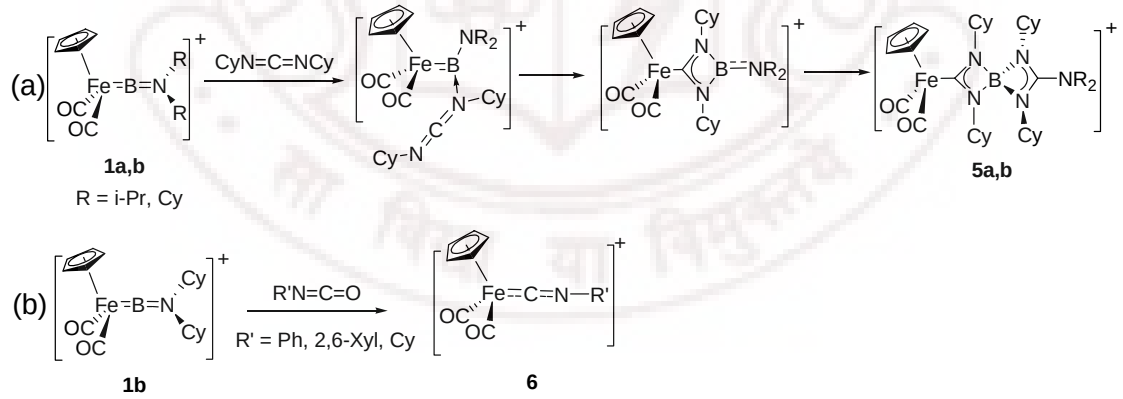


**Scheme 1.2:** Schematic Representation of the Reactions of **1a,b** (a) Insertion Reaction with CyNCNCy and (b) Oxygen atom abstraction Reaction with R′NCO.

It has been shown[24] that both carbodiimide and isocyanate substrates prefer insertion into the Fe=B bond rather than the B=N bond of the borylene complex. In case of isocyanates, the net metathesis reaction is a competitive pathway to

insertion. The metathesis pathway is facile for isocyanate substrates if initial coordination at the boron atom occurs via the oxygen atom (kinetically favored). Insertion chemistry is feasible when the isocyanate attacks initially via the nitrogen atom. However, further reaction of the mono-insertion product so formed with excess isocyanate offers a number of facile (low energetic barrier) routes to $[CpFe(CO)_2(CNR')]^+$ (**6**) rather than to the formation of the bis-insertion product $[CpFe(CO)_2C(NR')(O)B(NR')(O)CNR_2]^+$ (R' = Ph, 2,6-Xyl, Cy) (i.e. the direct analogue of the observed products (**5a,b**) from the carbodiimide reaction). Moreover, the presence of a number of facile competing reaction pathways for the formation of the final isonitrile products (**6**) indicate that the product distribution is better explained in terms of competing pathways, rather than differing extents of reaction along similar trajectories.

### [1.4.3] Chapter 4: Structure and Bonding in Mono and Dinuclear Metallacycles of $Cp_2M$ (M = Ti, Zr) with C2-Cumulenic Ligands XCCX (X = O, NH): Comparison with Metallacycles of 1,2,3-Butatriene and 1,3-Butadiyne

The unstable 14-electron titanocene $Cp_2Ti$ and zirconocene $Cp_2Zr$ have been playing a vital role in the synthetic organometallic chemistry,[25] olefin polymerization, [26] organometallic chemical vapour deposition,[27] C-C coupling and cleavage reactions.[28, 29] The carbene-type frontier orbitals of $Cp_2M$ (M = Ti, Zr) help in the reaction with unsaturated compounds such as 1,3-butadiynes and 1,2,3-butatrienes to form several mono and binuclear metallacycles.[30, 31] The structure and reactivity of these complexes are well studied both experimentally and theoretically. However, similar three and five membered 2,5-dihetero-substituted metallacycles are not reported yet. On the other hand, binuclear complexes of 2,5-dihetero

substituted metallacycles have been reported in the literature.[32] The structure and boding in the mono and binuclear metallacycles of $Cp_2M$ (M = Ti, Zr) with C2-cumulenes XCCX (X = O, NH) is investigated in this chapter (Scheme 1.3).

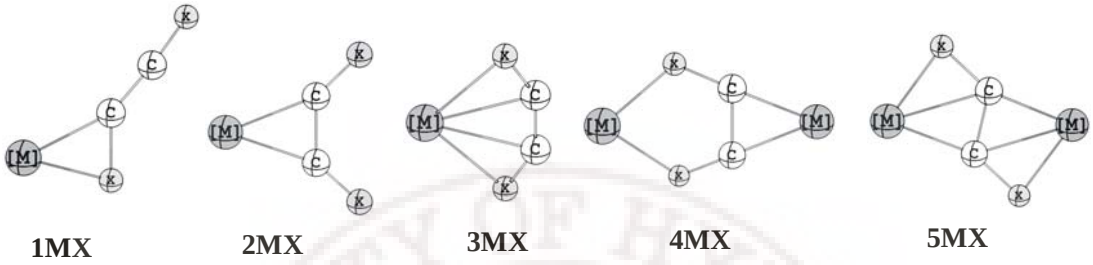


**Scheme 1.3:** Schematic representation of the mono and dinuclear complexes of $Cp_2M$ (M = Ti, Zr) with XCCX (X = O, NH, CH, $CH_2$). [M] represents $Cp_2M$ fragment.

The bonding analysis on the C2-cumulene ligands indicates that the ligand OCCO can be described as dianion of 1,3-butadiyne and the ligand HNCCNH as similar to 1,2,3-butatriene, where terminal $CH_2$ groups are replaced by isolobal NH groups having lone pair. The number of filled in plane π MOs are same in all these four C2-cumulenic ligands, but the two hetero-cumulenic ligands have two additional electrons in the perpendicular π MO. The ligands $H_2CCCCH_2$ and HNCCNH can interact with the $Cp_2M$ fragment through the terminal C-X (X = $CH_2$, NH) as well as central C-C π bond to form three membered metallacycles **1MX** and **2MX** (Scheme 1.3). On the other hand, three membered metallacycle **2MX** are not the stationary points on the potential energy surface for the ligands OCCO and HCCCCH. The interaction of the in-plane π MOs in **3ZrO** and **3MNH** is similar to that of the metallacyclocumulene and metallacyclopentyne. However, the anti-bonding interaction in the third filled perpendicular π MO results in distortion of the

five membered ring of **3ZrO** and **3MNH**. The relative stability of the five membered metallacycle **3MX** as compared to three-membered metallacycle **1MX** increases when X changes from O to $CH_2$. This trend is more pronounced in Zr complexes due to the bigger size of Zr. All the cis- binuclear complexes except **4MCH** are non-planar and the bending of the metallocene fragments from the plane of XCCX are larger for X = NH and O. The rehybridization of the in-plane and perpendicular π MO probably results in the bending of the two metallocene fragments in **4MX** with respect to XCCX plane. Unlike the cis-dimetallabicycles, the two $Cp_2M$ fragments in **5MX** are in the same plane with respect to XCCX ligand.

### [1.4.4] Chapter 5: *mno* Rule for Condensed Boranes versus Mingos' Rule for Condensed Transition Metal Clusters: The missing link

In this chapter, the topographic and electronic similarities between the poly-condensed transition metal clusters and polyhedral borane clusters are investigated with the help of electron-counting rules.[33-41] The correlation between the electron count for the polyhedral boranes (Wade's $n$ + 1 rule)[37] and for the transition metal clusters (PSEPT, 7$n$ + 1 rule)[38] can be understood from the isolobal analogy between BH and transition metal fragments. The relationship between the electron count of poly-condensed polyhedral boranes (*mno* rule)[39] and poly-condensed transition metal clusters (Mingos' rule)[41a,b] is not straightforward. The *mno* rule for condensed boranes and Mingos' rule for transition metal clusters are based on different sets of parameters and thus one to one correspondence between these two rules is missing. In this chapter, a total valence electron count for the condensed transition metal

clusters is proposed which establishes the missing link between the electron count for condensed boranes (*mno* rule), and transition metal clusters (Mingos' rule). According to this rule, $m + n + o + 6n - 3(m - 1) = 7n - 2m + o + 3$ ($n$ = number of vertices, $m$ = number of polyhedra, $o$ = number of single vertex sharing) number of electron pairs are necessary for the stability of *closo* polycondensed transition metal clusters. The additional electron pairs required for *nido* and *arachno* polyhedra, one and two respectively, are to be added separately. Comparison of this electron count with Mingos' rule gives a relation between $n_s$ (number of shared vertices), $y_b$ (number of bonds between the shared atoms) and $m$ (number of polyhedra) as $y_b = 2n_s - 3(m - 1) + o$. The rule is also extended as $m + n + o + p + 6x - x_s/n_s\{3(m - 1)\}$, (where $x$ = number of transition metals, $x_s$ = number of shared transition metals and $n_s$ = number of shared atoms) to the incorporate the electron counts of the metallaboranes. This rule converts to *mno* rule (where $x = x_s = 0$) for condensed boranes and $7n - 2m + o + 3$ rule (where $x = n$, $x_s = n_s$) for condensed transition metal clusters.

## [1.5] References


1. Dirac, P. A. M. *Proc. R. Soc.* **1929**, *123*, 714.
2. Schrödinger, E. *Phys. Rev.* **1926**, *28*, 1049.
3. (a) Levine, I. N. *Quantum Chemistry*, 5th Edition, Prentice Hall, NJ, 2000. (b) McQuarrie, D. A. *Quantum Chemistry*, Oxford University Press, California, 1983. (c) Pilar, F. L. *Elementary Quantum Chemistry*, Mc-Graw Hill Publishing Co., NewYork, 1968. (d) Chandra, A. K. *Introductory Quantum Chemistry*, Tata Mc-Graw Hill Publishing Co., New Delhi, 1988. (e) Szabo, A.; Ostlund, N. S. *Modern Quantum Chemistry*, Mc-Graw Hill Publishing Co., NewYork, 1982.
4. (a) Hehre, W. J.; Radom, L.; Schleyer, P. v. R.; Pople, J. A. *Ab-initio Molecular Orbital Theory*, John Wiley & Sons, Inc., New York, 1986. (b) Pople, J. A.; Beveridge, D. L. *Approximate Molecular Orbital Theory*, Mc-Graw Hill Publishing Co., NewYork, 1970. (c) Lowe, J. P. *Quantum Chemistry*, Academic Press, New York, 1978. (d) Schaefer III, H. F. *The Electronic Structure of Atoms and Molecules*, Addison-Wesley, Massachusetts, USA, 1972. (e) Foresman, J. B.; Frisch, A. *Exploring Chemistry with Electronic Structure Methods,* Gaussian Inc. Pittsburgh, USA. 2004 (f) Richards, W. G.; Cooper, D. L. *Ab initio Molecular Orbital Calculations for Chemists*, Clarendon Press, Oxford, 1983. (g) Jensen, F. *Introduction to Computational Chemistry*, John Wiley & Sons, New York, 1999.
5. Hohenberg, P. C.; Kohn, W. *Phys. Rev.* **1964**, *136,* B864.
6. Kohn, W.; Sham, L. *Phys. Rev.* **1965,** *140*, A1133.

7. (a) Parr, R. G.; Yang, W. *Density Functional Theory of Atoms and Molecules,* Oxford University Press, Oxford, 1989. (b) Dreisler, R. M.; Gross, E. K. V. *Density Functional Theory: An Approach to the Quantum Many-body Problem*, Springer-Verlag, Berlin, 1990. (c) Hohenberg, P. C.; Kohn, W.; Sham, L. J. *Advances in Quantum Chemistry*, Vol. 21, Academic Press, 1990. (d) Kohn, W.; Becke, A. D.; Parr, R. G. *J. Phys. Chem*. **1996**, *100*, 12974. (e) Geerlings, P.; De Proft, F.; Langenaeker, W. *Chem. Rev*. **2003**, *103*, 1793.
8. Born, M.; Oppenheimer, J. R. *Ann. Physik* 1927, *84*, 457.
9. (a) Hartree, D. R. *Proc. Cambridge Phil. Soc.* **1928**, *24*, 89. (b). Fock, V. *Z. Phys.* **1930***, 61,*126.
10. McWeeny, R. *Int. J. Quant. Chem.* **1967**, *15*, 351.
11. Møller, C.; Plesset, M. S. *Phys. Rev.* **1934**, *46*, 618.
12. (a) Hurley, A. C. *Electron Correlation in Small Molecules* Academic Press, London, 1977. (b) Wilson, S. *Electron Correlation in Molecules* Clarendon Press, Oxford, 1984. (c) Raghavachari, K.; Anderson, J. B. *J. Phys. Chem.* **1996**, *100*, 12960.
13. (a) Purvis, G. D., III; Bartlett, R. J. *J. Chem. Phys.* 1982, 76, 1910. (b) Raghavachari, K.; Trucks, G. W.; Pople, J. A.; Head-Gordon, M. *Chem. Phys. Lett.* 1989, 157, 479. (c) Watts, J. D.; Gauss, J.; Bartlett, R. J. *J. Chem. Phys.* 1993, 98, 8718.
14. Slater, J. C. *Phys. Rev.* **1930**, *36*, 57.
15. Boys, S. F. *Proc. R. Soc. (London)* **1950**, *A200*, 542.

16. Frenking, G.; Seijo, L.; Bohme, M.; Dapprich, S.; Ehlers, A. W.; Jonas, V.; Neuhaus, A.; Otto, M.; Stegmann, R.; Veldkamp, A.; Vyboishchikov, S. F.; *Reviews in Computational Chemistry*; Lipkowitz, K. B., Boyd, D. B., Eds.; VCH: New York, 1996, *8*, 63.

17. (a) Becke, A. D. *J. Chem. Phys.* **1993**, *98*, 5648. (b) Becke, A. D. *Phys. Rev. A* **1988**, *38*, 3098. (c) Lee, C.; Yang, W.; Parr, R. G. *Phys. Rev. B* **1988**, *37*, 785. (d) Hay, P. J.; Wadt, W. R. *J. Chem. Phys.* **1985**, *82*, 270. (e) Wadt, W. R.; Hay, P. J. *J. Chem. Phys.* **1985**, *82*, 284. (f) Hay, P. J.; Wadt, W. R. *J. Chem. Phys.* **1985**, *82*, 299.

18. Gaussian 03, Revision C.02, Frisch, M. J.; Trucks, G. W.; Schlegel, H. B.; Scuseria, G. E.; Robb, M. A.; Cheeseman, J. R.; Montgomery, Jr., J. A.; Vreven, T.; Kudin, K. N.; Burant, J. C.; Millam, J. M.; Iyengar, S. S.; Tomasi, J.; Barone, V.; Mennucci, B.; Cossi, M.; Scalmani, G.; Rega, N.; Petersson, G. A.; Nakatsuji, H.; Hada, M.; Ehara, M.; Toyota, K.; Fukuda, R.; Hasegawa, J.; Ishida, M.; Nakajima, T.; Honda, Y.; Kitao, O.; Nakai, H.; Klene, M.; Li, X.; Knox, J. E.; Hratchian, H. P.; Cross, J. B.; Bakken, V.; Adamo, C.; Jaramillo, J.; Gomperts, R.; Stratmann, R. E.; Yazyev, O.; Austin, A. J.; Cammi, R.; Pomelli, C.; Ochterski, J. W.; Ayala, P. Y.; Morokuma, K.; Voth, G. A.; Salvador, P.; Dannenberg, J. J.; Zakrzewski, V. G.; Dapprich, S.; Daniels, A. D.; Strain, M. C.; Farkas, O.; Malick, D. K.; Rabuck, A. D.; Raghavachari, K.; Foresman, J. B.; Ortiz, J. V.; Cui, Q.; Baboul, A. G.; Clifford, S.; Cioslowski, J.; Stefanov, B. B.; Liu, G.; Liashenko, A.; Piskorz, P.; Komaromi, I.; Martin, R. L.; Fox, D. J.; Keith, T.; Laham, M. A.; Peng, C. Y.; Nanayakkara, A.; Challacombe, M.; Gill, P.

M. W.; Johnson, B.; Chen, W.; Wong, M. W.; Gonzalez, C.; and Pople, J. A. Gaussian, Inc., Wallingford CT, 2004.

19. Kays, D. L.; Day, J. K.; Ooi, L.-L.; Aldridge, S. *Angew. Chem. Int. Ed.* **2005**, *44*, 7457.
20. Kays, D. L.; Day, J. K.; Aldridge, S.; Harrington, R. W.; Clegg, W. *Angew. Chem., Int. Ed*. **2006**, *45*, 3513.
21. De, S.; Parameswaran, P.; Jemmis, E. D. *Inorg. Chem.* **2007,** *46*, 6091.
22. Pierce, G. A.; Aldridge, S.; Jones, C.; Gans-Eichler, T.; Stasch, A.; Coombs, N. D.; Willock, D. J. *Angew. Chem. Int. Ed*. **2007**, *46*, 2043.
23. Pierce, G. A.; Vidovic, D.; Kays, D. L.; Coombs, N. D.; Thompson, A. L.; Jemmis, E. D.; De, S.; Aldridge, S. *Organometallics* **2009**, *28*, 2947.
24. De, S.; Pierce, G. A.; Vidovic, D.; Kays, D. L.; Coombs, N. D.; Jemmis, E. D.; Aldridge, S. *Organometallics* **2009**, *28*, 2961.
25. Togni, A., Halterman, R. L. (Eds.), *Metallocenes: Synthesis, Reactivity, Applications*, Wiley-VCH, Weinheim, 1998, Vols. 1 and 2 and references therein.
26. (a) Alt, H. G.; Köppl, A. *Chem. Rev.* **2000**, *100*, 1205. (b) Resconi, L.; Cavallo, L.; Fait, A.; Piemontesi, F. *Chem. Rev.* **2000**, *100*, 1253. (c) Kaminsky, W. J. *Chem. Soc., Dalton Trans.* **1998**, 1413. (d) Bochmann, M. J. *Chem. Soc., Dalton Trans.* **1996**, 255. (e) Brintzinger, H. H.; Fischer, D.; Mulhaupt, R.; Rieger, B.; Waymouth, R. M. *Angew. Chem., Int. Ed. Engl.* **1995**, *34*, 1143.
27. (a) Choukroun, R.; Donnadieu, B.; Zhao, J.-S.; Cassoux, P.; Lepetit, C.; Silvi, B. *Organometallics* **2000**, *19*, 1901. (b) Choukroun, R.; Cassoux, P.

*Acc. Chem. Res.* **1999**, *32*, 494. (c) Choukroun, R.; Donnadieu, B.; Zhao, J.; Cassoux, P.; Lepetit, C.; Silvi, B. *Organometallics* **2002**, *19*, 1901. (d) Danjoy, C.; Zhao, J. S.; Donnadieu, B.; Legros, J.-P.; Valade, L.; Choukroun, R.; Zwick, A.; Cassoux, P. *Chem. Eur. J.* **1998**, *4*, 1100.

28. (a) Sato, F.; Urabe, H.; Okamoto, S. *Chem. Rev.* **2000**, *100*, 2835. (b) Rosenthal, U.; Pellny, P.-M.; Kirchbauer, F. G.; Burlakov, V. V. *Acc. Chem. Res.* **2000**, *33*, 119. (c) Ohff, A.; Pulst, S.; Peulecke, N.; Arndt, P.; Burlakov, V. V.; Rosenthal, U. *Synlett.* **1996**, 111. (d) Negishi, E.; Takahashi, T. *Acc. Chem. Res.* **1994**, *27*, 124. (e) Buchwald, S. L.; Nielsen, R. B. *Chem. Rev.* **1988**, *88*, 1047. (f) Miura, K.; Funatsu, M.; Saito, H.; Ito, H.; Hosomi, A. *Tetrahedron Lett.* **1996**, *37*, 9059. (g) Rosenthal, U.; Burlakov, V. V. In *Titanium and Zirconium in Organic Synthesis, Marek, I.* (Ed.), Wiley-VCH, Weinheim, 2002, p. 355. (h) Rosenthal, U.; Burlakov, V. V.; Arndt, P.; Baumann, W.; Spannenberg, A. *Organometallics* **2003**, *22*, 884. (i) Rosenthal, U. *Angew. Chem., Int. Ed.* **2004**, *43*, 3882. (j) Pulst, S.; Arndt, P.; Heller, B.; Baumann, W.; Kempe, R.; Rosenthal, U. *Angew. Chem., Int. Ed. Engl.* **1996**, *35*, 1112. (k) Pellny, P.-M.; Peulecke, N.; Burlakov, V. V.; Tillack, A.; Baumann, W.; Spannenberg, A.; Kempe, R.; Rosenthal, U. *Angew. Chem., Int. Ed. Engl.* **1997**, *36*, 2615.

29. (a) Rosenthal, U.; Görls, H. *J. Organomet. Chem.* **1992**, *439*, C36. (b) Rosenthal, U.; Ohff, A.; Tillack, A.; Baumann, W.; Görls, H. *J. Organomet. Chem.* **1994**, *468*, C4. (c) Erker, G.; Frömberg, W.; Mynott, R.; Gabor, B.; Krüger, C. *Angew. Chem., Int. Ed. Engl.* **1986**, *25*, 463. (d) Erker, G. *Angew. Chem., Int. Ed. Engl.* **1989**, *28*, 397. (e) Erker, G.; Frömberg, W.;

Benn, R.; Mynott, R.; Angermund, D.; Kruger, C. *Organometallics* **1989**, *8*, 911. (f) Teuben, J. H.; de Liefde Meijer, H. J. *J. Organomet. Chem.* **1969**, *17*, 87. (g) Sekutowski, D. G.; Stucky, G. D. *J. Am. Chem. Soc.* **1976**, *98*, 1376. (h) Wood, G. L.; Knobler, C. B.; Hawthorne, M. F. *Inorg. Chem.* **1989**, *28*, 382. (i) Cuenca, T.; Gómez, R.; Gómez-Sal, P.; Rodriguez, G. M.; Royo, P. *Organometallics* **1992**, *11*, 1229. (j) Varga, V.; Mach, K.; Hiller, J.; Thewalt, U.; Sedmera, P.; Polasek, M. *Organometallics* **1995**, *14*, 1410. (k) Metzler, N.; Nöth, H. *J. Organomet. Chem.* **1993**, *454*, C5. (l) Cano, A.; Cuenca, T.; Galakhov, M.; Rodríguez, G. M.; Royo, P.; Cardin, C. J.; Convery, M. A. *J. Organomet. Chem.* **1995**, *493*, 17. (m) Lang, H.; Blau, S.; Nuber, B.; Zsolnai, L. *Organometallics* **1995**, *14*, 3216. (n) Heshmatpour, F.; Wocadlo, S.; Massa, W.; Dehnicke, K. *Acta Crystallogr.* **1995**, *C51*, 2225. (o) Hsu, D. P.; Davis, W. M.; Buchwald, S. L. *J. Am. Chem. Soc.* **1993**, *115*, 10394.

30. Rosenthal, U.; Pellny, P.-M.; Kirchbauer, F. G.; Burlakov, V. V. *Acc. Chem. Res.* **2000**, *33*, 119.

31. (a) Rosenthal, U.; Burlakov, V. V.; Arndt, P.; Baumann, W.; Spannenberg, A. *Organometallics* **2005**, *24*, 456, and references therein. (b) Bach, M. A.; Burlakov, V. V.; Arndt, P.; Baumann, W.; Spannenberg, A.; Rosenthal, U. *Organometallics* **2005**, *24*, 3047. (c) Suzuki, N.; Aihara, N.; Takahara, H.; Watanabe, T.; Iwasaki, M.; Saburi, M.; Hashizume, D.; Chihara, T. *J. Am. Chem. Soc*. **2004**, *126*, 60. (d) Suzuki, N.; Watanabe, T.; Iwasaki, M.; Chihara, T. *Organometallics* **2005**, *24*, 2065. (e) Rosenthal, U.; Ohff, A.; Baumann, W.; Kempe, R.; Tillack, A.; Burlakov, V. V. *Organometallics*

**1994**, *13*, 2903. (f) Rosenthal, U.; Pulst, S.; Ohff, A.; Tillack, A.; Baumann, W.; Kempe, R.; Burlakov, V. V. *Organometallics* **1995**, *14*, 2961. (g) Pulst, S.; Kirchbauer, F. G.; Heller, B.; Baumann, W.; Rosenthal, U. *Angew. Chem. Int. Ed. Engl.* **1998**, *37*, 1925. (h) Rosenthal, U.; Ohff, A.; Baumann, W.; Kempe, R.; Tillack, A.; Burlakov, V. V. *Angew. Chem. Int. Ed. Engl.* **1994**, *33*, 1605. (i) Rosenthal, U.; Burlakov, V. V.; Arndt, P.; Baumann, W.; Spannenberg, A.; Shur, V. B. *Eur. J. Inorg. Chem.* **2004**, 4739. (j) Erker, G.; Venne-Duncker, S.; Kehr, G.; Kleigrewe, N.; Fröhlich, R.; Mück-Lichtenfeld, C.; Grimme, S. *Organometallics* **2004**, *23*, 4391. (k) Pellny, P.-M.; Kirchbauer, F. G.; Burlakov, V. V.; Baumann, W.; Spannenberg, A.; Rosenthal, U. *J. Am. Chem. Soc.* **1999**, *121*, 8313.

32. (a) Hessen, B.; Blenkers, J.; Teuben, J. H.; Helgesson G.; Jagner, S. *Organometallics*, **1989**, *8*, 830. (b) Lentz, D.; Brüdgam, I.; Hartl, H. *Angew. Chem., Int. Ed. Engl.*, **1984**, *23*, 525 and references cited therein. (c) Cotton, F. A.; Roth, W. J. *J. Am. Chem. Soc.* **1983**, *105*, 3734. (d) Cotton, F. A.; Duraj, S. A.; Roth, W. J. *J. Am. Chem. Soc.* **1984**, *106*, 6987. (e) Seidel, W. W.; Schaffrath, M.; Pape, T. *Angew. Chem., Int. Ed.* **2005**, *44*, 7798.
33. (a) Lewis, G. N. *J. Am. Chem. Soc.* **1916**, *38*, 762. (b) Abegg, R. *Z. Anorg. Chem.* **1904**, *39*, 330.
34. Sidgwick, N. V. *The electronic theory of valency*; Cornell University Press: Ithaca, NY, 1927.
35. Hückel, E. *Z. Phys.* **1931**, *70*, 204.
36. Lipscomb, W. N. *Boron Hydrides*, Benjamin, New York, 1963.

37. (a) Wade, K. *Chem. Commun*. **1971**, 792. (b) Wade, K. *Adv. Inorg. Chem. Radiochem.* **1976**, *18*, 1.

38. (a) Mingos, D. M. P. *Nature (London), Phys. Sci.* **1972**, *236*, 99. (b) Mason, R.; Thomas, K. M.; Mingos, D. M. P. *J. Am. Chem. Soc.* **1973**, *95*, 3802.

39. Jemmis, E. D.; Balakrishnarajan, M. M.; Pancharatna, P. D. *J. Am. Chem. Soc.* **2001**, *123*, 4313.

40. (a) Ciani, G.; Sironi, A. *J. Organomet. Chem.* **1980**, *197*, 233-248. (b) Lauher, J. W. *J. Am. Chem. Soc*. **1978**, *100*, 5305. (c) Teo, B. K. *Inorg. Chem.* **1985**, *24*, 115-116.

41. (a) Mingos, D. M. P. *Acc. Chem. Res*. **1984**, *17*, 311. (b) Mingos, D. M. P. *J. Chem. Soc., Chem. Commun.* **1983**, 706. (c) Mingos, D. M. P.; Welch, A. J. *J. Chem. Soc., Dalton Trans*. **1980**, 1674. (d) Mingos, D. M. P. *J. Chem. Soc., Dalton Trans*. **1974**, 133. (e) Mingos, D. M. P. *Inorg. Chem.* **1985**, *24*,114-115.

# CHAPTER 2

## REACTIVITY OF CATIONIC TERMINAL Fe-BORYLENE COMPLEX: MECHANISM FOR BORON METATHESIS

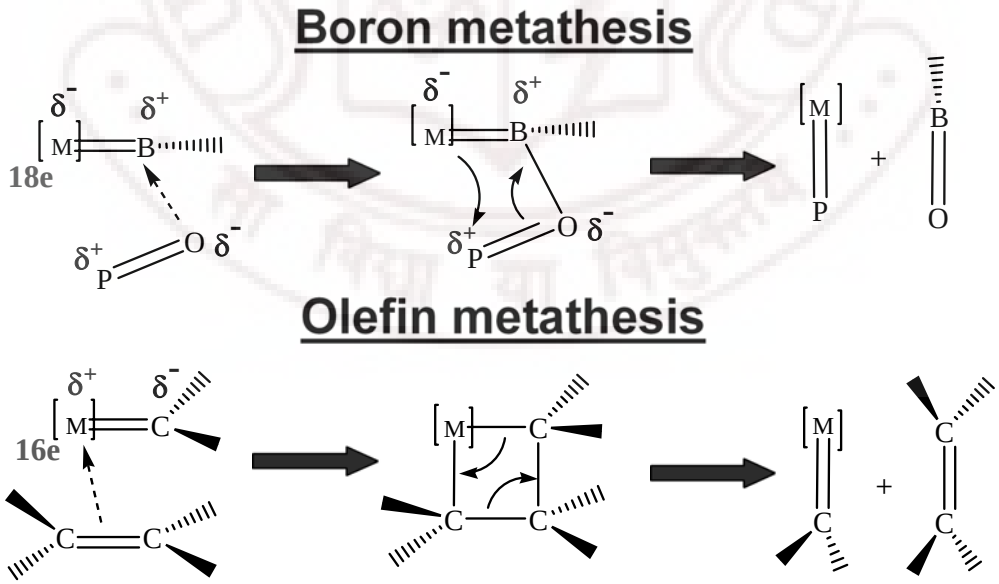

## Abstract

The mechanism of the boron metathesis reaction of the transition-metal-aminoborylene complex $Cp(CO)_2FeBN(CH_3)_2^+$ (**8**) with EX, where EX = $H_3PO$ (**9ap**), $H_3AsO$ (**9bp**), $H_3PS$ (**9aq**), $H_3AsS$ (**9bq**), $CH_3CHCH_2$ (**9cr**), $(NH_2)_2CCH_2$ (**9dr**), $H_2CO$ (**9ep**), and $(NH_2)_2CO$ (**9dp**) was investigated at the B3LYP/LANL2DZ level. The analysis of bonding and charge distribution shows that the Fe-borylene complex (**8**) is a Fischer-type carbene analogue. The attack of the olefin takes place at the metal end of the M=C bond of the metal-carbene complex in olefin metathesis and proceeds via [2 + 2] cycloaddition, while in boron metathesis, the initial attack of the substrates takes place at the positively charged B atom of the Fe-borylene complex and forms the preferred acyclic intermediate. The energetics of boron metathesis is comparable to that of the olefin metathesis. Substrates that are polar and a have low-lying $\sigma^*$ molecular orbital (weak $\sigma$ bond) prefer the boron metathesis reaction. The relative stability of the metathesis products is controlled by the strength of the Fe-E and B-X bonds of the products **13** and **14**, respectively. The possibility of a $\beta$-hydride-transfer reaction in the Fe-borylene complex has also been investigated.

## [2.1] Introduction

It is fascinating to compare and contrast the chemistry of the two adjacent elements in the periodic table, boron and carbon.[1] Differences among them are plentiful. Carbon provides the basic structural framework for life, while boron is needed only in trace quantities to sustain it. Compounds of carbon provide the best examples for two-center, two-electron bonding. In contrast, boron and its compounds ushered in multicenter bonding. Despite these differences, there are several aspects common to both carbon and boron.[2-5] Advances in the chemistry of one element in a particular direction, however, can go faster than those of the other. Hydroboration, for example, was discovered in 1948 and led to a Nobel Prize for H. C. Brown.[2] It took another 30 years for hydrocarbation to be established.[3]

Olefin metathesis,[4] discovered in 1967, provides a reverse scenario. The versatility of the metathesis reaction in chemistry is recognized by the award of 2005 Nobel Prize to Robert Grubbs, Richard Schrock and Yves Chauvin.[6] The metathesis reactions involving atoms such as Si,[7] S[8], Ga,[9] and N[10] have been slowly coming to light. There are limited examples of metathesis involving $MeB{=}C(SiMe_3)_2$,[11] and these metathesis reactions proceed through [2 + 2] cycloaddition and the regiospecificity is decided by the polarity of both B=C and the attacking double bonds. Despite the fact that there are several transition-metal-borylene complexes known,[12] no metathesis reactivity studies on those complexes have been reported to date. Even though there is a close relationship between transition-metal-borylene complexes and metal-carbene complexes, most of the earlier studies of the reactivity of borylene complexes toward unsaturated substrates containing C=C and C=O

bonds have shown the borylene ligand to undergo a displacement reaction[13] rather than the cycloaddition or metathesis reactions, which are commonly observed in metal-carbenes. Recently, metathesis reactions of the transition-metalaminoborylene complex $[Cp(CO)_2FeBN(i\text{-}Pr)_2]^+(BAr^f_4)^-$ ($Ar^f$ = 3,5-$(CF_3)_2C_6H_3$) (**1**) with AX (**2**), where A = $Ph_3P$, $Ph_3As$; X = O, S, were reported by Aldridge and co-workers (Scheme 2.1a).[14] It led to the isolation of $[Cp(CO)_2Fe(A)]^+(BAr^f_4)^-$ (**4**) and ($i$-Pr)$_2$NBX (**5**). An addition-substitution pathway through intermediate **3** (Scheme 2.1a) was suggested for the reaction. The amino(oxo)boryl intermediate $Cp(CO)_2FeBN(i\text{-}Pr)_2OPPh_3^+$ (**3**, where A = $Ph_3P$, X = O) was isolated for the reaction of $Ph_3PO$ and the Fe-borylene complex **1**.

The reaction of $Ph_2CO$ with **1**, however, does not follow the metathesis pathway; a ligand transformation process, Meerwein-Ponndorf $\beta$-hydride transfer from an isopropyl substituent of the aminoborylene ligand to the coordinated ketone, takes place instead (Scheme 2.1b).[15] Obviously, not all unsaturated substrates are suitable to undergo metathesis with the borylene complex. This raises many interesting questions about the details of the reaction, the characteristics of the metal-borylene complex and the unsaturated substrates likely to undergo boron metathesis. It will also be intriguing to probe the detailed mechanism and the energetics of the boron metathesis reaction. These questions are especially attractive in view of the interest in finding parallels in the chemistry of boron and carbon[1b-f,3b] and prompted the study of these reactions using the model borylene complex $Cp(CO)_2FeBN(CH_3)_2^+$ (**8**) with the unsaturated substrates $H_3PO$ (**9ap**), $H_3AsO$ (**9bp**), $H_3PS$ (**9aq**), $H_3AsS$ (**9bq**), $CH_3HCCH_2$ (**9cr**), $(NH_2)_2CCH_2$ (**9dr**), $H_2CO$

(**9ep**) and $(NH_2)_2CO$ (**9dp**) (Scheme 2.2). The boron metathesis reaction of the derivative of the first three substrates with the Fe-borylene complex (**1**) is observed experimentally. The substrates **9cr**, **9dr**, **9ep** and **9dp** were chosen so that the reactivity of the Fe-borylene complex toward alkenes and carbonyl compounds could be examined.

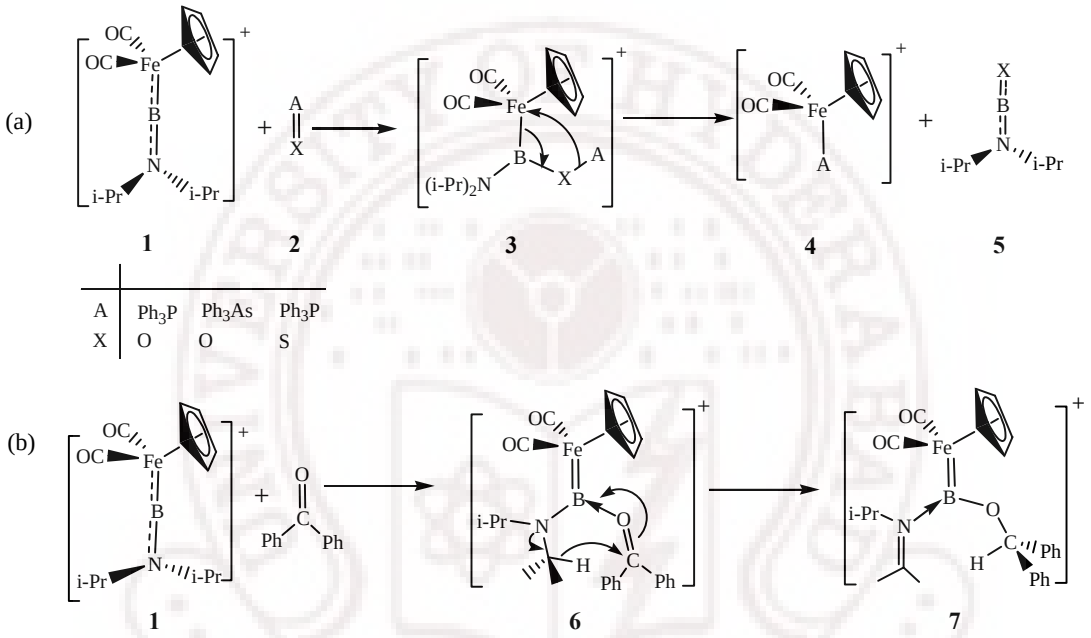


**Scheme 2.1:** Schematic representation of the reactions of **1**: (a) metathesis reaction with AX and (b) $\beta$-hydride-transfer reaction with $Ph_2CO$.

## [2.2] Computational Details

All structures were optimized using the hybrid HF-DFT method, B3LYP/LANL2DZ, based on Becke's three-parameter functional including the Hartree-Fock exchange contribution with a nonlocal correction for the exchange potential proposed by Becke[16,17a,b] together with the nonlocal correction for the correlation energy suggested by Lee et al.[16,17c] The LANL2DZ basis set uses the

effective-core potential of Hay and Wadt.[16,18] The nature of the stationary points was characterized by vibrational frequency calculations. The Gaussian03 program package was used in this study.[19] The charge distributions were obtained by NBO analysis.[20]

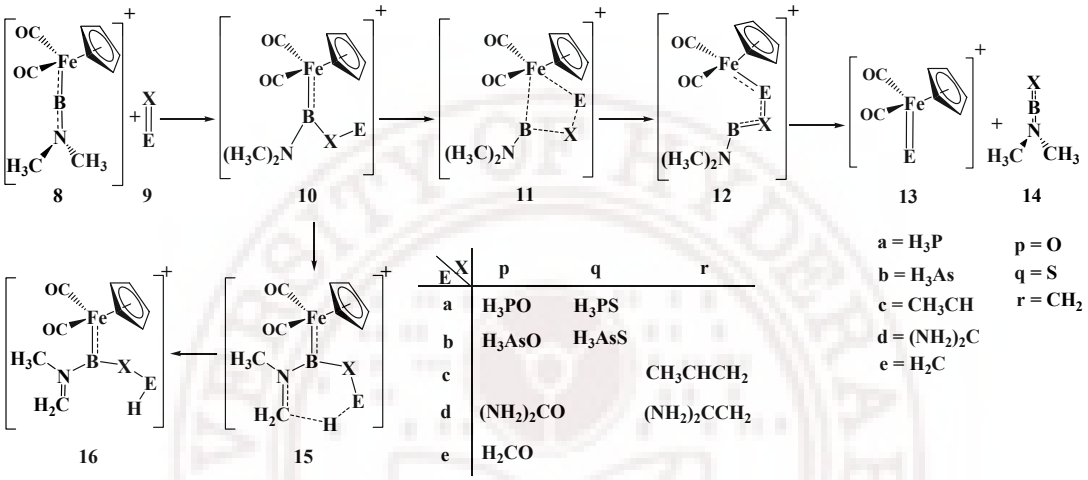


**Scheme 2.2:** Schematic representation of the mechanism of boron metathesis and $\beta$-hydride-transfer reaction of the Fe-borylene complex **8** with EX.

Scheme 2.2 shows the numbering used. The structures are numbered using Arabic numerals. The various substrates (EX) are represented by the combination of two letters. E is represented by five letters (**a** = $H_3P$, **b** = $H_3As$, **c** = $CH_3CH$, **d** = $(NH_2)_2C$ and **e** = $H_2C$) and X is represented by three letters (**p** = O, **q** = S and **r** = $CH_2$). For example, **10ap** describes structure number **10** in which the substrate (EX) attached to the Fe-borylene complex is $H_3PO$, which will correspond to the entry under row **a** and column **p** in scheme 2.2. The structure numbers **13a** and **14p**, for example, represent the final metathesis products where **a** corresponds to $H_3P$ and **p** corresponds to O.

## [2.3] Results and Discussion

The reactants for olefin metathesis are metal-carbene complexes and olefins, while metal-borylene complexes and polar substrates are the reactants for boron metathesis. Though the structure and bonding of borylene complexes are described in the literature,[12d,15,21] a brief recapitulation for the Fe-borylene complex $Cp(CO)_2FeBN(CH_3)_2^+$ (**8**) is given in order to understand the reaction. The details of the mechanism of the metathesis reaction obtained from the theoretical calculations are discussed next, followed by the competitive $\beta$-hydride transfer reaction. Even though the aminoborylene complex is formally isolobal to the vinylidene complex,[5] the more general carbene complex for olefin metathesis was taken as the reference for comparison.

### [2.3.1] Electronic Structure of the Fe-Borylene Complex $Cp(CO)_2FeBN(CH_3)_2^+$

All the theoretical studies on metal-borylene complexes show that the metal-boron bond is formed by the $\sigma$ donation from the boron to the metal and the $\pi$ back-donation from the metal to boron.[12d,15,21] The calculated geometrical parameters of the Fe-borylene complex are close to the experimentally reported values (Table 2.1).[14] It is possible to anticipate from the difference in the electronegativity of the B and Fe atoms that the Fe-borylene complex **8** is a Fischer-type carbene analogue with a polarization of charge, making Fe the negative end. The analysis of natural charge distribution on the Fe-borylene complex **8** shows negative charge on Fe (-0.38) and positive charge on B (+0.95). The charges on the fragments, +0.34 on $Cp(CO)_2Fe$ and +0.66 on $BN(CH_3)_2$, also indicate the electropositive nature of B as

**Table 2.1:** Important bond lengths (in Å) of all the molecules. Experimental values are given in parenthesis.

| Molecule | Bond distance (Å) | | | | |
|---|---|---|---|---|---|
| | **Fe-B** | **B-N** | **B-X** | **E-X** | **M-E** |
| **8** | 1.861 (1.859) | 1.355 (1.324) | - | - | - |
| **9ap** | - | - | - | 1.619 | - |
| **9bp** | - | - | - | 1.707 | - |
| **9aq** | - | - | - | 2.136 | - |
| **9bq** | - | - | - | 2.203 | - |
| **9cr** | - | - | - | 1.350 | |
| **9dr** | - | - | - | 1.365 | - |
| **9dp** | - | - | - | 1.258 | - |
| **9ep** | - | - | - | 1.241 | - |
| **10ap** | 2.033 (2.057) | 1.402 (1.397) | 1.512 (1.469) | 1.648 (1.540) | 3.796 |
| **10bp** | 2.038 | 1.404 | 1.503 | 1.731 | 3.904 |
| **10aq** | 2.017 | 1.404 | 2.096 | 2.209 | 4.111 |
| **10bq** | 2.006 | 1.400 | 2.123 | 2.288 | 4.544 |
| **10dr** | 2.060 | 1.422 | 1.642 | 1.507 | 3.972 |
| **10dp** | 2.013 | 1.405 | 1.523 | 1.310 | 3.881 |
| **10ep** | 2.018 | 1.392 | 1.538 | 1.269 | 3.787 |
| **11ap (TS)** | 2.164 | 1.391 | 1.398 | 1.810 | 2.719 |
| **11bp (TS)** | 2.164 | 1.392 | 1.401 | 1.868 | 2.798 |
| **11aq (TS)** | 2.221 | 1.399 | 1.870 | 2.472 | 2.825 |
| **11ep** | 2.353 | 1.377 | 1.355 | 1.487 | 2.024 |
| **12ep** | 3.987 | 1.346 | 1.263 | 1.548 | 1.987 |
| **13a** | - | - | - | - | 2.329 |
| **13b** | - | - | - | - | 2.405 |
| **13c** | | | | | 1.826 |
| **13d** | - | - | - | - | 1.962 |
| **13e** | - | - | - | - | 1.796 |
| **14p** | - | 1.380 | 1.241 | - | - |
| **14q** | - | 1.378 | 1.665 | - | - |
| **14r** | - | 1.374 | 1.403 | - | - |
| **15dr (TS)** | 1.985 | 1.529 | 1.608 | 1.555 | 4.484 |
| **15dp (TS)** | 1.964 | 1.525 | 1.412 | 1.466 | 4.373 |
| **15ep (TS)** | 1.949 | 1.472 | 1.476 | 1.327 | 4.251 |
| **16dr** | 1.983 | 1.551 | 1.585 | 1.555 | 4.540 |
| **16dp** | 1.991 | 1.599 | 1.357 | 1.548 | 3.677 |
| **16ep** | 1.983 | 1.596 | 1.360 | 1.465 | 3.669 |

compared to Fe. The molecular orbital (MO) analysis shows the $\sigma$ donation from B to Fe and the $\pi$ back-donation from Fe to B (Scheme 2.3).

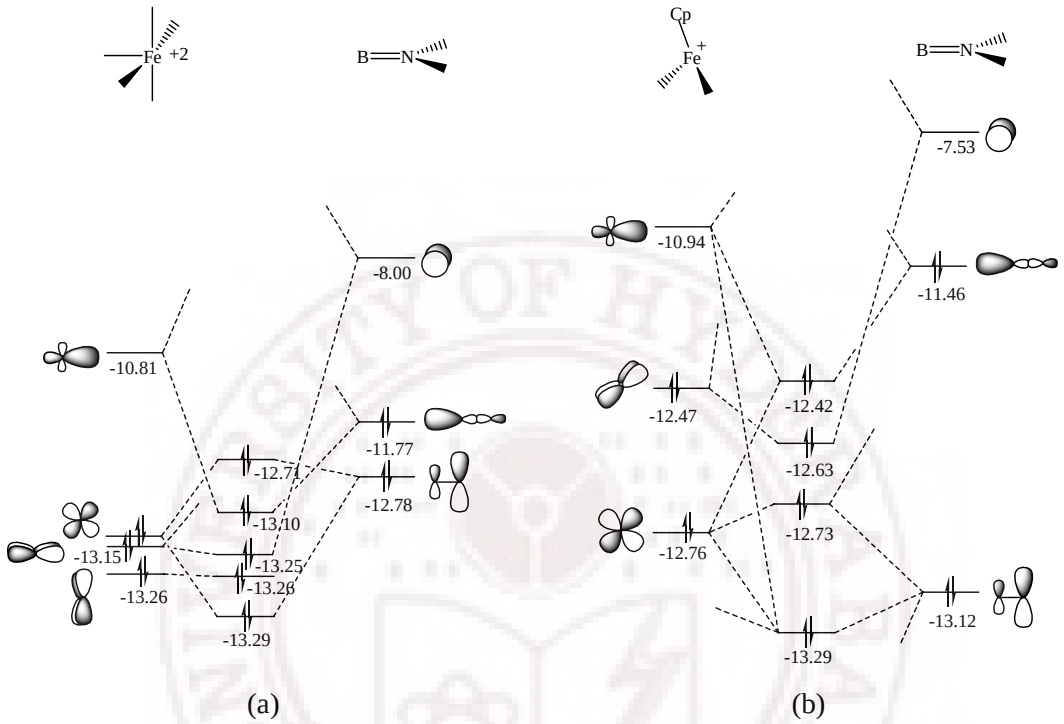


**Scheme 2.3:** Schematic representation of $\sigma$ donation from B to vacant d orbital of Fe and $\pi$ back donation from filled d orbital of Fe to vacant p orbital on B. The figure depicts the interaction diagram of (a) $(CO)_5Fe^{2+}$ and $BN(CH_3)_2$ fragments in $(CO)_5FeBN(CH_3)_2^{2+}$, isoelectronic to $Cp(CO)_2FeBN(CH_3)_2^{+}$ and (b) $Cp(CO)_2Fe^{+}$ and $BN(CH_3)_2$ fragments in $Cp(CO)_2FeBN(CH_3)_2^{+}$ using Extended Hückel (CACAO) program. The energy values are given in eV.

Generally, metal-carbenes involved in olefin metathesis are 16- or 14-electron complexes,[6,22] while the Fe-borylene **8** is an 18-electron complex with greater negative charge on the metal. The highest-occupied molecular orbital (HOMO) of the Fe-borylene complex is a nonbonding metal orbital, whereas the lowest-unoccupied molecular orbital (LUMO) is a $\pi$*-MO localized mainly on the B atom (Scheme 2.4a). This is in contrast to the carbene complexes that undergo olefin metathesis, where the HOMO is generally a $\pi$ MO between the metal and the carbon

and the LUMO is a d orbital on the metal (Scheme 2.4b). Hence, the electrophilic center is the B atom in the Fe-borylene complex and the metal atom in the metal-carbene complexes. As a result, the unsaturated substrates prefer to interact with the B atom in the Fe-borylene complex and with the metal atom in the metal-carbene complexes.

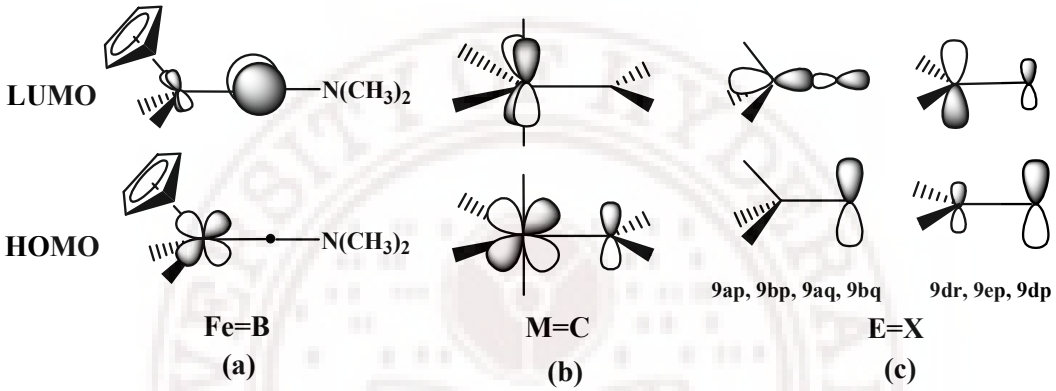


**Scheme 2.4:** Schematic representation of the HOMO and LUMO of (a) Fe-borylene complex, (b) metal-carbene complex and (c) substrates.

### [2.3.2] Metathesis Reaction of the Fe-Borylene Complex $Cp(CO)_2FeBN(CH_3)_2^+$

In order to understand the mechanism for boron metathesis reaction of transition-metal-borylene complexes, the model complex **8** and the substrates $H_3PO$ (**9ap**), $H_3AsO$ (**9bp**), $H_3PS$ (**9aq**), $H_3AsS$ (**9bq**), $CH_3HCCH_2$ (**9cr**), $(NH_2)_2CCH_2$ (**9dr**), $H_2CO$ (**9ep**) and $(NH_2)_2CO$ (**9dp**) were used (Scheme 2.2). The energetics of the boron metathesis reaction, evaluated using reaction 2.1, gives insight into the feasibility of boron metathesis with various substrates.

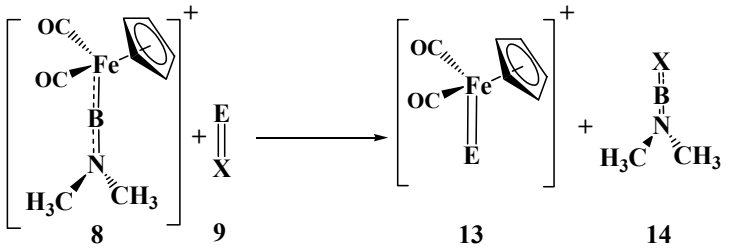


8 9 13 14 **(2.1)**

**Table 2.2**: Energies (ΔE in kcal/mol) from reaction 2.1 and distribution of natural charges on E and X in the substrates **9**.[a]

| **Substrate** | **9ap** | **9bp** | **9aq** | **9bq** | **9cr** | **9dr** | **9ep** | **9dp** |
|---|---|---|---|---|---|---|---|---|
| **ΔE** | -74.4 | -76.0 | -43.8 | -41.4 | +45.5 | -6.2 | -1.7 | -33.2 |
| **Δ*c*** | 2.09 | 2.28 | 0.98 | 1.26 | 0.25 | 1.03 | 0.73 | 1.54 |
| Charge on E | +1.12 | +1.29 | +0.46 | +0.69 | -0.18 | +0.41 | +0.23 | +0.84 |
| Charge on X | -0.97 | -0.98 | -0.52 | -0.57 | -0.43 | -0.62 | -0.51 | -0.70 |

[a]Note that Δ*c* is the difference between the natural charge on E and X.

The reaction energies of the Fe-borylene complex **8** with the substrates $H_3PO$ (**9ap**), $H_3AsO$ (**9bp**), $H_3PS$ (**9aq**) and $H_3AsS$ (**9bq**) are calculated to be exothermic (Table 2.2). The substrates **9ap** and **9bp**, which have the same X substituent (X = O), show almost similar reaction energies. Similarly, the substrates **9aq** and **9bq** (X = S) also have comparable reaction energies. The analysis of charge distribution (Table 2.2) shows that the more polar E-X bonds (**9ap** and **9bp**) give more exothermic reactions as compared with the less polar E-X bonds (**9aq** and **9bq**). Owing to the lower polarity of propene (**9cr**), the reaction is largely endothermic (Table 2.2); therefore, the reaction mechanism for **9cr** was not investigated. The reaction of more polar $H_2CO$ (**9ep**) is calculated to be exothermic by 1.7 kcal/mol. In order to understand the effect of electron-donating substituents, the H and $CH_3$ groups on carbon in **9cr** and **9ep** were substituted by $NH_2$ groups. The reaction of

the resultant diaminoalkene (**9dr**) is exothermic by 6.2 kcal/mol. Similarly, the reaction of **9dp** is more exothermic as compared with **9ep**. It is clear from the energetics that the more polar substrates like $H_3PO$ (**9ap**), $H_3AsO$ (**9bp**), $H_3PS$ (**9aq**) and $H_3AsS$ (**9bq**) are preferred for boron metathesis reaction (Table 2.2). The experimental observation of the boron metathesis reaction for the derivatives of the substrates **9ap**, **9bp** and **9bq** supports this result.

**Table 2.3:** Reactions to estimate the relative stabilities of Fe-E and B-X Bonds in **13** and **14**.

| **Reaction** | **ΔE (kcal/mol)** | |
|---|---|---|
| $H_3PO + (CH_3)_2NBS \rightarrow H_3PS + (CH_3)_2NBO$ | -30.7 | (2.2a) |
| $H_3AsO + (CH_3)_2NBS \rightarrow H_3AsS + (CH_3)_2NBO$ | -34.5 | (2.2b) |
| $(NH_2)_2CO + (CH_3)_2NBCH_2 \rightarrow (NH_2)_2CCH_2 + (CH_3)_2NBO$ | -27.0 | (2.2c) |
| $Cp(CO)_2FeC(NH_2)_2^+ + H_3PO \rightarrow Cp(CO)_2FePH_3^+ + (NH_2)_2CO$ | -41.2 | (2.3a) |
| $Cp(CO)_2FeCH_2^+ + H_3PO \rightarrow Cp(CO)_2FePH_3^+ + H_2CO$ | -72.7 | (2.3b) |
| $Cp(CO)_2FeC(NH_2)_2^+ + H_3AsO \rightarrow Cp(CO)_2FeAsH_3^+ + (NH_2)_2CO$ | -42.8 | (2.3c) |
| $Cp(CO)_2FeCH_2^+ + H_3AsO \rightarrow Cp(CO)_2FeAsH_3^+ + H_2CO$ | -74.3 | (2.3d) |

The energetics of the boron metathesis reaction can be analyzed using the relative stabilities of the Fe-E and B-X bonds of the products **13** and **14** as compared to the Fe-B and E-X bonds of the reactants **8** and **9**. Reactions 2.2 and 2.3 (Table 2.3) are used to explain these relative stabilities. The preference for hard-hard and soft-soft interactions explains the greater stability of the B-O bond compared with the B-S bond (reactions 2.2a and 2.2b). Reaction 2.2c specifies that the formation of the B-C bond (**14r)** is less favorable than that of the B-O bond (**14p**). Hence, the order of stability of the B-X bond in **14** is B-O (**14p**) > B-C (**14r**) > B-S (**14q**). The formation of the Fe-P (**13a**) and Fe-As (**13b**) bonds is 41.2 and 42.8 kcal/mol more

favorable when compared with the Fe-C$(NH_2)_2$ bond formation in **13d** (reactions 2.3a and 2.3c). Similarly, the reactions 2.3b and 2.3d show that the Fe-P (**13a**) and Fe-As (**13b**) bonds are 72.7 and 74.3 kcal/mol more stable than the Fe-$CH_2$ bond **(13e)**. The comparison of reactions 2.3a,b and 2.3c,d indicates that the Fe-C bond in Fe-C$(NH_2)_2$ is more stable than the Fe-C bond in Fe-$CH_2$. The $\pi$-donor $NH_2$ ligands raise the energy of the p orbital on the carbene, making it a better $\sigma$ donor and a poor $\pi$ acceptor to the metal. As a result, the Fischer carbene **13d** (Fe-C$(NH_2)_2$) is more stable in comparison with **13e** (Fe-$CH_2$). Hence, the order of stability of the Fe-E bond is as follows: Fe-As (**13b**) > Fe-P (**13a**) > Fe-C$(NH_2)_2$ (**13d**) > Fe-$CH_2$ (**13e**).

The greater exothermicity of the reaction 2.1 for the substrates $H_3PO$ (**9ap**) and $H_3AsO$ (**9bp**) can be attributed to the formation of the more stable B-O bond in **14p** as well as the Fe-P and Fe-As bonds in **13a** and **13b**. The reactions for the substrates $H_3PS$ (**9aq**) and $H_3AsS$ (**9bq**) are less exothermic than those for the substrates $H_3PO$ (**9ap**) and $H_3AsO$ (**9bp**). This is partially due to the formation of the less stable B-S bond in **14q**. The substrate **9cr** gives the least stable products due to the formation of the less stable B-C (**14r**) and Fe-$CH_2$ (**13e**) bonds. The relative stabilities of the Fe-C$(NH_2)_2$ (**13d**) and Fe-$CH_2$ (**13e**) bonds as well as the B-O (**14p**) and B-C (**14r**) bonds explain the order of energies (Table 2.2) for the reactions of the substrates **9dr**, **9ep** and **9dp**. The reaction energies for the substrates are in the order **9dp** (B-O and Fe-C$(NH_2)_2$) > **9dr** (B-C and Fe-C$(NH_2)_2$) > **9ep** (B-O and Fe-$CH_2$).

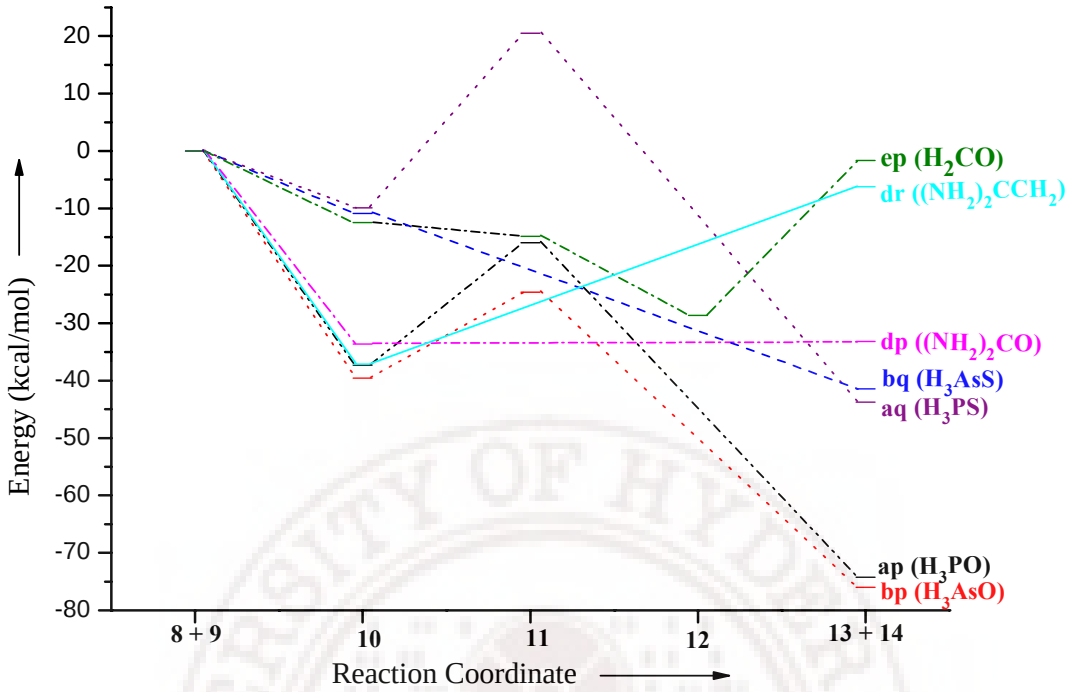


**Figure 2.1:** Reaction energy profile for metathesis reaction of the Fe-borylene complex (**8**) with the substrates (**9**) indicating the relative energies of the intermediates (**10, 11ep** and **12**), the transition states (**11ap**, **11bp** and **11aq**) and the products (**13** and **14**).

Let us now discuss the details of the individual steps involved (Figure 2.1). The first step of the reaction is the formation of acyclic intermediate **10**, where X of EX forms a bond with B (Scheme 2.2). The HOMO of the Fe-borylene complex (**8**) is a d orbital and the LUMO is a $\pi^*$ MO largely localized on B (Scheme 2.4a). The HOMO of the substrates **9ap**, **9bp**, **9aq** and **9bq** is a lone pair on more electronegative X and LUMO is the $\sigma^*$ MO at the E-X bond (Scheme 2.4c). On the other hand, HOMO of **9dr**, **9ep** and **9dp** is a $\pi$ MO, which is mainly localized on X and the LUMO is the $\pi^*$ MO mainly localized on E. Hence, the acyclic intermediate **10** is formed by the donation of electrons from the HOMO of EX to the empty p orbital on the B atom (LUMO). This is in contrast to the formation of the four-membered cyclic intermediate in olefin metathesis by the attack of the $\pi$ MO of

olefin to the LUMO on metal. An acyclic intermediate $Cp(CO)_2FeBN(i\text{-}Pr)_2OPPh_3^+$ (**3**, where A = $Ph_3P$, X = O) was isolated for the reaction of $Ph_3PO$ and Fe-borylene complex **1**.[14] The geometrical parameters of **10ap** are comparable to this experimentally reported structure (Table 2.1). The Fe-B-X-E dihedral angle varies within a range of 0-20° in **10ap** (18.0°), **10bp** (22.4°) and **10aq** (1.2°), but the Fe-B-S-As dihedral angle in **10bq** is 67.8°. The larger value of this dihedral angle arises from the nonbonded interaction between the large $H_3As$ group and the ligands on Fe. The donation of $\pi$ electrons from EX to the empty p orbital on B is also reflected in the elongated E-X, Fe-B and B-N bond distances in intermediate **10** (Table 2.1). The substrates **9dr**, **9dp** and **9ep** also form the acyclic intermediates **10dr**, **10dp** and **10ep**.

The descending order of negative charge on X in **9** is as follows: **9bp** > **9ap** >**9dp** > **9bq** > **9dr** > **9aq** > **9ep** (Table 2.2), while the order of stability of the intermediate **10** is **10bp** > **10ap** > **10dr** > **10dp** > **10ep** > **10bq** > **10aq** (Figure 2.1). The stability of **10dr** and **10ep** is not in accordance with the order of the negative charge on X. The analysis of charge distribution shows that **10ep** should be the least stable intermediate and **10dr** should be less stable than **10dp** and **10bq**. The stability of **10dr** over **10dp** is also not in tune with the greater stability of the B-O bond compared with the B-C bond (reaction 2.2c). The pyramidal N atom in **9dr** becomes planar in the intermediate **10dr** and results in the delocalization of electrons in the $BCH_2C(NH_2)_2$ moiety, which causes the additional stabilization. The extent of stabilization gained by **10ep** compared with **10bq** and **10aq** is attributed to the formation of the more stable B-O bond in **10ep** rather than the weak B-S bond in

**10bq** and **10aq**. Thus, in general, the intermediate **10** is more stable when X of EX has more negative charge. After the donation of $\pi$ electrons from EX to the empty p orbital on the B atom, a decrease in the positive charge on the B atom and in the negative charge on X in the intermediate **10** is observed (Table 2.3).

**Table 2.3**: Natural charges on Fe, B, N, E (E = $H_3P$, $H_3As$, $H_2C$, $(NH_2)_2C$) and X (X = O, S, $CH_2$) in intermediate **10**.

| Molecule | Charge on | | | | |
|---|---|---|---|---|---|
| | **Fe** | **B** | **N** | **E** | **X** |
| **10ap** | -0.31 | +0.96 | -0.81 | +1.15 | -1.00 |
| **10bp** | -0.33 | +0.96 | -0.81 | +1.36 | -1.03 |
| **10aq** | -0.32 | +0.65 | -0.85 | +0.52 | -0.24 |
| **10bq** | -0.33 | +0.67 | -0.84 | +0.74 | -0.32 |
| **10dr** | -0.31 | +0.82 | -0.84 | +0.62 | -0.88 |
| **10dp** | -0.31 | +0.93 | -0.83 | +0.88 | -0.74 |
| **10ep** | -0.30 | +0.93 | -0.81 | +0.31 | -0.59 |

The transition states **11ap**, **11bp** and **11aq** are 21.3, 15.0 and 30.4 kcal/mol higher in energy than the respective intermediates **10**. Here the major interaction is between the filled metal d orbital (HOMO) and the $\sigma^*$ MO (LUMO), which is more localized on positively charged E (Scheme 2.4c). Therefore, the greater the positive charge on E in **10**, the lower the barrier for the formation of the products (Figure 2.1). The natural charges on E in **10ap**, **10bp** and **10aq** are +1.15, +1.36 and +0.52, respectively (Table 2.3). The descending order of charges on E in **10**, **10bp** > **10ap** > **10aq**, agrees with the ascending order of the energy barrier, **11bp** < **11ap** < **11aq**. It is possible that the nonbonded interaction between $H_3As$ and the ligands on Fe,

which results in the dihedral angle of 67.8° in **10bq**, prevents the approach of $H_3As$ toward the metal center. A transition state for this step could not be located. The cyclic intermediate **11ep** is similar to the intermediates in olefin metathesis and is formed by the donation of electrons from the d orbital of Fe (HOMO) to the empty $\pi^*$ orbital (LUMO) at the O-C bond (Scheme 2.4a and c). The C-O $\sigma$ bond in **11ep** is not considerably affected in comparison to **11ap**, **11bp** and **11aq** and thus the four-membered cyclic intermediate can be stabilized. The structures **11dp** and **11dr** could not be located on the potential energy surface, probably due to the destabilizing non-bonded interaction between the ligands of the Fe-borylene complex and the substrates.

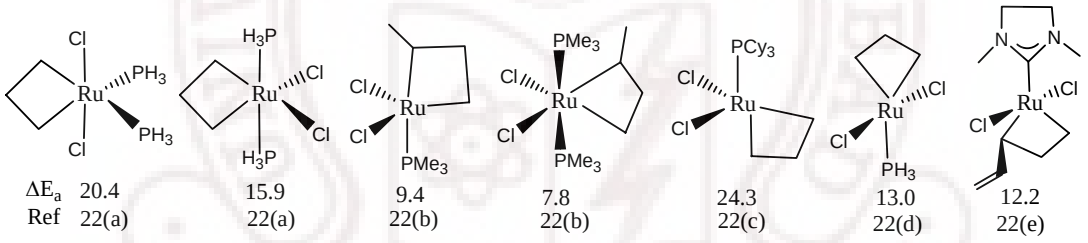


**Figure 2.2:** Four-membered transition states of different olefin metathesis reactions from the literature. The energy barriers ($\Delta E_a$ in kcal/mol) for the formation of the transition states and reference numbers are given below each structure.

The transition states **11ap**, **11bp** and **11aq** lead to the products **13** and **14** by breaking the Fe-B and E-X bonds. The energetics of the boron metathesis is greatly influenced by the bond energy of the Fe-E and B-X bonds in the products. The cyclic intermediate **11ep** goes to the products **13e** and **14p** via another acyclic intermediate **12ep**. The intermediates similar to **12ep** are not stationary points on the potential energy surfaces for the other substrates. The calculated energy barriers for the boron metathesis reaction are within the range of 15-30 kcal/mol. Figure 2.2

shows various four-membered transition states of the olefin metathesis reaction available in the literature.[22] The energy barriers for the formation of the transition states in the metathesis reaction of the Fe-borylene complex are in the range of those obtained for the olefin metathesis.

### [2.3.3] $\beta$-Hydride Transfer versus Boron Metathesis

The reaction of $Ph_2CO$ and $[Cp(CO)_2FeBN(i\text{-}Pr)_2]^+(BAr^f_4)^-$ (**1**) does not follow the metathesis pathway; the ligand transformation process, similar to the Meerwein-Ponndorf $\beta$-hydride transfer from an isopropyl substituent of the aminoborylene ligand to the coordinated ketone, takes place instead (Scheme 2.1b). In order to understand the energetics involved for this $\beta$-hydride transfer in comparison to the boron metathesis reaction, the possible $\beta$-hydride-transfer products for all the substrates were calculated. The intermediate **10** can give either metathesis products (**13** and **14**) or hydride-transfer product (**16**) (Scheme 2.2). The metathesis products are formed by the donation of metal d electrons to the LUMO of the EX and the hydride-transfer product is formed by the interaction of $\beta$-hydrogen with the LUMO of EX. Therefore, the preference of $\beta$-hydride transfer over metathesis depends upon the relative energies of these two interactions.

Figure 2.3 shows the correlation diagram connecting the HOMO, $\sigma^*$ and $\pi^*$ MO levels of the substrates as well as the HOMO and LUMO of the Fe-borylene complex **8**. It is clear from the diagram that the substrates **9ap**, **9bp**, **9aq** and **9bq** have a low-lying $\sigma^*$ MO and the substrates **9dr**, **9ep** and **9dp** have a low-lying $\pi^*$

MO. This difference in energy levels is due to the weaker $\sigma$ bond in **9ap**, **9bp**, **9aq** and **9bq** compared with that in **9dr**, **9ep** and **9dp**. The interaction of the hydride from the $CH_3$ group in $N(CH_3)_2$ with the low-lying $\sigma^*$ MO of **9ap**, **9bp**, **9aq** and **9bq** leads to the rupture of the E-X bond. As a result, $\beta$-hydride-transfer products could not be observed for these substrates.

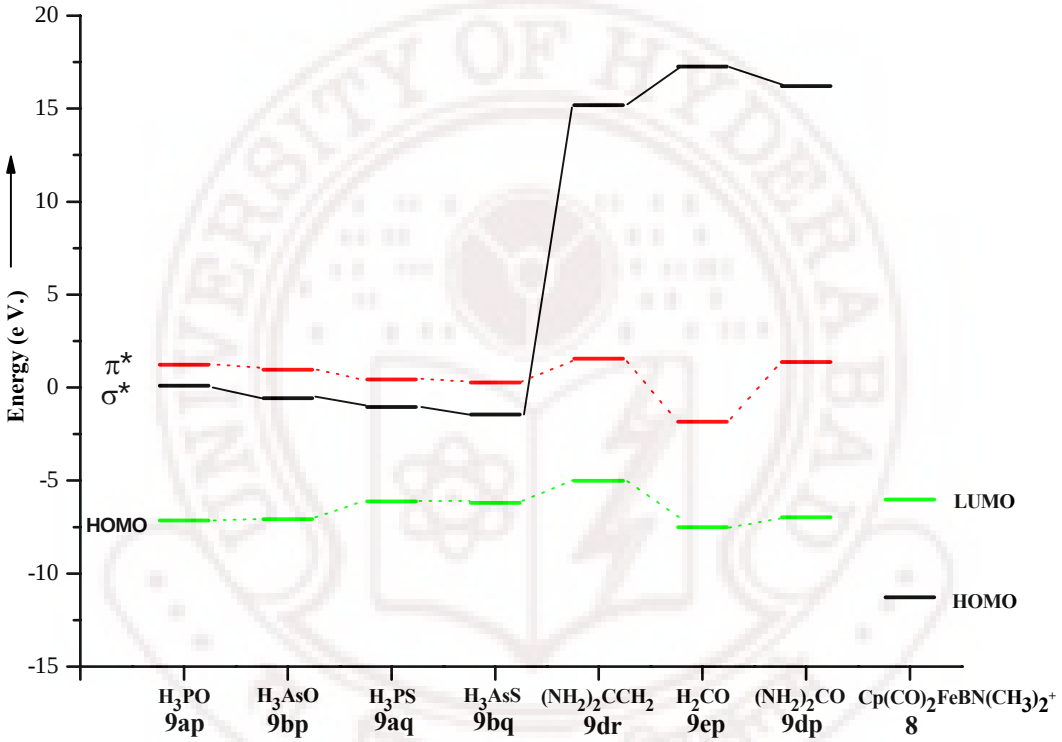


**Figure 2.3:** Correlation diagram between the HOMO, $\sigma^*$ and $\pi^*$ MO levels of the substrates **9**. The HOMO and LUMO levels of **8** are also shown.

On the other hand, in the boron metathesis reaction, the metal d electrons (HOMO) are donated to the $\sigma^*$ MO of the E-X bond, resulting in four membered cyclic transition states (**11**). This transition state then undergoes Fe-B and E-X bond breaking and leads to the metathesis products **13** and **14** (Scheme 2.2). The $\beta$-hydride transfer is the competitive reaction to boron metathesis for the substrates with a low-lying $\pi^*$ MO (**9dr**, **9ep** and **9dp**) (Figure 2.3). The substrates that have a

low-lying $\sigma^*$ MO (**9ap**, **9bp**, **9aq** and **9bq**) prefer boron metathesis to $\beta$-hydride transfer. Hence, substrates with a polar bond and a weak $\sigma$ bond would be ideal for boron metathesis.

On the contrary, the hydride donates its electrons to the low-lying $\pi^*$ MO of **9dr**, **9ep** and **9dp** and leads to the $\beta$-hydride-transfer products **16dr**, **16dp** and **16ep** through a six-membered cyclic transition state (**15**) (Scheme 2.2). The donation of metal d electrons to the $\pi^*$ MO can form a four-membered cyclic intermediate as the E-X $\sigma$ bond remains unbroken. However, the formation of the cyclic intermediate **11ep** is only observed for the small substrate **9ep** ($H_2CO$). The larger size of $(NH_2)_2C$ in **9dr** and **9dp** prevents their approach toward the metal center and hence, intermediates **11dr** and **11dp** could not be located on the potential energy surface. This indicates that the substrates having a low-energy $\sigma^*$ MO prefer the metathesis reaction over the $\beta$-hydride transfer. Both $\beta$-hydride transfer and metathesis reactions may take place when the substrates have a low-lying $\pi^*$ MO. These reactions are also influenced by the steric nature of the substrate as well as the ligands on the metal-borylene complexes.

The relative energetics for the $\beta$-hydride transfer in comparison to the metathesis reaction, acquired by taking the intermediate **10** as the reference, is shown in figure 2.4. The energy barriers for the formation of the transition states **15dr**, **15ep** and **15dp** are 52.6, 15.6 and 51.1 kcal/mol, respectively.

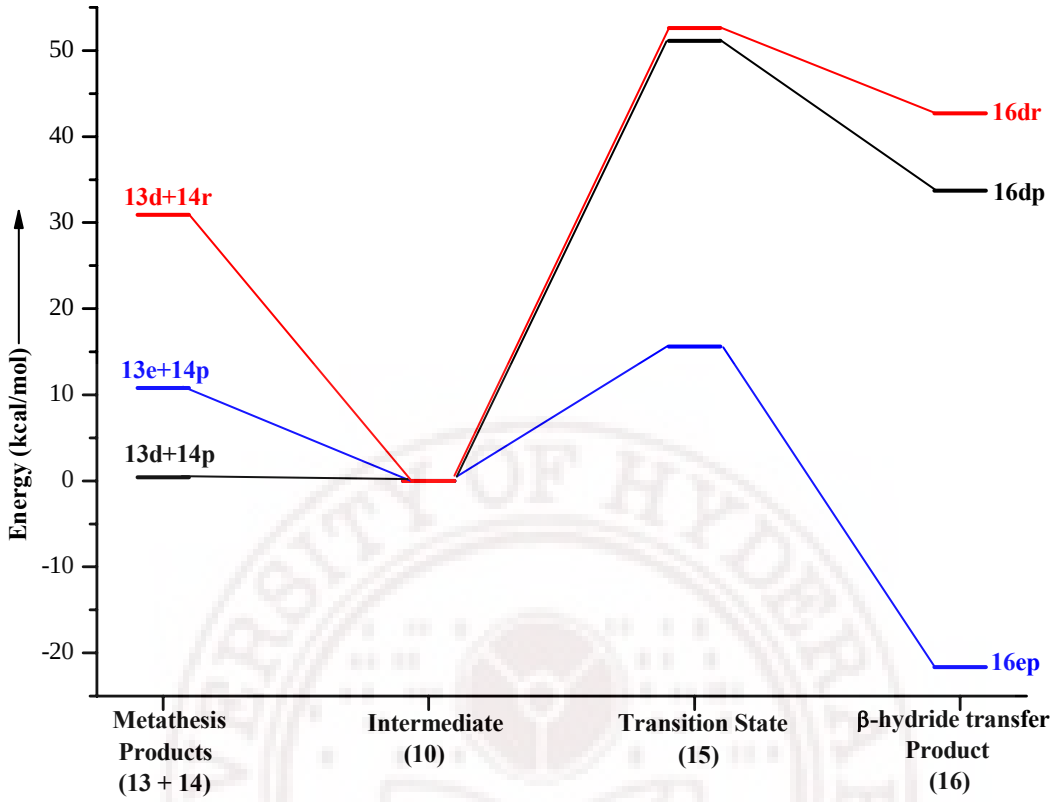


**Figure 2.4:** Relative energies of the metathesis products (**13** and **14**), the transition states (**15**) and hydride-transfer products (**16**) for the substrates **9dr**, **9ep** and **9dp** with respect to intermediate **10**.

The order of stability of the hydride-transfer products is **16ep** > **16dp** > **16dr**. The structure **16ep** is more stable than that of **10ep**, whereas both **16dp** and **16dr** are less stable than the corresponding intermediates **10**. It is also more stable than the metathesis products **13e** and **14p** (Figure 2.4). On the other hand, the hydride-transfer products **16dp** and **16dr** are less stable than the corresponding metathesis products. The $NH_2$ group in **10dp** and **10dr** is planar and stabilized by conjugation whereas that in the transition states (**15dr** and **15dp**) as well as in the hydride-transfer products (**16dp** and **16dr)** is pyramidal. This results in the high barrier for the transition states **15dp** and **15dr** and the formation of corresponding hydride-transfer products becomes unfavorable. The greater stability of **16ep**

compared with **10ep** is also attributed to the delocalization present in the $CH_2NBO$ fragment. The nature of the $\beta$-hydride-transfer products is almost similar to the corresponding intermediates (**10**). Thus, the relative stabilities between the metathesis products and the $\beta$-hydride-transfer product in comparison to the intermediate **10** depend on the stability of the Fe-E bond formed in the metathesis product **13**. Since the Fe-C bond in Fe-$C(NH_2)_2$ is more stable than the Fe-C bond in Fe-$CH_2$, the metathesis product formation of the substrates **9dp** and **9dr** is more favorable than that of the corresponding $\beta$-hydride-transfer products. Since the Fe-$CH_2$ bond in **13e** is less stable, the metathesis product formation for **9ep** is less favorable compared with the formation of $\beta$-hydride-transfer product **16ep**. This supports the experimental observation for the formation of the $\beta$-hydride-transfer product for the reaction of $Ph_2CO$ with **1**.

The substituents without a $\beta$-hydrogen atom on boron can be used to direct the reactivity of borylene complexes toward metathesis. In summary, $\beta$-hydride transfer from the ligand on boron may be a competitive reaction to boron metathesis. The substrates having a low-energy $\sigma^*$ MO prefer boron metathesis to hydride transfer.

## [2.4] Conclusions

The metathesis reaction of the Fe-borylene complex takes place with the initial attack of the electronegative end (X) of the substrate EX on the B atom, leading to an acyclic intermediate **10**. The positively charged E of this acyclic

intermediate accepts electrons from the metal d orbital and forms a four-membered intermediate or transition state, which depends on the $\sigma^*$ and $\pi^*$ levels of the substrate EX. The boron metathesis is more favorable for those substrates that have a low-lying $\sigma^*$ MO (weak $\sigma$ bond). The $\beta$-hydride transfer is a competitive reaction to boron metathesis for the substrates having a low-energy $\pi^*$ MO. The relative stability of the products is controlled by the strength of both Fe-E and B-X bonds. The energetics of the boron metathesis reaction is comparable to that of the olefin metathesis. The metathesis reactions of the Fe-borylene complex **8** with all the substrates (Scheme 2.2) indicate the role of polarity in tuning the reaction in a preferred direction.

Similar transition-metal-borylene complexes with other metals are good candidates for boron metathesis reactions using polar substrates. Experimentally aryl-borylene and boryl complexes are also known to undergo different types of reactions with substrates containing double bonds, e.g., C=C and C=O. These complexes are not yet explored for the metathesis, but the present study points to a rich chemistry awaiting for the reactions of arylborylene and boryl complexes toward metathesis.

## [2.5] References


1. (a) Earnshaw, A.; Greenwood, N. N. *Chemistry of the Elements*, Pergamon: First Edition Oxford, 1984. (b) Jemmis, E. D.; Jayasree, E. G. *Acc. Chem. Res*. **2003**, *36*, 816. (c) Prasad, D. L. V. K.; Balakrishnarajan, M. M.; Jemmis, E. D. *Phys. Rev. B.* **2005**, *72*, 195102. (d) Jemmis, E. D.; Balakrishnarajan, M. M.; Pancharatna, P. D. *Chem. Rev.* **2002,** *102*, 93. (e) Jemmis, E. D.; Jayasree, E. G.; Parameswaran, P. *Chem. Soc. Rev.* **2006**, *35*, 157. (f) Pathak, B.; Pandian, S.; Hosmane, N.; Jemmis, E. D. *J. Am. Chem. Soc.* **2006,** *128*, 10915. (g) Fehlner, T. P. In *Electron Deficient Boron and Carbon Clusters* Ed: Olah, G. A.; Wade, K.; Williams, R. E. Wiley, New York, 1991, pp. 287.
2. Brown, H. C. *Hydroboration*, (Ed: W. A.; Benjamin), New York, 1962.
3. (a) Casey, C. P.; Fagan, P. J. *J. Am. Chem. Soc.* **1982,** *104,* 4950. (b) Jemmis, E. D.; Prasad, B. V. *Organometallics* **1992,** *11*, 2528.
4. (a) Grubbs, R. H. *Handbook of Metathesis*; Ed: Wiley-VCH: Weinheim, Germany, 2003. (b) Mecking, S.; Held, A.; Bauers, F. M. *Angew. Chem., Int. Ed.* **2002**, *41*, 544. (c) Connon, S. J.; Blechert, S. *Angew. Chem., Int. Ed.* **2003**, *42*, 1900. (d) Trnka, T. M.; Grubbs, R. H. *Acc. Chem. Res.* **2001**, *34*, 18. (e) Pietraszuk, C.; Fischer, H.; Rogalski, S.; Marciniec, B. *J. Organomet. Chem.* **2005**, *690*, 5912.
5. Terry, M. R.; Mercando, L. A.; Kelley, C.; Geoffroy, G. L.; Nombel, P.; Lugan, N.; Mathieu, R.; Ostrander, R. L.; Owens-Waltermire, B. E.; Rheingold, A. L. *Organometallics* **1994**, *13*, 843.

6. (a) Chauvin, Y. *Angew. Chem. Int. Ed*. **2006**, *45*, 3741. (b) Grubbs, R. H. *Angew. Chem. Int. Ed*. **2006**, *45*, 3760. (c) Schrock, R. R. *Angew. Chem. Int. Ed*. **2006**, *45*, 3748.
7. (a) Teng, W.; Englich, U.; Ruhlandt-Senge, K. *Angew. Chem. Int. Ed*. **2003**, *42*, 3661. (b) Miller, R. L.; Maifeld, S. V.; Lee, D. *Org. Lett.* **2004**, *6*, 2773.
8. Arisawa, M.; Fujimoto, K.; Morinaka, S.; Yamaguchi, M. *J. Am. Chem. Soc.* **2005,** *127*, 12226.
9. Downs, A. J.; Greene, T. M.; Johnsen, E.; Brain, P. T.; Morrison, C. A.; Parsons, S.; Pulham, C. R.; Rankin, D. W. H.; Aarset, K.; Mills, I. M.; Page, E. M.; Rice, D. A. *Inorg. Chem.* **2001**, *40*, 3484.
10. (a) Hazari, N.; Mountford, P. *Acc. Chem. Res.* **2005**, *38*, 839. (b) McCowan, C. S.; Caudle, M. T. *Dalton Trans.* **2005**, 238. (c) Bailey, B. C.; Fout, A. R.; Fan, H.; Tomaszewski, J.; Huffman, J. C.; Gary, J. B.; Johnson, M. J. A.; Mindiola, D. J. *J. Am. Chem. Soc.* **2007**, *129*, 2234.
11. Paetzold, P.; Englert, U.; Finger, R.; Schmitz, T.; Tapper, A.; Ziembinski, R. *Z. Anorg. Allg. Chem*. **2004**, *630*, 508.
12. (a) Braunschweig, H.; Herbst, T.; Rais, D.; Seeler, F. *Angew. Chem. Int. Ed*. **2005**, *44*, 7461. (b) Braunschweig, H.; Kollann, C.; Englert, U. *Angew. Chem. Int. Ed*. **1998**, *37*, 3179. (c) Braunschweig, H.; Colling, M.; Kollann, C.; Stammler, H. G.; Neumann, B. *Angew. Chem. Int. Ed*. **2001**, *40*, 2298. (d) Braunschweig, H.; Colling, M.; Hu, C.; Radacki, K. *Angew. Chem. Int. Ed*. **2003**, *42*, 205. (e) Braunschweig, H.; Forster, M.; Radacki, K. *Angew. Chem. Int. Ed*. **2006**, *45*, 2132. (f) Wrackmeyer, B. *Angew. Chem. Int. Ed*. **1999**, *38*, 771. (g) Cowley, A. H.; Lomelı, V.; Voigt, A. *J.*

*Am. Chem. Soc.* **1998,** *120,* 6401. (h) Coombs, D. L.; Aldridge, S.; Coles, S. J.; Hursthouse, M. B. *Organometallics* **2003,** *22,* 4213. (i) Coombs, D. L.; Aldridge, S.; Rossin, A.; Jones, C.; Willock, D. J. *Organometallics* **2004,** *23,* 2911. (j) Irvine, G. J.; Rickard, C. E. F.; Roper, W. R.; Williamson, A.; Wright, L. J. *Angew. Chem. Int. Ed*. **2000**, *39,* 948. (k) Braunschweig, H.; Rais, D.; Uttinger, K. *Angew. Chem. Int. Ed*. **2005**, *44,* 3763. (l) Braunschweig, H.; Kollann, C.; Rais, D. *Angew. Chem. Int. Ed.* **2006**, *45*, 5254.

13. Coombs, D. L.; Aldridge, S.; Rossin, A.; Jones, C.; Willock, D. J. *Organometallics* **2004,** *23,* 2911.
14. (a) Kays, D. L.; Day, J. K.; Ooi, L.-L.; Aldridge, S. *Angew. Chem. Int. Ed*. **2005**, *44,* 7457. (b) Kays, D. L.; Rossin, A.; Day, J. K.; Ooi, L. L.; Aldridge, S. *Dalton Trans.* **2006**, 399.
15. Kays, D. L.; Day, J. K.; Aldridge, S.; Harrington, R. W.; Clegg, W. *Angew. Chem. Int. Ed*. **2006**, *45*, 3513.
16. Hehre, W. J.; Radom, L.; Schleyer, P. v. R.; Pople, J. A. *Ab Initio Molecular Orbital Theory*; Wiley: New York, **1986**.
17. (a) Becke, A. D. *J. Chem. Phys.* **1993**, *98,* 5648. (b) Becke, A. D. *Phys. Rev. A* **1988**, *38,* 3098. (c) Lee, C.; Yang, W.; Parr, R. G. *Phys. Rev. B* **1988**, *37*, 785.
18. (a) Hay, P. J.; Wadt, W. R. *J. Chem. Phys.* **1985**, *82,* 270. (b) Wadt, W. R.; Hay, P. J. *J. Chem. Phys.* **1985**, *82,* 284. (c) Hay, P. J.; Wadt, W. R. *J. Chem. Phys.* **1985**, *82,* 299.

19. Gaussian 03, Revision C.02, Frisch, M. J.; Trucks, G. W.; Schlegel, H. B.; Scuseria, G. E.; Robb, M. A.; Cheeseman, J. R.; Montgomery, Jr., J. A.; Vreven, T.; Kudin, K. N.; Burant, J. C.; Millam, J. M.; Iyengar, S. S.; Tomasi, J.; Barone, V.; Mennucci, B.; Cossi, M.; Scalmani, G.; Rega, N.; Petersson, G. A.; Nakatsuji, H.; Hada, M.; Ehara, M.; Toyota, K.; Fukuda, R.; Hasegawa, J.; Ishida, M.; Nakajima, T.; Honda, Y.; Kitao, O.; Nakai, H.; Klene, M.; Li, X.; Knox, J. E.; Hratchian, H. P.; Cross, J. B.; Bakken, V.; Adamo, C.; Jaramillo, J.; Gomperts, R.; Stratmann, R. E.; Yazyev, O.; Austin, A. J.; Cammi, R.; Pomelli, C.; Ochterski, J. W.; Ayala, P. Y.; Morokuma, K.; Voth, G. A.; Salvador, P.; Dannenberg, J. J.; Zakrzewski, V. G.; Dapprich, S.; Daniels, A. D.; Strain, M. C.; Farkas, O.; Malick, D. K.; Rabuck, A. D.; Raghavachari, K.; Foresman, J. B.; Ortiz, J. V.; Cui, Q.; Baboul, A. G.; Clifford, S.; Cioslowski, J.; Stefanov, B. B.; Liu, G.; Liashenko, A.; Piskorz, P.; Komaromi, I.; Martin, R. L.; Fox, D. J.; Keith, T.; Laham, M. A.; Peng, C. Y.; Nanayakkara, A.; Challacombe, M.; Gill, P. M. W.; Johnson, B.; Chen, W.; Wong, M. W.; Gonzalez, C.; and Pople, J. A. Gaussian, Inc., Wallingford CT, 2004.

20. (a) Reed, A. E.; Curtiss, L. A.; Weinhold, F. *Chem. Rev.* **1988**, *88*, 899. (b) Weinhold, F.; Carpenter, J. E. In *The Structure of Small Molecules and Ions; Plenum Press: New York* **1988**, *227*.

21. (a) Boehme, C.; Uddin, J.; Frenking, G. *Coord. Chem. Rev.* **2000**, *197*, 249. (b) Frenking, G.; Fröhlich, N. *Chem. Rev.* **2000,** *100*, 717. (c) Ehlers, A. W.; Baerends, E. J.; Bickelhaupt, F. M.; Radius, U. *Chem. Eur. J.* **1998**, *4*, 210. (d) Radius, U.; Bickelhaupt, F. M.; Ehlers, A. W.; Goldberg, N.; Hoffmann,

R. *Inorg. Chem.* **1998,** *37,* 1080. (e) Coombs, D. L.; Aldridge, S.; Jones, C.; Willock, D. J. *J. Am. Chem. Soc.* **2003**, *125*, 6356. (f) Aldridge, S.; Rossin, A.; Coombs, D. L.; Willock, D. J. *Dalton Trans.* **2004**, 2649. (g) Musaev, D. G.; Morokuma, K. *J. Phys. Chem.* **1996,** *100,* 6509. (h) Dickinson, A. A.; Willock, D. J.; Calder, R. J.; Aldridge, S. *Organometallics* **2002,** *21,* 1146.

22. (a) Bernardi, F.; Bottoni, A.; Miscione, G. P. *Organometallics* **2003**, *22*, 940. (b) Fomine, S.; Vargas, S. M.; Tlenkopatchev, M. A. *Organometallics* **2003**, *22*, 93. (c) Janse van Rensburg, W.; Steynberg, P. J.; Meyer, W. H.; Kirk, M. M.; Forman, G. S. *J. Am. Chem. Soc.* **2004,** *126,* 14332. (d) Suresh, C. H.; Koga, N. *Organometallics* **2004**, *23*, 76. (e) Lippstreu, J. J.; Straub, B. F. *J. Am. Chem. Soc.* **2005**, *127*, 7444. (f) Burdett, K. A.; Harris, L. D.; Margl, P.; Maughon, B. R.; Mokhtar-Zadeh, T.; Saucier, P. C.; Wasserman, E. P. *Organometallics* **2004,** *23,* 2027.

# CHAPTER 3

# REACTIVITY OF CATIONIC TERMINAL Fe-BORYLENE COMPLEX TOWARD CARBODIIMIDE AND ISOCYANATE: INSERTION VERSUS METATHESIS REACTIONS

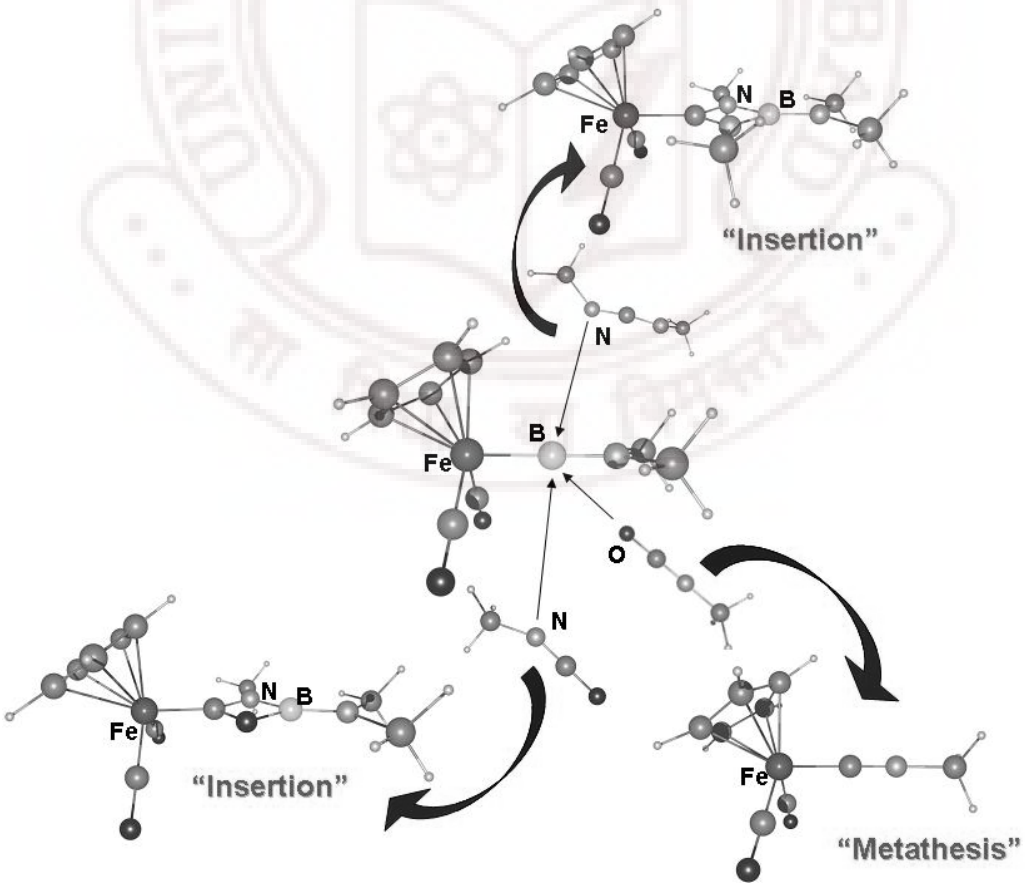

# Abstract

The reactions of terminal borylene complexes of the type $[CpFe(CO)_2(BNR_2)]^+$ (R = *i*-Pr, Cy) with heteroallenes have been investigated. Reaction with dicyclohexylcarbodiimide (CyNCNCy) gives a bis-insertion product, in which one equiv of carbodiimide is assimilated into each of the Fe=B and B=N double bonds to form a spirocyclic boronium system. In contrast, isocyanates (R′NCO, R′ = Ph, 2,6-Xyl, Cy; Xyl = $C_6H_3Me_2$) react to give isonitrile complexes of the type $[CpFe(CO)_2(CNR')]^+$, via a net oxygen abstraction (or formal metathesis) process. Both carbodiimide and isocyanate substrates are shown to prefer initial attack at the Fe=B bond rather than the B=N bond of the borylene complex. Further mechanistic studies revealed that the carbodiimide reaction ultimately leads to the bis-insertion compounds $[CpFe(CO)_2C(NCy)_2B(NCy)_2CNR_2]^+$, rather than to the isonitrile system $[CpFe(CO)_2(CNCy)]^+$, on the basis of both thermodynamic (product stability) and kinetic considerations (barrier heights). The mechanism of the initial carbodiimide insertion process is unusual in that it involves coordination of the substrate at the (borylene) ligand followed by migration of the metal fragment, rather than a more conventional process: i.e., coordination of the unsaturated substrate at the metal followed by ligand migration. In the case of isocyanate substrates, metathesis products are competitive with those from the insertion pathway. Direct, single-step metathesis reactivity to give products containing a coordinated isonitrile ligand (i.e. $[CpFe(CO)_2(CNR')]^+$) is facile if initial coordination of the isocyanate at boron occurs

via the oxygen donor (which is kinetically favored); insertion chemistry is feasible when the isocyanate attacks initially via the nitrogen atom. However, even in the latter case, further reaction of the mono-insertion product so formed with excess isocyanate offers a number of facile (low energetic barrier) routes which also generate $[CpFe(CO)_2(CNR')]^+$, rather than the bis-insertion product $[CpFe(CO)_2C(NR')(O)B(NR')(O)CNR_2]^+$ (i.e., the direct analogue of the observed products in the carbodiimide reaction).

## [3.1] Introduction

Transition metal borylene complexes have received significant recent attention, from structure, bonding and reactivity perspective, due, in part, to similarities with classical organometallic ligand systems such as Fischer carbenes and vinylidenes.[1-3] A range of fundamental reaction types have been demonstrated, including metathesis, insertion and hydride transfer chemistries.[3] For example, it has been reported that the cationic aminoborylene complex $[CpFe(CO)_2BN(i\text{-}Pr)_2]^+$ (**1a**) undergoes metathesis reactions with $Ph_3PO$, $Ph_3PS$ and $Ph_3AsO$ (Scheme 3.1a),[3g] but, by contrast, undergoes a Meerwein-Ponndorf type hydride transfer reaction with $Ph_2CO$ (Scheme 3.1b).[3i] Theoretical studies in chapter 1 suggest that the metathesis reaction is favorable for substrates having a low-lying σ* orbital, and hydride transfer is a competitive reaction for substrates having a low-lying π* orbital.[4]

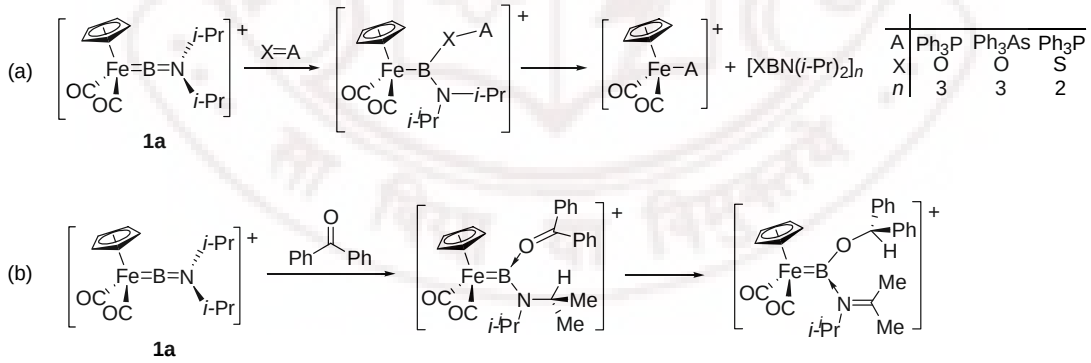


**Scheme 3.1**: Experimentally observed reactivity of $[CpFe(CO)_2BN(i\text{-}Pr)_2]^+$ (**1a**): (a) metathesis reactions with AX (A = $Ph_3P$, $Ph_3As$; X = O, S); and (b) hydride transfer with $Ph_2CO$.

Interestingly, the reaction of the same borylene complex **1a**, or its dicyclohexylamino counterpart $[CpFe(CO)_2(BNCy_2)]^+$ (**1b**) with dicyclohexylcarbodiimide (CyNCNCy) gives an insertion product, in which two

equivalents of carbodiimide are assimilated, one into each of the Fe=B and B=N double bonds to form the spirocyclic complexes **4a,b** (Scheme 3.2a).[3e] Preliminary theoretical results show that the insertion of the first carbodiimide molecule into the Fe=B bond is preferred over the B=N bond.[5]

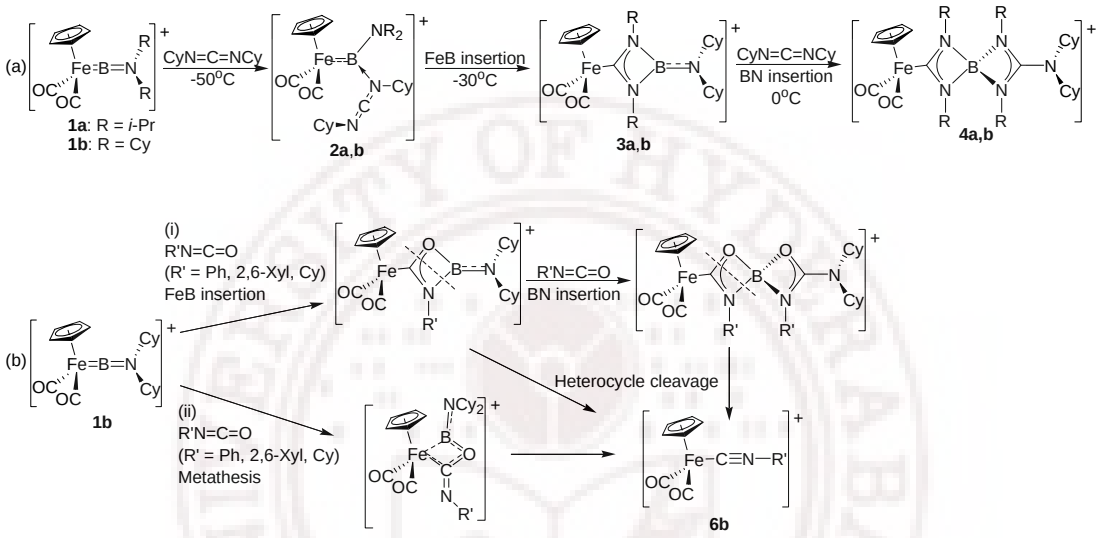


**Scheme 3.2**: Potential mechanisms for the reactions of aminoborylene complexes **1a** and **1b** with heteroallenes: (a) insertion of CyNCNCy; and (b) oxygen atom abstraction from isocyanates, R'NCO (R' = Ph, 2,6-Xyl, Cy).

In contrast to the chemistry found with CyNCNCy, the reaction of isocyanates (R'NCO; R' = Ph, 2,6-Xyl, Cy) with **1b** gives an entirely different type of product i.e. $[CpFe(CO)_2(CNR')]^+$ (**6b**) via a net oxygen abstraction process from the heteroallene precursor.[3r] In theory, such isonitrile complexes could be the result of a number of different mechanistic pathways (Scheme 3.2b), including (i) cleavage of the 4-membered heterocyclic rings of intermediate(s) formed by insertion chemistry analogous to that seen for carbodiimides and (ii) a via a single metathesis step. It is interesting to note that in situ monitoring of the reaction of **1b** with PhNCO by electrospray mass spectrometry (ESI-MS) reveals peaks consistent with

an intermediate - for which the measured value of m/z, the isotope profile and the exact mass determination are consistent with a compound equivalent to **1b** plus two molecules of PhNCO – and which subsequently converts to $[CpFe(CO)_2(CNPh)]^+$ (i.e. **6b**).[3r]

To rationalize the difference in the reactivity of **1a,b** towards carbodiimide and isocyanates substrates we have studied the mechanisms for both reactions using quantum chemical methods. Moreover, given the results of VT-NMR experiments,[3r] which imply a highly unusual mechanism for the insertion chemistry of CyNCNCy with **1a,b** (i.e. coordination of the substrate at the (borylene) ligand followed by migration of the metal fragment rather than the more conventional coordination at the metal followed by ligand migration) we were interested in mapping this reaction profile computationally. Of particular interest was an in-depth rationale for the observed preference for the insertion of the carbodiimide into the Fe=B bond (c.f. the B=N bond). These studies were additionally designed to shed light on the differing reactivity of cationic terminal borylene complexes towards delocalized heteroallene substrates, as compared to molecules containing simple isolated C=O (hydride transfer),[3i] or C=N bonds (simple coordination at boron).[3i] Finally, since the isonitrile complex products resulting from the reaction of isocyanates with **1a,b** can conceivably be obtained either from initial insertion or metathesis steps, a comprehensive mechanistic study was also thought to be of use in understanding which of these (precedented) reaction pathways is the more likely to operate for this particular substrate class.

## [3.2] Computational Details

All structures were optimized using the hybrid HF-DFT method, B3LYP/LANL2DZ, based on Becke's three-parameter functional including Hartree-Fock exchange contributions with a non-local correction for the exchange potential proposed by Becke,[6,7a,b] together with the non-local correction for the correlation energy suggested by Lee et al.[6,7c] The LANL2DZ basis set uses the effective core potential (ECP) of Hay and Wadt.[6,8a-c] The nature of the stationary points were characterized by vibrational frequency calculations. The Gaussian 03 program package was used in this study;[9] reaction energies are given in terms of the free energy change (ΔG, in kcal/mol), while orbital energies are given in Hartrees.

In order to verify the validity of the structural simplifications employed (e.g., Me versus Cy, *i*-Pr, Ph, etc.) and of level of theory, viz. B3LYP/LANL2DZ, we have performed energy calculations on the optimized geometries (at the B3LYP/LANL2DZ level) of the isomeric intermediates **2d**,**e** (with various substituents at both R and R′) using both B3LYP and BP86 methods and the def2-TZVPP basis set.[7b,d,e,8d] The trends in the energy difference between **2d**,**e** (with various substituents) are very similar at the higher levels of theory. The average error and the mean absolute deviation of the relative energies of the isomers **2d**,**e** at the B3LYP/LANL2DZ level as compared to B3LYP/def2-TZVPP are -5.2 and 5.2 kcal/mol, respectively. Similar values for the BP86/def2-TZVPP level are 0.5 and 2.0 kcal/mol, respectively. Thus, the relative energies at the B3LYP/LANL2DZ level are overestimated by an average of 5.2 kcal/mol as compared to the B3LYP/def2-TZVPP level. This systematic deviation in the energies of model

complexes between the B3LYP/LANL2DZ level employed and B3LYP/def2-TZVPP does not affect the relative stability of the thermodynamically most stable products reported in this chapter.

## [3.3] Results and Discussion

Detailed computational studies were carried out to get an insight into the mechanism of the reaction of carbodiimide and isocyanate with $N(i\text{-}Pr)_2$- and $NCy_2$-substituted borylene complexes **1a,b**. For computational efficiency, the bulky R and R' groups both in the borylenes themselves, and in the CyNCNCy and R'NCO molecules were replaced by Me. We have used a self-consistent combination of Arabic numerals and letters to represent specific complexes, which are key to the study. The structures corresponding to experimentally known species are represented by **a** and **b**, while **c**-**e** are used for the model complexes. Thus, the iron borylene complexes with $N(i\text{-}Pr)_2$ and $NCy_2$ substituents are represented as **1a** and **1b** respectively, with the corresponding (model) $NMe_2$ complex being **1c**. Furthermore, intermediates obtained in the (experimentally determined) reactions of **1a,b** with CyNCNCy or R'NCO (R' = Ph, 2,6-Xyl, Cy; where Xyl = $C_6H_3(Me)_2$) are similarly indicated by the letters **a** or **b** after the structure number (Scheme 3.2b). Intermediate and product species obtained from the reactions of the model compound $[CpFe(CO)_2(BNMe_2)]^+$ (**1c**) with MeNCNMe are represented by the suffix **c**. For the reaction of **1c** with the model isocyanate substrate MeNCO, there are two possibilities for the attack of the MeNCO molecule i.e. via initial O- or N-coordination. The intermediates in the O-attack pathway are represented by the

suffix **d** while those derived from the N-attack pathway are represented by the suffix **e**. To avoid the complexity of drawing three-dimensional structures, we have used a representative schematic as shown in scheme 3.3. First, we will discuss the mechanism of insertion of carbodiimide into the Fe=B and B=N bonds of **1a,b**; the mechanisms of the more complex reactions with isocyanates are discussed later.

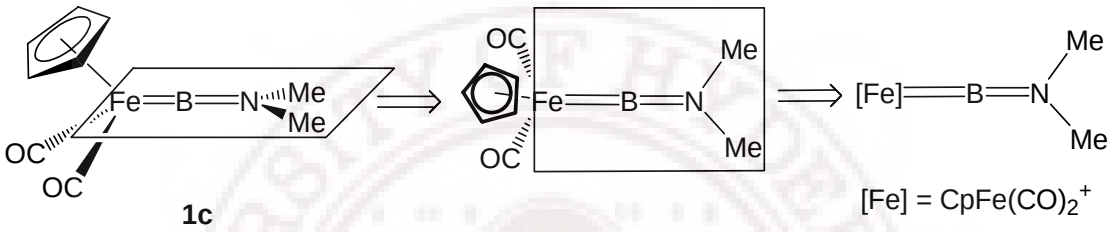


**Scheme 3.3**: Schematic representation followed throughout the chapter: projection of the three-dimensional structure (in this case of **1c**), where the $[CpFe(CO)_2]^+$ fragment is represented by the symbol [Fe].

### [3.3.1] Mechanistic Study of the Insertion of Carbodiimide into the Fe=B and B=N Bonds of 1a and 1b

The reaction of **1a,b** with one equivalent of CyNCNCy has been shown crystallographically to give the mono-insertion product **3a,b**, in which the carbodiimide molecule has undergone insertion into the Fe=B bond of the complex; when two equivalents of carbodiimide are used the bis-insertion products **4a,b** are rapidly formed (Scheme 3.2a).[3e] Computational studies were carried out to understand the mechanisms of these reactions using the model systems **1c** and MeNCNMe.

### [3.3.1.1] Reaction with One Equivalent of Carbodiimide

The first step of the reaction is the interaction of the carbodiimide (MeNCNMe) with the iron borylene complex **1c**, to form the acyclic intermediate **2c** (Scheme 3.4). The formation of this intermediate is calculated to be exothermic by 24.4 kcal/mol. This can be attributed to the donation of one of the nitrogen-centered lone pairs (the HOMO of MeNCNMe; figure 3.1a) of the carbodiimide to the LUMO of **1c** (Figure 3.1b), which is mainly located on the boron atom. A closely related intermediate $[CpFe(CO)_2\{BNCy_2(CyNCNCy)\}]^+$ (**2b**) has been characterized by low temperature NMR spectroscopy as an intermediate in the reaction of **1b** with CyNCNCy (Scheme 3.2a).[3e] Similar acyclic intermediates of this type have been isolated from the reactions of **1a** with $Ph_3PO$ (Scheme 3.1a)[3g] and *i*-$PrN{=}CMe_2$.[3i]

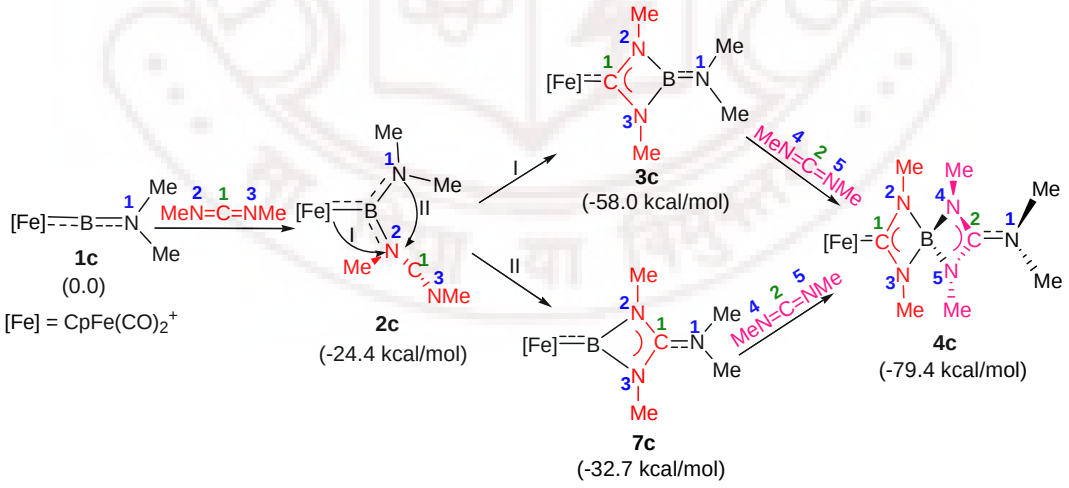


**Scheme 3.4**: Schematic representations of two possible pathways for the formation of spirocyclic complex **4c** by the reaction of **1c** with two equivalents of MeNCNMe. All energies ΔG, in kcal/mol

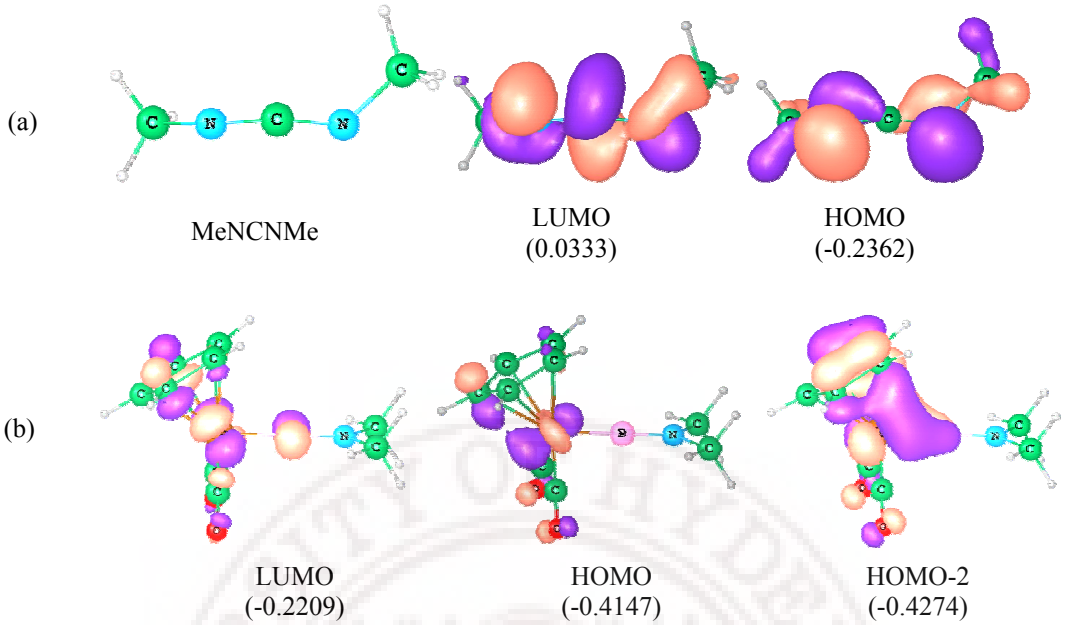


**Figure 3.1**: Important molecular orbitals of (a) the carbodiimide MeNCNMe and (b) the model iron borylene complex **1c**. Energies are given in Hartrees.

In the model intermediate **2c**, the planar MeNCNMe moiety lies approximately perpendicular to the least squares plane defined by the $FeBNMe_2$ unit (Figure 3.2). **2c** can then undergo insertion into the Fe=B (pathway I) or B=N (pathway II) bond to form complexes **3c** or **7c** respectively (Scheme 3.4). Complex **3c**, formed by insertion into the Fe=B bond, is thermodynamically more stable than complex **7c** (the B=N insertion product) by 25.3 kcal/mol; a similar trend has been suggested in preliminary DFT studies.[5] The relative energy difference between the intermediates **3c** and **7c** is similar for both Cy (26.8 kcal/mol)[5a] and Me (25.3 kcal/mol) substituents. This further reconfirms our calculations with the model complexes using Me substituents. Such a finding is, of course, consistent with the experimental isolation of complex **3b** (Scheme 3.2a).[3g]

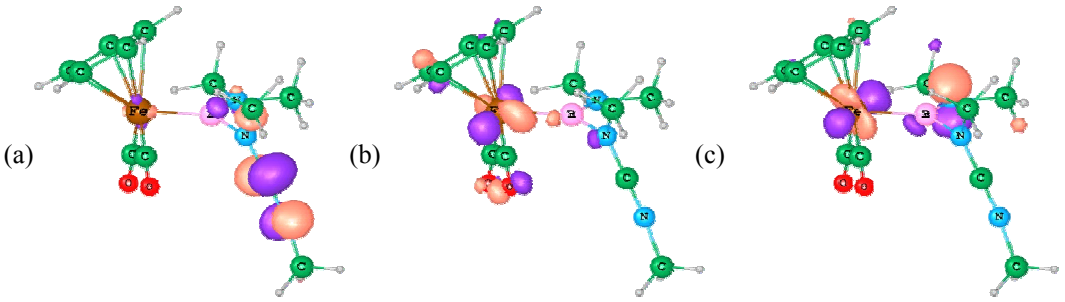


**Figure 3.2**: Important molecular orbitals of the intermediate borylene-carbodiimide complex **2c**. Energies are given in Hartrees.

These findings imply that the first insertion step of the MeNCNMe molecule is thermodynamically more favorable at the Fe=B bond rather than the B=N bond. The HOMO of complex **2c** is mainly iron d orbital in character (Figure 3.2b), while the LUMO is a C-N $\pi$* orbital (Figure 3.2a), thus offering a facile pathway for formation of a Fe-C bond and ultimate formation of complex **3c**. By contrast, complex **7c** can be formed by interaction between the LUMO and the HOMO-2 of **2c** (a lone pair type orbital at N; figure 3.2c). From an orbital energy perspective, (Figure 3.2), the iron-centered HOMO (-0.3590 a.u.) is clearly likely to be a better donor orbital than the lower lying HOMO-2 (-0.3745 a.u.), thus implying that the experimental formation of complex **3c** (rather than **7c**) may be due to more favorable orbital interactions. In addition, the larger negative charge calculated by Mulliken population analysis on iron (-0.998) as compared to nitrogen (-0.136) offers an alternative electrostatic rationale for the observed regiochemistry of insertion. In simplistic terms, the nitrogen lone pair is utilized in the formation of the B-N1 $\pi$ bond and is consequently less available (lower lying); this is reflected in the planar geometry around N1 and similarities between the B-N1 bond distances in **1c** (1.355

Å), **2c** (1.360 Å) and classical B=N double bonds, such as those found in $[R(R')N{=}B{=}NR(R')]^+$ [R = *t*-Bu, R' = $CH_2Ph$; 1.324(6) Å].[10] Furthermore, since the relative energy of the intermediate in the insertion reaction at the B=N bond (i.e. **7c**) is very high in comparison to the corresponding intermediate for insertion into the Fe=B bond (and experimental evidence also points to Fe=B insertion), we did not explore further reaction paths for B=N insertion. A detailed mechanistic study of the insertion reaction at the Fe=B bond is explored below (Scheme 3.5).

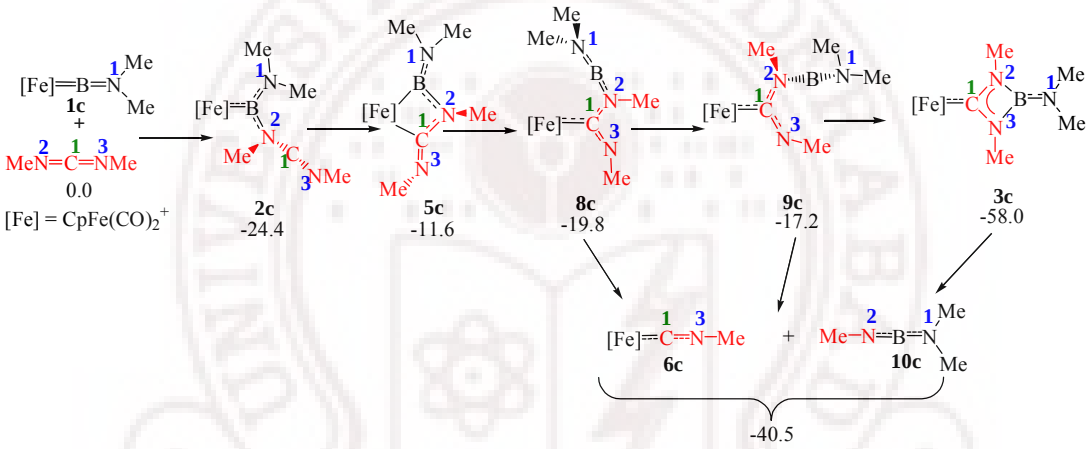


**Scheme 3.5**: Schematic representation of the mechanism of insertion of one molecule of MeNCNMe into the Fe=B bond of **1c** (includes only the intermediates). All energies ΔG, in kcal/mol.

The formation of the acyclic donor-acceptor adduct **2c** from **1c** by the coordination of the carbodiimide MeNCNMe at boron is exothermic by 24.4 kcal/mol (Scheme 3.5 and Figure 3.3). The corresponding transition state (**1c-2c**) is only 5.3 kcal/mol higher in energy than the reactants themselves (Figure 3.3), consistent with the high reactivity of the borylene towards nucleophilic attack.[3s-v,11] The formation of a similar complex has previously been reported in the metathesis reactions of **1a**,[3g] and related species containing imine donors have been structurally

characterized.[3i] In addition the boron-centered electrophilicity of **1c** is supported by the calculated Mulliken charge at boron (+0.683, c.f. -0.937 at iron).

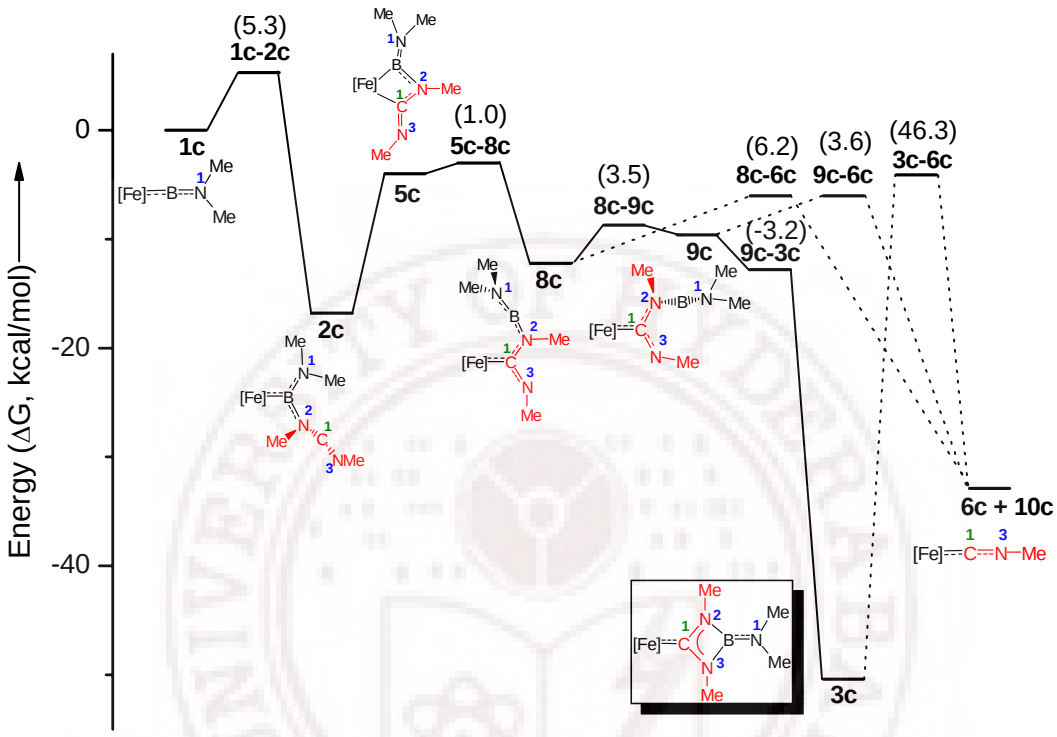


**Figure 3.3**: Potential energy diagram (including intermediates and transition states) for insertion of one molecule of MeNCNMe into the Fe=B bond of **1c** (Scheme 3.5). The dotted line indicates the formation of the dissociated products. All energies ΔG, in kcal/mol.

Mechanistically, the next step in the formation of **3c** is the formation of the four-membered metallacyclic intermediate **5c** by the interaction of the HOMO of **2c**, which is mainly concentrated at iron (Figure 3.2b) with the LUMO, which is ostensibly the C1-N3 π* anti-bonding molecular orbital (Figure 3.2a). As a result, the C1-N3 bond distance in **5c** (1.261 Å) is somewhat longer than the corresponding distance in **2c** (1.179 Å). Moreover, in **5c** the methyl substituents on N1 and N2 do not lie in the same plane (dihedral angle ∠N1BN2C = 20.1°) presumably to avoid unfavorable steric interactions. Thus, the non-planar structure of the complex **5c** can

be attributed to the optimization of the mutually repulsive interactions between the methyl groups on N1 and N2, and the bonding pair-lone pair repulsive interaction between N2-Me and the lone pair on N3. The 4-membered metallacycle **5c** is less stable than the acyclic complex **2c** by 12.8 kcal/mol. Nevertheless, a similar metallacyclic intermediate has been suggested in the metathesis reaction of the **1a** with various unsaturated substrates,[4] and has been isolated in the reaction of the closely related neutral borylene complex $CpMn(CO)_2B(t\text{-}Bu)$ with CyNCNCy or $Ph_2CO$.[3h]

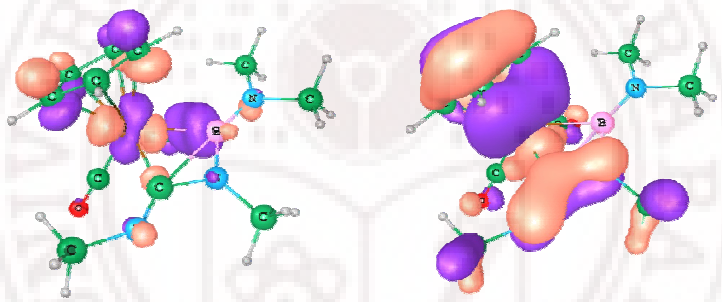


**Figure 3.4**: Fe-B antibonding and C-N π molecular orbitals of the metallacycle **5c**. Energies are given in Hartrees.

The cyclic intermediate **5c** can then undergo scission of the Fe-B bond to form a second acyclic intermediate (**8c**) which is more stable than **5c** by 8.2 kcal/mol; the energy barrier for this process is 1.0 kcal/mol. Since the Fe-B bond in **5c** is likely to be weaker (ca. 85.5 kcal/mol) than the C-N bond (179.5 kcal/mol),[2f,12] metallacycle cleavage in **5c** via Fe-B bond breakage is likely to be more feasible than breakage of the C-N bond. In addition, the LUMO of the intermediate **5c** is the Fe-B $\sigma^*$ orbital (Figure 3.4), and donation of C-N $\pi$ electron density (from the HOMO-5) to the Fe-B $\sigma^*$ orbital therefore results in Fe-B bond breakage to form **8c**.

Consequently, this interaction leads to the elongation of the C1-N2 bond in **8c** (1.503 Å) compared to the C1-N2 bond in **5c** (1.401 Å). The C1-N2 bond length in **8c** is in the range expected for C-N single bonds, and facile rotation about C1-N2 can therefore give a further acyclic intermediate **9c**. This rotation brings N3 closer to the boron center in **9c** (*d*(N3-B) = 3.272 Å) when compared to the corresponding distance in **8c** (*d*(N3-B) = 3.570 Å). The intermediate **9c** is less stable than intermediate **8c** by 2.6 kcal/mol and the energy barrier for this rotation is 3.5 kcal/mol. The C1-N2 bond in the intermediate **9c** (1.604 Å) is also elongated with respect to that in **5c** (1.401 Å); at this point dissociation at the C1-N2 bond could conceivably yield the metathesis products **6c** and **10c**. The energy barriers for the dissociation of **8c** or **9c** (via breakage of the C1-N2 bond) to give the common metathesis products **6c** and **10c** are 6.2 and 3.6 kcal/mol, respectively, and the reactions are exothermic by 20.7 and 23.3 kcal/mol. However, it seems more likely at this point that the intermediate **9c** would undergo a very facile cyclization to give **3c** by the donation of the lone pair at N3 into the B-N2 $\pi^*$ orbital. The formation of **3c** from **9c** is exothermic by 40.8 kcal/mol and the corresponding energy barrier is -3.2 kcal/mol, indicating a very flat potential energy surface for the cyclization process.[13] A cyclic intermediate similar to **3c** has been isolated from the reaction of CyNCNCy with **1b** (Scheme 3.2a).[3g]

Once formed, the possibility for dissociation of **3c** into the metathesis products **6c** and **10c** appears to be fairly remote, due to a very high energy barrier (46.3 kcal/mol) for this process and its inherent endothermicity (17.5 kcal/mol). Experimentally, the absence of $[CpFe(CO)_2(CNCy)]^+$ among the products of the reaction of **1b** with CyNCNCy, and the correspondingly high isolated yields of

insertion products are consistent with these predictions. On the other hand, the exothermicity of the conversion of the **9c** to **3c** (40.8 kcal/mol) and the low energy barrier (-3.2 kcal/mol) suggests that the reaction of carbodiimide with the **1c** would proceed via the pathway **2c** → **5c** → **8c** → **9c** → **3c**. The unusual stability of cyclic product **3c** can be attributed to π delocalization in the 4-membered ring (Figure 3.5). The exocyclic B-N1 π orbital of the complex **3c** is also further delocalized into the 4-membered ring (Figure 3.5), and is therefore characterized by a slightly longer B-N1 linkage (1.373 Å) when compared to the B-N1 distance in the model borylene complex **1c** (1.355 Å). From a bond strength perspective, the presence of three strong B-N (92.7 kcal/mol) and C-N bonds (179.5 kcal/mol) presumably also contributes to the high stability of **3c**.[14]

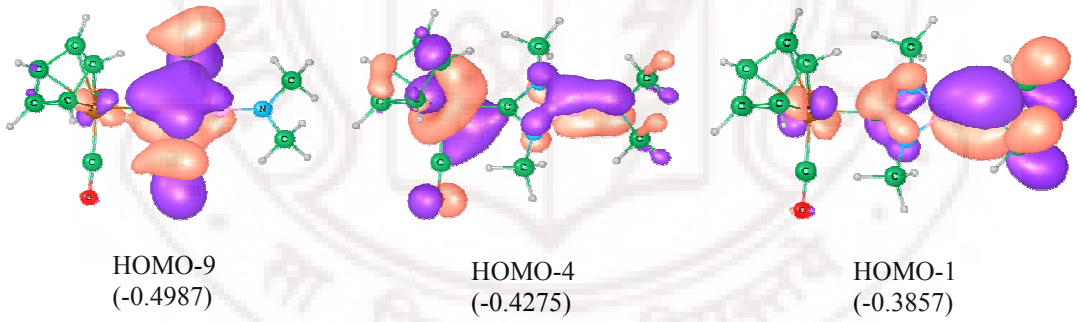


**Figure 3.5**: Important molecular orbitals of the mono(insertion) product **3c** obtained from **1c** and one equivalent of MeNCNMe, showing the delocalization in the plane of the 4-membered N2CN3B ring. Energies are given in Hartrees.

### [3.3.1.2] Reaction with Two Equivalents of Carbodiimide

The product **3c**, generated by the insertion of one molecule of carbodiimide into the Fe=B bond of **1c**, can undergo further reaction with a second molecule of carbodiimide. Indeed, variable temperature NMR experiments imply that the

corresponding reaction of cyclohexyl substituted complex **3b** with CyNCNCy is facile at -20°C. In a similar fashion to the first insertion step, the lone pair of one of the nitrogen atoms of the second molecule of carbodiimide (MeNCNMe) attacks the electrophilic boron centre atom to form an intermediate, in this case **11c** (Scheme 3.6).

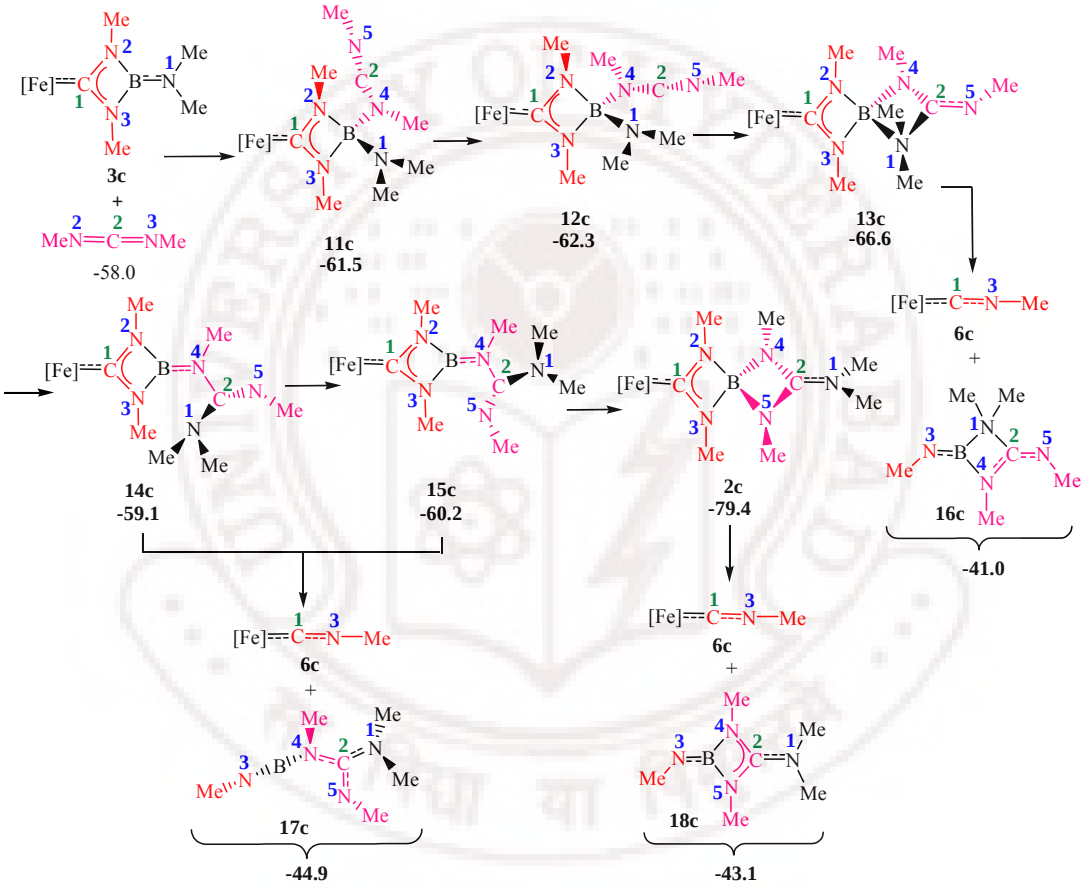


**Scheme 3.6**: Schematic representation of the mechanism for the insertion of a second molecule of MeNCNMe into the B=N bond of **3c** (includes only the intermediates). All energies ΔG, in kcal/mol.

This reaction is both kinetically favorable due to a low energy barrier (1.7 kcal/mol) and exothermic (by 3.5 kcal/mol; Figure 3.6). From **11c**, rotation about the B-N4 bond gives the closely related intermediate **12c**, in which C2 is significantly

closer to N1 (*d*(C2-N1) = 2.767 Å, c.f. 3.639 Å in **11c**). The relative energies of **11c** and **12c** are very close, differing by only 0.8 kcal/mol. The next reaction step is the formation of the bicyclic intermediate **13c** by the interaction of the lone pair at N1 with the LUMO of the (second) carbodiimide fragment, which is mainly located at C2. This ring-closure process is exothermic by 4.3 kcal/mol; the resulting (second) 4-membered ring is planar and perpendicular to the existing C1N2BN3 ring. An alternative mechanism for the formation of **13c** from **3c** is a concerted [2+2] cycloaddition process involving interaction of the B-N1 π orbital with the C2-N4 $\pi^*$ orbital.[15] The transition state corresponding to this [2+2] cycloaddition process could not be located. Conceivably, this reflects the fact that the B-N1 π bond in **3c** is stabilized due to delocalization into the existing 4-membered ring (Figure 3.5).

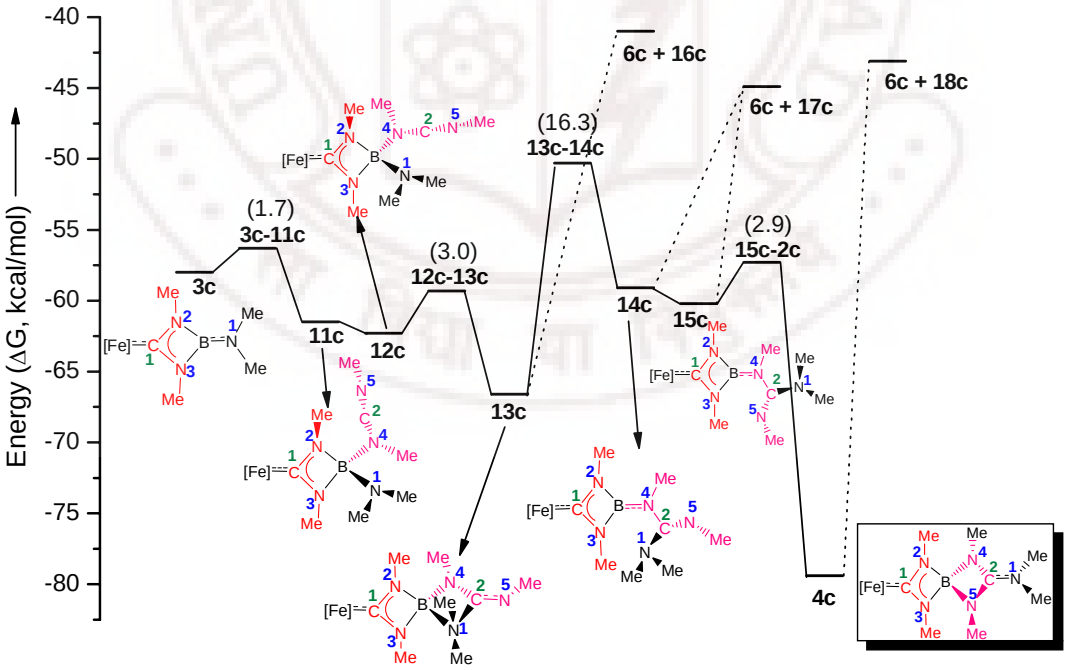


**Figure 3.6**: Potential energy diagram (including intermediates and transition states) for the insertion of a second molecule of MeNCNMe into the B=N bond of the intermediate **3c** (Scheme 3.6). The dotted line indicates the formation of the dissociated products. All energies ΔG, in kcal/mol.

The final products in the reactions of **1a,b** with two equivalents of CyNCNCy are the spirocyclic systems **4a**,**b** (Scheme 3.2a). The formation of the related model compound **4c** from the intermediate **13c** can take place via further (acyclic) intermediates **14c** and **15c** (Scheme 3.6 and Figure 3.6) the formation of which necessitates rearrangement of the second heterocycle. The breakage of the B-N1 bond (1.655 Å) in the intermediate **13c** leads to the formation of **14c**; this reaction is endothermic by 7.5 kcal/mol and the corresponding energy barrier is 16.3 kcal/mol. From **14c**, subsequent rotation about the C2-N4 bond generates **15c**, which is 1.1 kcal/mol lower in energy. Both **14c** and **15c** are structurally similar to the intermediate **3c** (Scheme 3.6), with one of the methyl groups attached to N1 (in **3c**) being formally replaced by a $C(NMe)NMe_2$ group. This is reflected in similar geometrical parameters and energies for the cyclic components of three intermediates. Rotation about the C2-N4 bond in **14c** to form **15c** brings N5 close to the boron atom, such that donation of the lone pair of N5 to the p-orbital at boron gives the final bis-insertion product **4c**. This final coordination step reaction is exothermic by 19.2 kcal/mol.

A further reaction consideration, which is particularly relevant given the experimental findings with isocyanates,[3r] is that any or all of the intermediates **13c**, **14c**, **15c** and **4c** could potentially undergo breakage of the C1-N2 and B-N3 bonds to form the isonitrile complex **6c** (together with the corresponding boron-containing products **16c**, **17c** and **18c**).[16] It should be noted (Figure 3.6) that all combinations of the dissociation products (**6c** and **16c**, **17c** and **18c**) are significantly higher in energy than the corresponding precursors (**13c**, **14c**, **15c** and **2c**). This can be attributed, at least in part, to the high bond dissociation energy of the B-N and C-N

bonds,[14] and explains the experimental observation that only the double insertion products **4a**,**b** are isolated from the reactions of **1a**,**b** with excess CyNCNCy, with no trace of the dissociation product $[CpFe(CO)_2(CNCy)]^+$ being detected (Scheme 3.2a).

### [3.3.2] Mechanistic Study of the Reaction of Isocyanates with 1b

The reactions of the borylene complex **1b** with isocyanates R'NCO (R' = Ph, 2,6-Xyl, Cy) have been shown by crystallographic and in situ ESI-MS experiments to give the isonitrile products $[CpFe(CO)_2CNR']^+$ (**6b**, R' = Ph, 2,6-Xyl, Cy; scheme 3.2b),[3r] in contrast to the corresponding reaction with CyNCNCy, which gives the bis-insertion product **4b** (Scheme 3.2a).[3e] In an attempt to understand the underlying reasons for the differing product distributions obtained for superficially similar heteroallene substrates, a further series of calculations was carried out utilizing (in the first place) the model systems **1c** and MeNCO.

#### [3.3.2.1] Reaction with One Equivalent of Isocyanate

Unlike the reaction of carbodiimides, an additional complication is that the initial interaction of an isocyanate molecule with the borylene ligand can take place via O-attack at boron (to give **2d**) or via N-attack (to give **2d**; scheme 3.7). Both pathways can then lead to the insertion products **3d** (net insertion into the Fe=B bond) and/or **7d** (net insertion into the B=N bond). As in the case of the borylene-carbodiimide complex **2c** (Schemes 2 and 4), the HOMO of the donor-acceptor adduct **2d** is mainly iron d-orbital in character and the lone pair orbital at N2 is

much lower lying. Therefore, from the orbital energy perspective, the MeNCO insertion product **3d** (insertion into Fe=B bond) is not only more stable than **7d** (by 21.0 kcal/mol) but its formation is also more facile. Hence, we have studied the detailed mechanism only for the insertion into the Fe=B bond of **1c**; both O-attack (Scheme 3.8a) and the N-attack (Scheme 3.8b) pathways have been examined in an attempt to understand differences in reactivity between isocyanate and carbodiimide substrates.

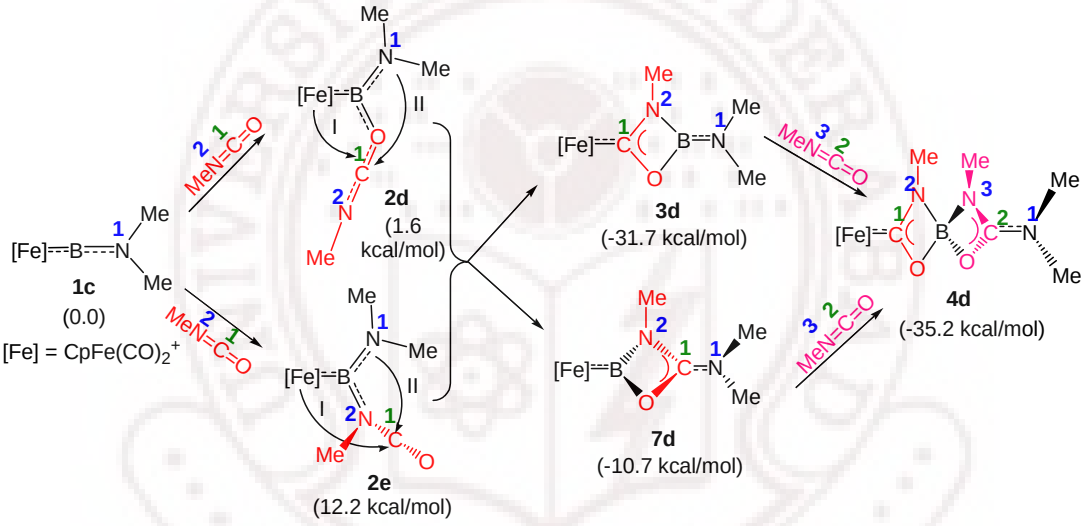


**Scheme 3.7**: Schematic representation of two possible pathways for the formation of spirocyclic complex **4d** by the reaction of model iron borylene complex **1c** and MeNCO. All energies ΔG, in kcal/mol.

In the O-attack and N-attack pathways, the formation of the acyclic intermediate **2d** or **2e** takes place by the attack of the lone pair at O or N, respectively, with the LUMO of **1c**, which is largely located at boron (Figure 3.1b). The energy change on formation of the N-bound isomer **2e** is endothermic by +12.2 kcal/mol, while that for the formation of **2d** is somewhat smaller at +1.6 kcal/mol. The corresponding energy barrier for the N-attack pathway is 18.2 kcal/mol while that for O-attack is only 3.0 kcal/mol (Figure 3.7).

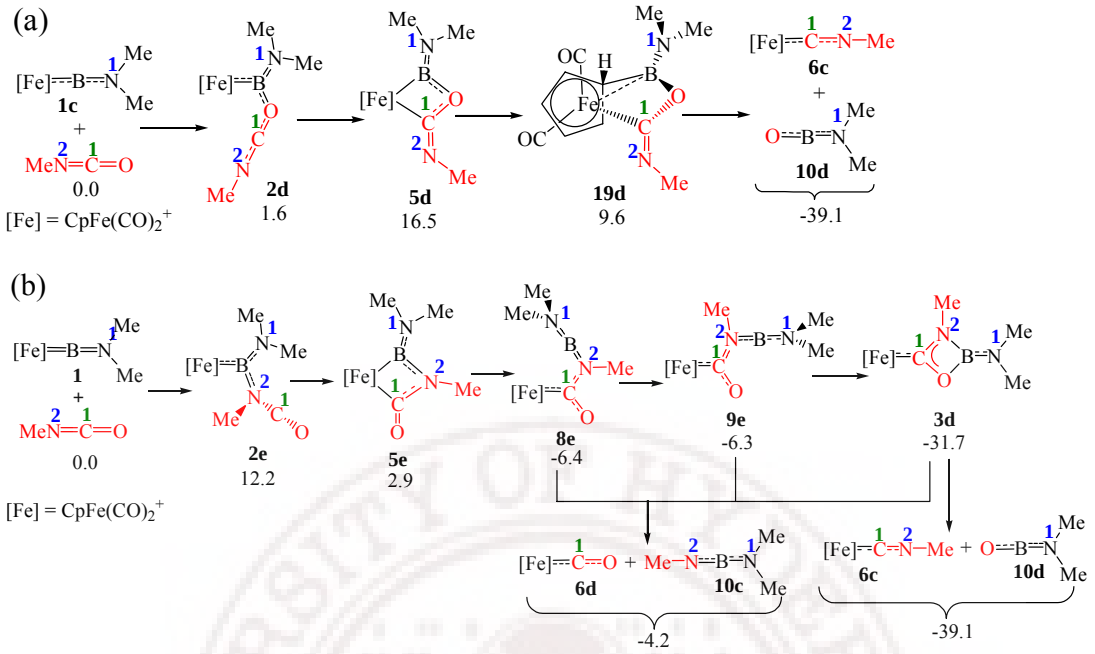


**Scheme 3.8**: Schematic representation of the mechanism of insertion of one molecule of MeNCO into the Fe=B bond of **1c** (includes only the intermediates): (a) O-attack pathway; and (b) N-attack pathway. All energies ΔG, in kcal/mol.

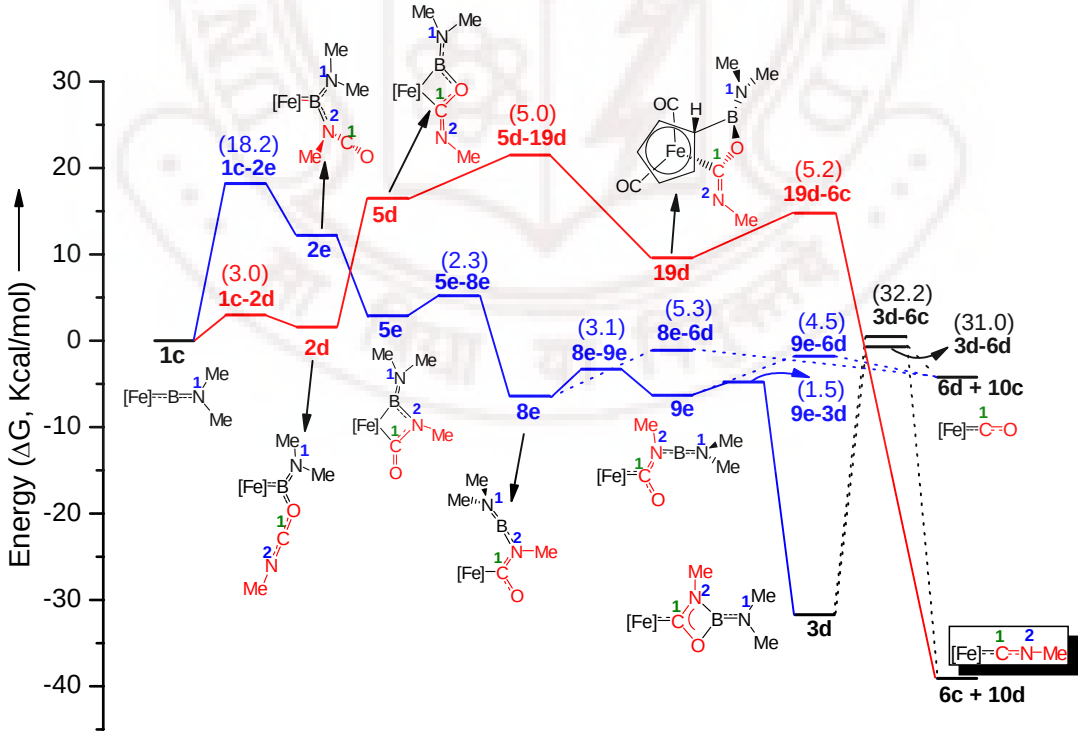


**Figure 3.7**: Potential energy diagram (including intermediates and transition states) for the reaction of one molecule of MeNCO into the Fe=B bond of **1c** (Scheme 3.8). The dotted line indicates the formation of the dissociated products. All energies ΔG, in kcal/mol.

The approach of the N2 centered lone pair of the isocyanate towards the boron atom is presumably more sterically encumbered due to the methyl substituent.[17] Such steric factors are also reflected in the geometry of **2e (**Figure 3.8), in which the methyl group attached to N2 lies in a plane perpendicular to that containing Fe, B and N1; a similar geometry is found for intermediate **2c**, formed in the reaction of **1c** with MeNCNMe (Figure 3.8). On the other hand, the MeNCO fragment in the O-bound isomer **2d** is able to lie in the FeBN1 plane (Figure 3.8). It is also to be noted that the negative charge, calculated by Mulliken population analysis, on O is much greater in magnitude (-0.262) than that on N (-0.005). Thus, both steric and electrostatic factors imply that the O-attack pathway is more facile than N-attack.

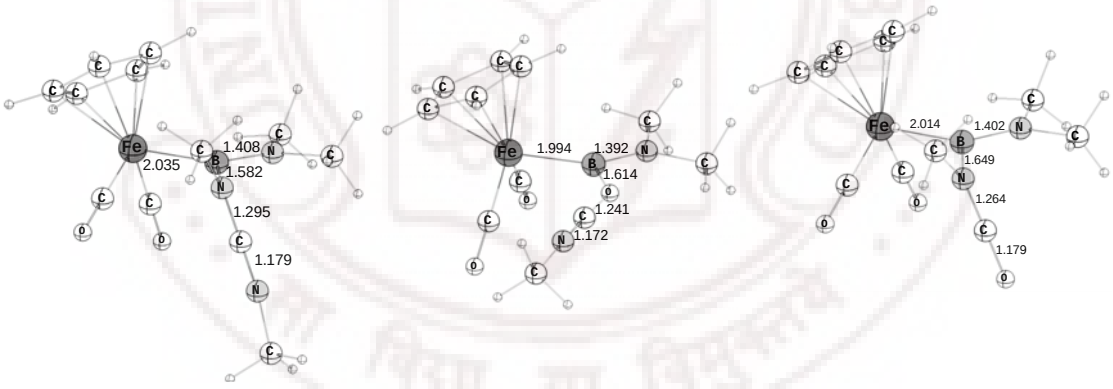


**2c** **2d** **2e**

**Figure 3.8:** Important bond lengths (Å) of the intermediates **2c**, **2d** and **2e**.

The next mechanistic step is the formation of the metallacyclic intermediates **5d** and **5e** by the donation of iron d-electron density into the LUMO+4 (-0.1476 a.u.) or LUMO (-0.2387 a.u.) of the intermediates **2d** or **2e**, respectively (Scheme 3.8); each acceptor orbital is formally antibonding in the NCO framework and mainly concentrated on C1 (Figure 3.9).

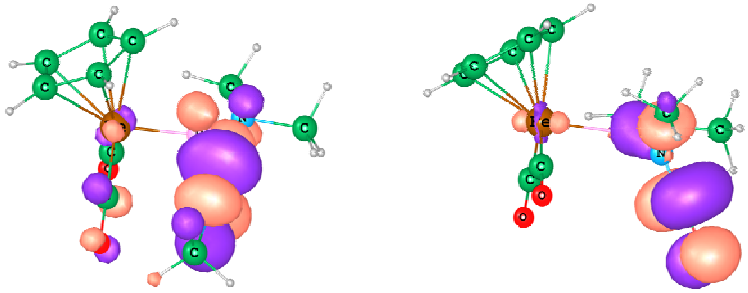

LUMO+4
(-0.1476)

**2d**

LUMO
(-0.2387)

**2e**

**Figure 3.9**: The LUMO+4 of the acyclic intermediate **2d** and LUMO of the alternative intermediate **2e**. Energies are given in Hartrees.

While the formation of cyclic intermediate **5d** from **2d** is endothermic by 14.9 kcal/mol, the formation of **5e** from **2e** is actually exothermic (by 9.3 kcal/mol). The interaction of the HOMO of the iron borylene complex (which is mainly iron d orbital in character) with the much more high-lying LUMO+4 makes **5d** less stable (compared to **5e**) by 13.6 kcal/mol. This is reflected in the elongated C1-O bond in **5d** (1.468 Å, c.f. 1.241 Å in **2d**); in contrast the bond lengthening is much less pronounced for **5e** (1.382 Å c.f. 1.264 Å for **2e**). Subsequent rearrangement of the intermediate **5d** to **19d** is exothermic by 6.9 kcal/mol and the energy barrier is 5.0 kcal/mol. The structure of the intermediate **19d** is rather unusual; the boron atom forms a bond with one of the carbon atoms of the Cp ring (*d*(B-C) = 1.690 Å) and the Fe-B bond is elongated (*d*(Fe-B) = 2.644 Å) to the extent that it is well outside the sum of the conventional covalent radii of iron and boron (ca. 2.05 Å).[18] This asymmetry is also reflected in the variation of calculated Fe-C(Cp) distances (shortest *d*(Fe-C) ) 2.219 Å; longest *d*(Fe-C) ) 2.324 Å) as well as in the C-C distances of the Cp ring itself (shortest *d*(C-C) ) 1.396 Å; longest *d*(C-C) ) 1.529 Å). The interaction of highly Lewis acidic borane fragments with the carbons of metal-

bound Cp ligands has previously been reported in a number of systems.[19] The intermediate **19d** dissociates at the C(Cp)-B and C1-O bonds into the metathesis products **6c** and **10d**. This reaction is highly exothermic (48.7 kcal/mol) and the corresponding energy barrier is 5.2 kcal/mol.

In contrast, the intermediate **5e**, formed by initial N-coordination, rearranges to form the acyclic intermediate **8e**. An intermediate similar to **8e** is also observed for the insertion of carbodiimide into **1c** (i.e. **8c**, scheme 3.5). The formation of the acyclic intermediate **8e** from **5e** by the breakage of the Fe-B bond is exothermic by 9.3 kcal/mol and the energy barrier is 3.3 kcal/mol. In a similar fashion to the carbodiimide chemistry, subsequent rotation about the C1-N2 bond in **8e** leads to the intermediate **9e**, which cyclizes to **3d** by the donation of the lone pair on oxygen to boron. The energy barrier for the formation of **9e** from **8e** is 3.1 kcal/mol and that of **3d** from **9e** is 1.5 kcal/mol. The formation of this additional donor-acceptor bond is exothermic by 25.4 kcal/mol. It should be noted that, as with the reaction of MeNCNMe with **1c**, both intermediates **8e** and **9e** can dissociate to give the metathesis products **6d** and **10c** via breakage of the C1-N2 bond. The energy barriers for these dissociation processes are 5.3 and 4.5 kcal/mol respectively. However, dissociation is endothermic by 2.2 kcal/mol. The insertion product **3d** can also undergo dissociation at both the C1-N2 and O-B bonds to give **6d** and **10c**, but this also is endothermic (in this case by 27.5 kcal/mol) and the corresponding energy barrier is 31.0 kcal/mol. On the other hand, dissociation in the alternative sense at the C1-O and B-N2 bonds to give **6c** and **10d** is exothermic by 7.4 kcal/mol. However, the energy barrier for this dissociation process is very high at 32.2 kcal/mol. The formation of the stronger B-O bond (192.6 kcal/mol) in **10d** plays a

major role in the stability of the dissociation products **6c** and **10d** over the insertion product **3d**.[4,14] This can be understood by the isodesmic equation (Scheme 3.9), which shows that the combined free energies of **3c** and **10d** are less than that of **3d** and **10c** by 25.7 kcal/mol. This analysis also indicates that the insertion product for carbodiimide (**3c**) is more stable than the insertion product for isocyanate (**3d**).

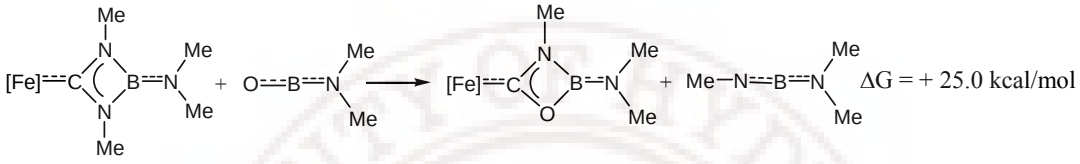


**3c** **10d** **3d** **10c**

**Scheme 3.9**: Isodesmic equation linking **3c**, **10d** and **3d**, **10c**.

To summarize, the initial interaction of the borylene complex with an isocyanate molecule via O-attack leads exclusively to metathesis product **6c**, whereas the N-attack pathway appears to generate the insertion product **3d**, with subsequent breakdown to give **6c** involving surmounting a large energy barrier, and that to give **6d** being strongly endothermic. The energy barrier for the initial O-attack step by MeNCO is 3.0 kcal/mol, while that for N-attack is 18.2 kcal/mol; the O-attack pathway is therefore kinetically more favorable. These computational results are consistent with the experimental observations that the reaction of iron borylene complex **1b** with R'NCO (R' = Ph, 2,6-Xyl, Cy), gives isonitrile complexes of the type $[CpFe(CO)_2(CNR')]^+$ as the major product in each case, these being both the thermodynamically and kinetically favorable products. However, the presence of small quantities of $[CpFe(CO)_3]^+$ (**6d**) implies that the N-attack pathway is also active, since the formation of **6d** via an initial O-coordination step is energetically

unfeasible. With this in mind, the kinetics of the initial O and N-attack steps provide further predictions concerning the product distributions using PhNCO and 2,6-XylNCO substrates.[3r] The presence of two methyl groups in the ortho positions of the phenyl ring in 2,6-XylNCO would be expected to make the approach of the N donor toward the boron atom more sterically encumbered. As a result, the O-attack pathway will be more preferred over the N-attack pathway and the isonitrile product analogous to **6c** will be obtained. The less bulky PhNCO substrate is more likely to be able to react through both O- and N-attack pathways. As a result, **6c** is obtained as the major product (via O-attack), but **6d** is also obtained as minor product (via N-attack). This is indeed observed experimentally for PhNCO. We have calculated the barrier for the initial step in the O- and N-attack pathways in the reaction of **1c** with PhNCO and 2,6-XylNCO. In the case of PhNCO, the energetic barriers for the O-attack (4.7 kcal/mol) and N-attack (18.3 kcal/mol) pathways are close in energy to those calculated for the model MeNCO system (Figure 3.7). However for 2,6-XylNCO, the energy barrier for the N-attack pathway increases significantly (23.9 kcal/mol) compared to PhNCO, while the barrier for O-attack (4.4 kcal/mol) remains essentially unchanged. Thus, the more bulky isocyanate prefers the O-attack pathway. It is interesting to note that the N-attack pathway leads to the insertion reaction, whereas the O-attack pathway, in effect, leads to a metathesis reaction. This supports the earlier finding that substrates containing more polar bonds have greater preference for metathesis reactivity over species containing less polar bonds.[4] Here, the more polar bond C-O (Mulliken charge difference, 0.174) undergoes an overall metathesis reaction (O-attack pathway), whereas the less polar C-N bond (Mulliken charge difference, 0.049) gives insertion (N-attack pathway).

Reactions where the C-N bond of an isocyanate undergoes insertion have been observed previously.[20]

Furthermore, in order to understand the effects of variation in substituent bulk at boron, we have computed the relative energy difference between the isomeric adducts **2d-R-R′** (formed via O attack) and **2e-R-R′** (formed via N attack) with various substituents (R = Me, Cy and R′ = Ph, 2,6-Xyl) (Table 3.1). It is evident from these calculated energy differences that the Cy substituent does not change the relative stability when R′ = Ph. However, the relative energy difference between the two isomers increases with R′ = 2,6-Xyl. This further precludes the formation of the metathesis product **6c** via the N-attack pathway as we observed experimentally. We have also obtained the energies of these isomers (**2d-R-R′** and **2e-R-R′**) at the B3LYP/def2-TZVPP and BP86/def2-TZVPP levels of theories as a representative test case in order to understand the reliability of the employed level of theory, viz. B3LYP/LANL2DZ.

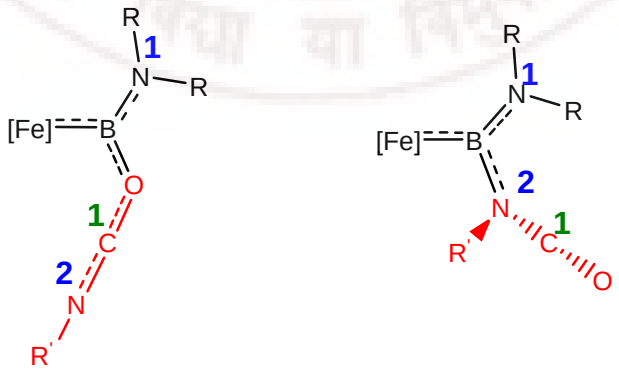


**2d-R-R'** **2e-R-R'**

**Table 3.1**: Relative energy (ΔE) of **2e-R-R'** with respect to **2d-R-R'**, deviation of energies from B3LYP/def2-TZVPP level of theory (ΔErr), average error ($\overline{\Delta Err}$) and mean absolute deviation ($\overline{|\Delta Err|}$). All the energies are in kcal/mol.

| R | R' | ΔE | | | ΔErr | |
|---|---|---|---|---|---|---|
| | | **B3LYP /def2-TZVPP //B3LYP /LANL2DZ** | **BP86 /def2-TZVPP //B3LYP /LANL2DZ** | **B3LYP /LANL2DZ** | **BP86 /def2-TZVPP //B3LYP /LANL2DZ** | **B3LYP /LANL2DZ** |
| Me | Me | 4.3 | 8.2 | 10.0 | -3.9 | -5.7 |
| Me | Ph | 6.0 | 5.9 | 11.7 | 0.1 | -5.7 |
| Me | 2,6-Xyl | 12.0 | 10.1 | 17.8 | 1.9 | -5.8 |
| Cy | Ph | 5.5 | 2.8 | 10.5 | 2.7 | -5.0 |
| Cy | 2,6-Xyl | 19.6 | 18.2 | 23.5 | 1.4 | -3.9 |
| $\overline{\Delta Err}$ | | | | | 0.5 | -5.2 |
| $\overline{\lvert\Delta Err\rvert}$ | | | | | 2.0 | 5.2 |

### [3.3.2.2] Reaction with Two Equivalents of Isocyanate

As outlined in the discussion above (and in Figure 3.7), the isocyanate insertion product **3d** has high energetic barriers for dissociation into either **6c** (32.2 kcal/mol) or **6d** (31.0 kcal/mol). Thus, in presence of two or more equivalents of isocyanate, **3d** can react further. The second molecule of isocyanate can also attack in one of two possible orientations viz. O- and N-attack (Scheme 3.10 and Figure 3.11) and each of these possibilities has been examined. The formation of the bicyclic intermediates **13d** and **13e** via O- and N-attack, respectively, can take place via a [2+2] cyclo-addition reaction between the B-N1 π orbital of **3d** (HOMO, Figure 3.10a) and the C2-N3 (HOMO) or C2-O (HOMO-2) π orbital of the isocyanates (Figure 3.10b); this type of [2+2] cycloaddition behavior has recent

literature precedent in the reactivity of strongly Lewis acidic boranes with heteroallenes.[15] In the current case, the [2+2] reactivity is reflected in a reduction in B-N1 multiple bond character and in increased bond lengths (1.630 Å for **13d**, 1.621 Å for **13e**) in comparison with **3d** (1.363 Å). The energetic barriers for the formation of **13d** via B-O bond formation (23.8 kcal/mol) and that of **13e** via B-N bond formation (20.5 kcal/mol) are comparable, while intermediate **13d** is less stable than intermediate **13e** by 19.5 kcal/mol (Figure 3.11). A similar trend in the stability of the cyclic intermediates **5d**,**e** was noted in the case of insertion of the first molecule of isocyanate (Scheme 3.8, Figure 3.7).

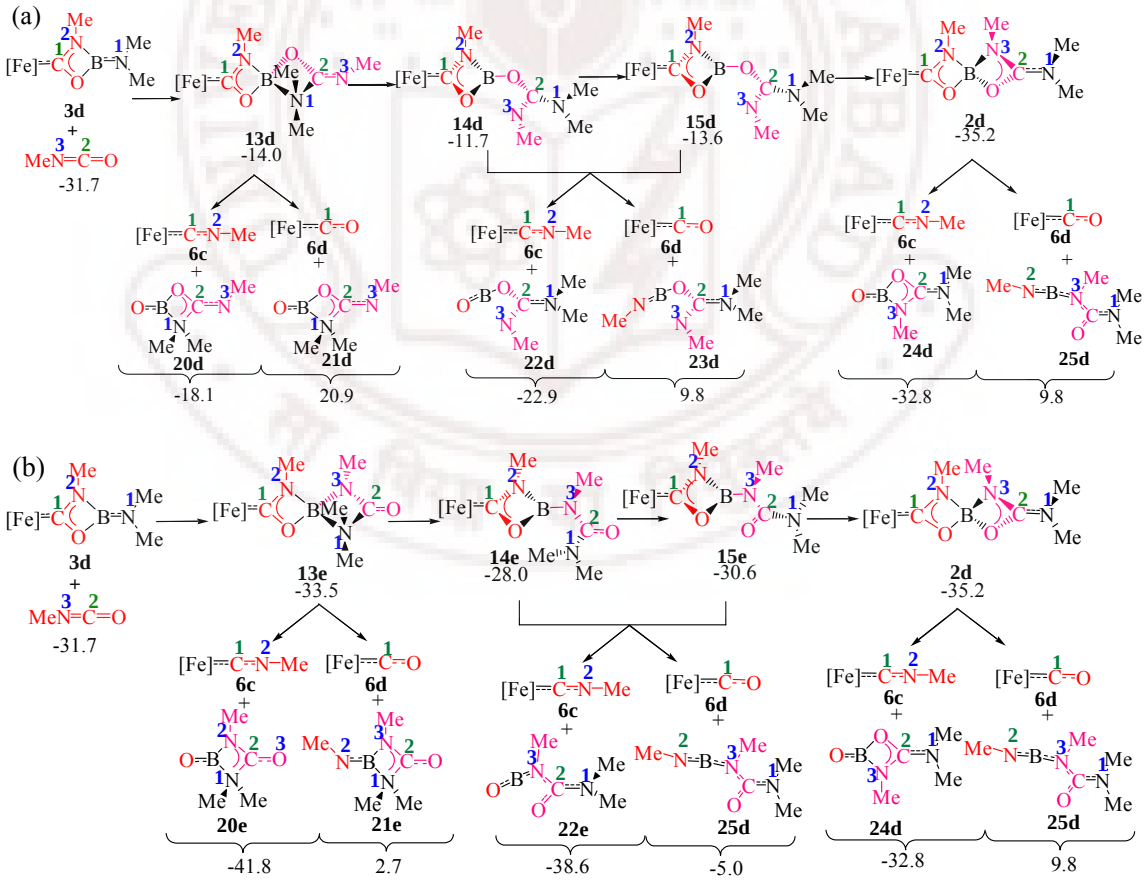


**Scheme 3.10**: Schematic representation of the mechanism of insertion of a second molecule of MeNCO into B=N bond of **3d** (includes only the intermediates): (a) O-attack pathway; and (b) N-attack pathway. All energies ΔG, in kcal/mol.

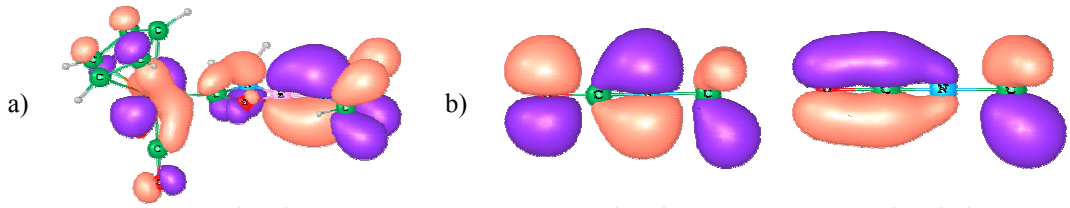


**Figure 3.10**: (a) The HOMO of the cyclic intermediate **3d** and (b) the HOMO and HOMO-2 of MeNCO. Energies are given in Hartrees.

The cyclic intermediates **13d** and **13e** can then dissociate in one of two possible ways, either by breaking the C1-O and B-N2 bonds (to give **6c**), or alternatively, by breaking the C1-N2 and B-O bonds (to give **6d**). In each case, the formation of **6c** is energetically far more profitable; dissociation of **13d** into **6c** (and **20d**) by breaking of the C1-O and B-N2 bonds is exothermic by 4.1 kcal/mol, while the formation of **6d** (and **21d**) is endothermic by 34.9 kcal/mol. Similarly, the dissociation of **13e** into **6c** (and **20e**) is exothermic by 8.3 kcal/mol, while formation of **6d** (and **21e**) is endothermic by 36.2 kcal/mol. The summation of the C-N (179.5 kcal/mol) and B-O (192.6 kcal/mol) bond enthalpies is estimated to be greater than that of the C-O (256.3 kcal/mol) and B-N bonds (92.7 kcal/mol) by ca. 23 kcal/mol.[14,21,22] Thus, from a thermodynamic perspective, the breaking of the C1-O and B-N2 bonds is more likely than the (stronger) C1-N and B-O bonds, and the isonitrile complex **6c** is a more feasible product than carbonyl complex **6d**. However, the energetic barriers to the formation of **6c** are not insignificant (20.9 kcal/mol from **13d**, 19.8 kcal/mol from **13e**). Thus, although dissociation to give the isonitrile product **6c** is thermodynamically favorable (via either route), the sizeable calculated barriers for the final dissociation step give an indication that the

intermediates **13d**,**e** might have significant lifetimes in solution. Such a finding is consistent with ESI-MS results for the **1b**/PhNCO system, which are consistent with measureable concentrations in solution of a species whose mass corresponds to borylene complex **1b** plus two equivalents of isocyanate.

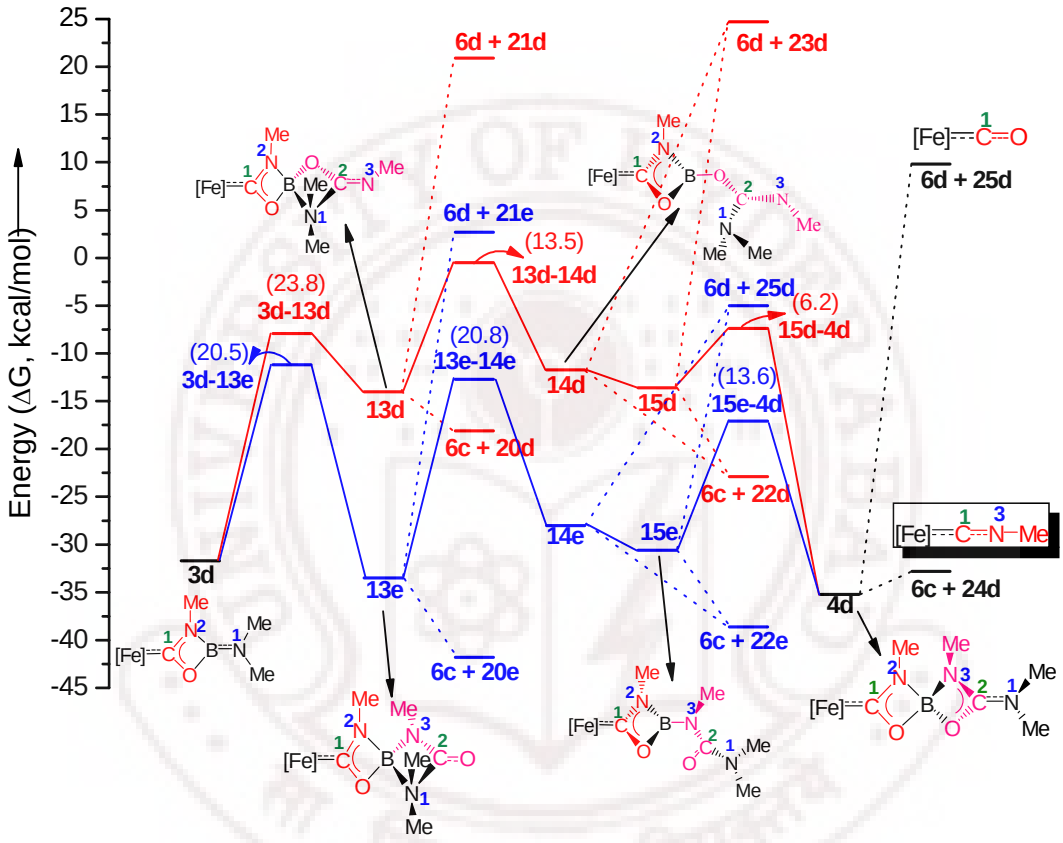


**Figure 3.11**: Potential energy diagram (including intermediates and transition states) for the reaction of MeNCO into the B=N bond of the complex **3d** (Scheme 3.10). The dotted line indicates the formation of the dissociated products. All energies ΔG, in kcal/mol.

On the other hand, the bicyclic intermediates **13d** and **13e** could also be converted to the bis-insertion product **4d** via the acyclic O-bound intermediates **14d** and **15d** or the more stable N-bound species **14e** and **15e** (Figure 3.11 and Scheme 3.10). The barrier for the formation of **14d** from **13d** by breakage of the B-N1 bond

is 13.5 kcal/mol; the corresponding barrier for the formation of **14e** from **13e** is 20.8 kcal/mol. That said, intermediate **14e** is more stable than **14d** by 14.4 kcal/mol. The intermediates **14d** and **14e** can then go on to form the closely related species **15d** and **15e** by simple rotation about the C2-O or C2-N3 bonds, respectively; **15d** and **15e** are marginally more stable than **14d** and **14e** by 1.9 and 2.8 kcal/mol, respectively. As with a number of earlier intermediate species, **15d** and **15e** can also dissociate into **6c** and other boron-containing products (**22d** and **22e**) by breakage of the C1-O and N2-B bonds. The dissociated products (i.e. isonitrile complex **6c** together with **22d**,**e**) arising from the breakage of the C1-O and N2-B bonds are more stable than the intermediates **15d** and **15e** by 9.3 and 10.6 kcal/mol respectively. The breakage of the C1-N2 and O-B bonds in **15d** and **15e**, on the other hand, leads to carbonyl complex **6d** (and the boron-containing products **23d** and **25d**); these dissociation processes are endothermic by 38.3 and 23.0 kcal/mol respectively. Alternatively, the bis-insertion product **4d**, analogous to the crystallographically authenticated final products formed with carbodiimide reagents, can be accessed from **15d** or **15e**. These steps are exothermic (by 22.6 and 4.6 kcal/mol respectively), and the corresponding energy barriers are 6.2 and 13.6 kcal/mol.

It is worth noting at this stage that, while the conversion of **13d**,**e** into **14d**,**e** (key steps in the formation of the bis-insertion product, **4d**) are endothermic by 2.3 and 5.5 kcal/mol (Figure 3.11), the alternative dissociation pathways for **13d**,**e** (to give **6c)** are actually exothermic by 4.1 and 8.3 kcal/mol respectively. Thus, it appears that the formation of the formal metathesis product **6c** from these intermediates is thermodynamically favorable; this then offers a further route to the

formation of the isonitrile products $[CpFe(CO)_2(CNR')]^+$ in keeping with the experimental observations for borylene complex **1b**.

The four membered rings BOC2N1 and BN3C2N1 in the bicyclic intermediates **13d** and **13e** are devoid of delocalization over all the four atoms of the ring because of tetra-coordination at N1. Hence, they are less stable than the final spirocyclic system **4d**, in which both rings in the bicyclic system allow for delocalization over the three atoms N, C and O. Nevertheless, the calculated energies of **13e** and **4d** are actually very close (1.7 kcal/mol). The possibility that **4d** can also dissociate into **6c** or **6d** has also been examined. **4d** is more stable than the dissociated products **6c** and **24d** by 2.4 kcal/mol, and than **6d** and **25d** by 45.4 kcal/mol. Thus it seems unlikely that the products of the reaction of **1b** with R'NCO (i.e. $[CpFe(CO)_2(CNR')]^+$) are derived from a species (i.e., **4d**) which is analogous to the bis-insertion products of the reaction of **1a**,**b** with CyNCNCy (i.e. **4a**,**b**) – since the final step would then be energetically uphill. During the progress of the reaction of **1b** and PhNCO, an ESI-MS peak was detected corresponding to an intermediate which has the mass of one equivalent of the borylene complex plus two equivalents of isocyanate. This intermediate is subsequently converted into the major isonitrile product $[CpFe(CO)_2(CNPh)]^+$. The fact that heterocycle cleavage in the bis-insertion product **4d** to give the dissociated products (**6c** and **24d**) is calculated to be significantly endothermic, means that this ESI-MS detected intermediate is unlikely to be **4d**. However, the formation of the **6c** from other insertion intermediates (e.g. **13d** and **13e**) which also have a mass consistent with the assimilation of two molecules of isocyanate by the borylene starting material, is thermodynamically feasible. This finding, together with the fact that the barriers to dissociation of **13d**,**e**

are relatively high (ca. 20 kcal/mol) – such that these species may attain measureable concentrations in solution – offers **13d**,**e** as more viable candidate intermediates.

## [3.4] Conclusions

We have compared the mechanisms for the reactions of the iron borylene complexes $[CpFe(CO)_2(BNR_2)]^+$, (R = *i*-Pr, Cy) with the carbodiimide CyNCNCy and with the isocyanates R'NCO (R' = Ph, 2,6-Xyl, Cy). It has been shown that both carbodiimide and isocyanate substrates prefer insertion into the Fe=B bond rather than the B=N bond of the borylene complex. Mechanistic studies reveal that the carbodiimide reaction ultimately leads to the bis-insertion compounds $[CpFe(CO)_2C(NCy)_2B(NCy)_2CNR_2]^+$ (R = *i*-Pr, Cy) rather than to the isonitrile systems $[CpFe(CO)_2(CNR')]^+$ (via a net metathesis reaction), on the basis of both thermodynamic (product stability) and kinetic considerations (barrier heights). In case of isocyanates, the net metathesis reaction is a competitive pathway to insertion. The metathesis pathway is facile for isocyanate substrates if initial coordination at the boron atom occurs via the oxygen donor (which is kinetically favored); insertion chemistry is feasible when the isocyanate attacks initially via the nitrogen atom. However, further reaction of the mono-insertion product so formed with excess isocyanate offers a number of facile (low energetic barrier) routes to $[CpFe(CO)_2(CNR')]^+$ rather than to the formation of the bis-insertion product $[CpFe(CO)_2C(NR')(O)B(NR')(O)CNR_2]^+$ (R' = Ph, 2,6-Xyl, Cy) (i.e. the direct analogue of the observed products from the carbodiimide reaction). Moreover, the

thermodynamic stability of these hypothetical spirocyclic species means that they are unlikely to be viable intermediates in the formation of the final isonitrile products, which are then better rationalized in terms of competing pathways, rather than differing extents of reaction along similar trajectories.

## [3.5] References


1. Billups, W. E.; Liufolin, M. A. *Buckminsterfullerene*; VCH Publishers: 1993. Terminal borylene complexes were first reported in 1998: (a) Cowley, A.H.; Lomeli, V.; Voigt, A. *J. Am. Chem. Soc.* **1998**, *120*, 6401. (b) Braunschweig, H.; C. Kollann, Englert, U. *Angew. Chem., Int. Ed.* **1998**, *37*, 3179. For recent reviews see: (c) Braunschweig, H.; Rais, D. *Heteroatom Chem.* **2005**, *16*, 566. (d) Braunschweig, H.; Kollann, C.; Rais, D. *Angew. Chem., Int. Ed.* **2006**, *45*, 5254. (e) Aldridge, S.; Kays, D.L. *Main Group Chem.* **2006**, *5*, 223. (f) Braunschweig, H.; Kollann, C.; Seeler, F. *Struct. Bond.* **2008**, *130*, 1.
2. For recent quantum chemical studies of borylene and related compounds, see, for example: (a) Bickelhaupt, F.M.; Radius, U.; Ehlers, A.W.; Hoffmann, R.; Baerends, E.J. *New J. Chem*. **1998**, *26*, 1. (b) Ehlers, A. W.; Baerends, E. J.; Bickelhaupt, F. M.; Radius, U. *Chem. Eur. J.* **1998**, *4*, 210. (c) Radius, U.; Bickelhaupt, F. M.; Ehlers, A. W.; Goldberg, N.; Hoffmann, R. *Inorg. Chem.* **1998**, *37,* 1080. (d) Boehme, C.; Frenking, G. *Chem. Eur. J.* **1999**, *5*, 2184. (e) Macdonald, C.L.B.; Cowley, A.H. *J. Am. Chem. Soc*. **1999**, *121*, 12113. (f) Uddin, J.; Boehme, C.; Frenking, G. *Organometallics* **2000**, *19*, 571. (g) Boehme, C.; Uddin, J.; Frenking, G. *Coord. Chem. Rev.* **2000**, *197*, 249. (h) Frenking, G.; Frohlich, N. *Chem. Rev.* **2000**, *100,* 717. (i) Chen, Y.; Frenking, G. *Dalton Trans*. **2001**, 434. (j) Uddin, J.; Frenking, G. *J. Am. Chem. Soc*. **2001**, *123*, 1683. (k) Bollwein, T.; Brothers, P.J.; Hermann, H.L.; Schwertfeger, P. *Organometallics* **2002**, *21*, 5236. (l)

Aldridge, S.; Rossin, A.; Coombs, D. L.; Willock, D. J. *Dalton Trans.* **2004**, 2649.

3. For examples of the fundamental patterns of reactivity demonstrated to date for terminal borylene complexes, see: [cycloaddition] (a) Braunschweig, H.; Herbst, T.; Rais, D.; Seeler, F. *Angew. Chem., Int. Ed.* **2005**, *44*, 7461. (b) Aldridge, S.; Jones, C.; Gans-Eichler, T.; Stasch, A.; Kays, D.L.; Coombs, N.D.; Willock, D.J. *Angew. Chem., Int. Ed.* **2006**, *45*, 6118. (c) Braunschweig, H.; Fernandez, I.; Frenking, G.; Radacki, K.; Seeler, F. *Angew. Chem., Int. Ed.* **2007**, *46,* 5215. [insertion] (d) Coombs, D.L.; Aldridge, S.; Rossin, A.; Jones, C.; Willock, D.J. *Organometallics* **2004**, *23*, 2911. (e) Pierce, G. A.; Aldridge, S.; Jones, C.; Gans-Eichler, T.; Stasch, A.; Coombs, N. D.; Willock, D. J. *Angew. Chem. Int. Ed*. **2007**, *46*, 2043. (f) Braunschweig, H.; Dewhurst, R.D.; Herbst, T.; Radacki, K. *Angew. Chem., Int. Ed.* **2008**, *47*, 5978. [metathesis] (g) Kays, D. L.; Day, J. K.; Ooi, L.-L.; Aldridge, S. *Angew. Chem. Int. Ed*. **2005**, *44*, 7457. (h) Braunschweig, H.; Burzler, M.; Radacki, K.; Seeler, F. *Angew. Chem., Int. Ed.* **2007**, *46*, 8071. [hydride transfer] (i) Kays, D. L.; Day, J. K.; Aldridge, S.; Harrington, R. W.; Clegg, W. *Angew. Chem. Int. Ed*. **2006**, *45*, 3513. [intermetal borylene transfer] (j) Braunschweig, H.; Colling, M.; Kollann, C.; Stammlker, H.G.; Neumann, B. *Angew. Chem., Int. Ed.* **2001**, *40*, 2298. (k) Braunschweig, H.; Colling, M.; Hu, C.; Radacki, K. *Angew. Chem., Int. Ed.* **2003**, *43*, 205. (l) Braunschweig, H.; Forster, M.; Radacki, K. *Angew. Chem., Int. Ed.* **2006**, *45*, 2132. (m) Braunschweig, H.; Radacki, K.; Rais, D.; Uttinger, K.; *Organometallics* **2006**, *25*, 5159. (n) Braunschweig, H.; Forster, M.;

Radacki, K.; Seeler, F.; Whittell, G.R. *Angew. Chem., Int. Ed.* **2007**, *46*, 5212. (o) Braunschweig, H.; Forster, M.; Kupfer, T.; Seeler, F. *Angew. Chem., Int. Ed.* **2008**, *47*, 5981. [substitution at metal centre] (p) Irvine, G.J.; Rickard, C.E.F.; Roper, W.R.; Williamson, A.; Wright, A. *Angew. Chem., Int. Ed.* **2000**, *39*, 948. (q) Blank, B.; Colling,-Hendelkens, Kollann. C.; Radacki, K.; Rais, D.; Uttinger, K.; Whittell, G.R.; Braunschweig, H. *Chem. Eur. J.* **2007**, *13*, 4770. (r) Pierce, G. A.; Vidovic, D.; Kays, D. L.; Coombs, N. D.; Thompson, A. L.; Jemmis, E. D.; De, S.; Aldridge, S. *Organometallics* **2009**, *28*, 2947. [addition/substitution at boron] (s) Rickard, C.E.F.; Roper, W.R.; Williamson, A.; Wright, L.J. *Organometallics* **2002**, *21*, 4862. (t) Coombs, D.L.; Aldridge, S.; Jones, C.; Willock, D.J. *J. Am. Chem. Soc.* **2003**, *125*, 6356. (u) Kays, D. L.; Rossin, A.; Day, J. K.; Ooi, L. L.; Aldridge, S. *Dalton Trans.* **2006**, 399. (v) Braunschweig, H.; Kraft, K.; Kupfer, T.; Radacki, K.; Seeler, F. *Angew. Chem., Int. Ed.* **2008**, *47*, 4931.

4. De, S.; Parameswaran, P.; Jemmis, E. D. *Inorg. Chem.* **2007**, *46*, 6091.
5. For preliminary DFT results see: (a) Pierce, G. A.; Coombs, N. D.; Willock, D. J.; Day, J. K.; Stasch, A.; Aldridge, S. *Dalton Trans.* **2007**, 4405. For related synthetic and mechanistic studies of boron amidinates and guanidinates see: (b) Jefferson, R.; Lappert, M.F.; Prokai, B.; Tilley, B.P. *J. Chem. Soc. A,* **1966**, 1585. (c) Ergezinger, C.; Weller, F.; Dehnicke, K. *Z. Naturforsch., Teil B* **1988**, *43*, 1621. (d) Ansorge, A.; Brauer, D.J.; Burger, H.; Dorrenbach, F.; Hagen, T.; Pawelke, G.; Weuter, W. *J. Organomet. Chem.* **1991**, *407*, 283. (e) Terry, M.R.; Mercando, L.A.; Kelley, C.;

Geoffroy, G.L.; Nombel, P.; Lugen, N.; Mathieu, R.; Ostrander, R.L.; Owens-Whitmire, B.E.; Rheingold, A.L. *Organometallics* **1994**, *13*, 843. (f) Blais, P.; Chivers, T.; Downward, A.; Parvez, M. *Can. J. Chem.* **2000**, *78*, 10. (g) Hill, N.J.; Moore, J.A.; Findlater, M.; Cowley, A.H. *Chem. Commun.* **2005**, 5462. (h) Hill, N.J.; Findlater, M.; Cowley, A.H. *Dalton Trans.* **2005**, 3229. (i) Findlater, M.; Hill, N.J.; Cowley, A.H. *Polyhedron* **2006**, *25*, 983. (j) Lu, Z.; Hill, N.J.; Findlater, M.; Cowley, A.H. *Inorg. Chim. Acta* **2007**, *360*, 1316. (k) Findlater, M.; Hill, N.J.; Cowley, A.H. *Dalton Trans.* **2008**, 4419.

6. Hehre, W. J.; Radom, L.; Schleyer, P. v. R.; Pople, J. A. *Ab Initio Molecular Orbital Theory*; Wiley: New York, 1986.
7. (a) Becke, A. D. *J. Chem. Phys.* **1993**, *98*, 5648. (b) Becke, A. D. *Phys. Rev. A* **1988**, *38*, 3098. (c) Lee, C.; Yang, W.; Parr, R. G. *Phys. Rev. B* **1988**, *37*, 785. (d) Perdew, J. P. *Phys. Rev. B* **1986**, *34*, 7406. (e) Perdew, J. P. *Phys. Rev. B* **1986**, *33*, 8822.
8. (a) Hay, P. J.; Wadt, W. R. *J. Chem. Phys.* **1985**, *82*, 270. (b) Wadt, W. R.; Hay, P. J. *J. Chem. Phys.* **1985**, *82*, 284. (c) Hay, P. J.; Wadt, W. R. *J. Chem. Phys.* **1985**, *82*, 299. (d) Weigend, F.; Ahlrichs, R. *Phys. Chem. Chem. Phys.* **2005**, *7*, 3297.
9. Gaussian 03, Revision C.02, Frisch, M. J.; Trucks, G. W.; Schlegel, H. B.; Scuseria, G. E.; Robb, M. A.; Cheeseman, J. R.; Montgomery, Jr., J. A.; Vreven, T.; Kudin, K. N.; Burant, J. C.; Millam, J. M.; Iyengar, S. S.; Tomasi, J.; Barone, V.; Mennucci, B.; Cossi, M.; Scalmani, G.; Rega, N.; Petersson, G. A.; Nakatsuji, H.; Hada, M.; Ehara, M.; Toyota, K.; Fukuda,

R.; Hasegawa, J.; Ishida, M.; Nakajima, T.; Honda, Y.; Kitao, O.; Nakai, H.; Klene, M.; Li, X.; Knox, J. E.; Hratchian, H. P.; Cross, J. B.; Bakken, V.; Adamo, C.; Jaramillo, J.; Gomperts, R.; Stratmann, R. E.; Yazyev, O.; Austin, A. J.; Cammi, R.; Pomelli, C.; Ochterski, J. W.; Ayala, P. Y.; Morokuma, K.; Voth, G. A.; Salvador, P.; Dannenberg, J. J.; Zakrzewski, V. G.; Dapprich, S.; Daniels, A. D.; Strain, M. C.; Farkas, O.; Malick, D. K.; Rabuck, A. D.; Raghavachari, K.; Foresman, J. B.; Ortiz, J. V.; Cui, Q.; Baboul, A. G.; Clifford, S.; Cioslowski, J.; Stefanov, B. B.; Liu, G.; Liashenko, A.; Piskorz, P.; Komaromi, I.; Martin, R. L.; Fox, D. J.; Keith, T.; Laham, M. A.; Peng, C. Y.; Nanayakkara, A.; Challacombe, M.; Gill, P. M. W.; Johnson, B.; Chen, W.; Wong, M. W.; Gonzalez, C.; and Pople, J. A. Gaussian, Inc., Wallingford CT, 2004.

10. Kolle, P.; Noth, H. *Chem. Ber.* **1986**, *119*, 313.
11. For related mechanistic studies of carbodiimide insertion reactivity towards main group and transition metal systems see, for example: (a) Holland, A. W.; Bergman, R. G. *J. Am. Chem. Soc.* **2002**, *124*, 9010. (b) Montilla, F.; Rio, D. d.; Pastor, A.; Galindo, A. *Organometallics* **2006**, *25*, 4996. (c) Brazeau, A. L.; Wang, Z.; Rowley, C. N.; Barry, S. T. *Inorg. Chem.* **2006**, *45*, 2276.
12. (a) East, A.L.L.; Johnson, C.S.; Allen, W.D. *J. Chem. Phys.* **1993**, *98*, 1299. (b) Harmony, M.D.; Laurie, V.W.; Kuczkowski, R.L.; Schwendeman, R.H.; Ramsay, D.A.; Lovas, F.J.; Lafferty, W.J.; Maki, A.G. *J. Phys. Chem. Ref. Data* **1979**, *8*, 619.

13. The imaginary frequency vector of the transition state **9c**-**3c** corresponds to the ring closing step (i.e. the attack of the lone pair on N3 to the B atom). It is to be noted that the Me group at the N3 in **9c** has to be rotated to undergo cyclization, but the structure with the lone pair on N3 facing towards the B atom is converged to **3c** on optimization. A partially optimized geometry of this structure is 1.5 kcal/mol lower in energy than the intermediate **9c**. This indicates that the structure with the lone pair on N3 facing toward B atom would have lower energy than **9c**. Since we calculate the energy barrier for the transition state **9c**-**3c** from the intermediate **9c**, the energy barrier turns out to be negative (-3.2 kcal/mol).
14. (a) Huheey, J.E.; Keiter, E.A.; Keiter, R.L. *Inorganic Chemistry: Principles of Structure and Reactivity* 4th edition; Harper Collins: New York, 1997. (b) Grant, D.J.; Dixon, D.A. *J. Phys. Chem. A.* **2006**, *110*, 12955.
15. For a proposal of a related [2+2] cycloaddition process, see: Brauer, D. J.; Buchheim-Spiegel, S.; Bürger, H.; Gielen, R.; Pawelke, G.; Rothe, J. *Organometallics* **1997**, *16,* 5321.
16. The boron containing dissociated products formed from intermediates **11c** and **12c** are not stable.
17. Unlike MeNCNMe (energy of lone pair on N = -0.2362 a.u.), the lone pair on N (-0.2834 a.u.) in MeNCO is greatly delocalized into the C-O π* orbital and as a result less available for donation. This is reflected in the corresponding energy barrier for the N-attack pathway in MeNCO (18.2 kcal/mol) as compared to the energy barrier in the case of MeNCNMe (5.2 kcal/mol).

18. Emsley, J. *The Elements*; Oxford University Press: Oxford, 1991.

19. See, for example, Aldridge, S.; Kays, D.L.; Al-Fawaz, A.; Jones, K.M.; Horton, P.N.; Hursthouse, M.B.; Harrington, R.W.; Clegg, W. *Chem. Commun.* **2006**, 2578, and references therein.

20. (a) Bernskoetter, W.H.; Olmos, A.V.; Pool, J.A.; Lobkovsky, E.; Chirik, P.J. *J. Am. Chem. Soc.* **2006**, *128*, 10696. (b) Tsai, C.-F.; Chen, H.-J.; Chang, J.-C.; Hung, C.-H.; Lai, C.-C.; Hu, C.-H.; Huang, J.-H. *Inorg. Chem.* **2004**, *43*, 2183. (c) Mitchell, G.P.; Tilley, T.D. *J. Am. Chem. Soc.* **1997**, *119*, 11236. (d) Kuninobu, Y.; Tokunaga, Y.; Kawata, A.; Takai, K. *J. Am. Chem. Soc.* **2006**, *128*, 202.

21. Gurvich, L.V.; Veyts, I.V.; Alcock, C.B. *Thermodynamic Properties of Individual Substances*, 4th edition; Hemisphere Publishing: New York, 1989.

22. (a) Huber, K.P.; Herzberg, G. *Molecular Spectra and Molecular Structure. IV. Constants of Diatomic Molecules*; Van Nostrand Reinhold Co.: New York, 1979. (b) Herzberg, G., *Electronic Spectra and Electronic Structure of Polyatomic Molecules*; Van Nostrand: New York, 1966. (c) Ruscic, B.; Curtis, L.; Berkowitz, J. *J. Chem. Phys.* **1984**, *80*, 3962.

# CHAPTER 4

## STRUCTURE AND BONDING IN MONO AND DINUCLEAR METALLACYCLES OF $Cp_2M$ (M = Ti, Zr) WITH C2-CUMULENIC LIGANDS XCCX (X = O, NH): A COMPARISON WITH METALLACYCLES OF 1,2,3-BUTATRIENE AND 1,3-BUTADIYNE

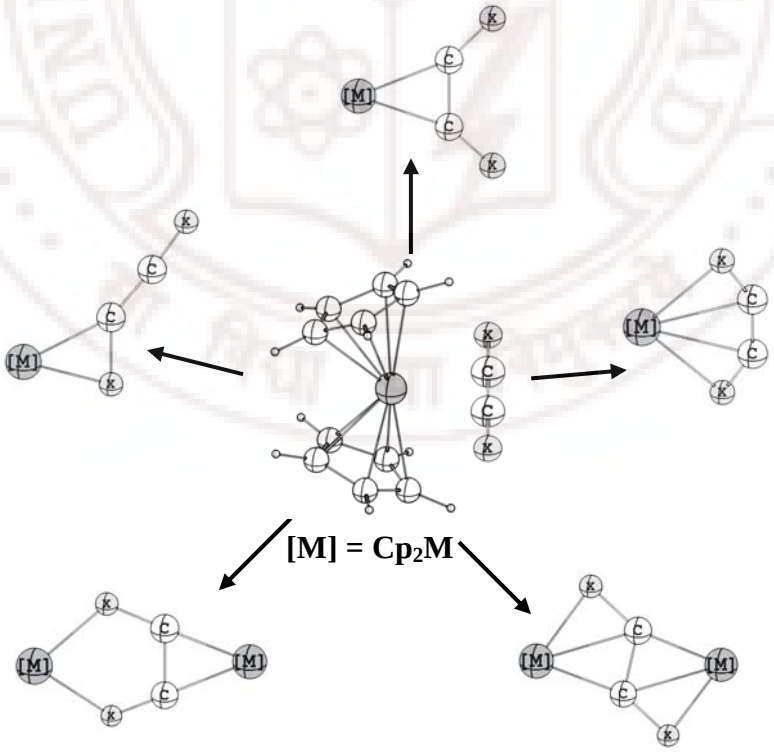

# Abstract

A comprehensive structural and bonding analysis of three- and five-membered metallacycles and cis- and trans- dinuclearmetallabicycles of $Cp_2M$ with the C2-cumulene ligands XCCX (X = O, NH) is presented. These are compared with the corresponding complexes of 1,2,3-butatriene and 1,3-butadiyne. The energetics for the conversion of the three membered metallacycles **1MX** to the five memebered metallacycles **3MX** revealed greater tendency for Zr to stabilize five memebered metallacycles. Unlike the metallacycles of 1,2,3-butatriene and 1,3-butadiyne the cis-dinuclear metallabicycles of heterocumulene ligands were calculated to be more stable as compared to their trans isomers. The energy barrier for the cis to trans conversion of the dinuclearbimetallacycles (**4MX** to **5MX**) was calculated to be very high. Fragment molecular orbital analysis showed that the structural and energetic differences of the metallacycles of C2-heterocumulenic ligands can be attributed to the additional occupancy in the perpendicular π molecular orbital $\Psi_{\perp}^{3}$ as compared to 1,2,3-butatriene and 1,3-butadiyne.

## [4.1] Introduction

The unstable 14-electron titanocene $Cp_2Ti$ and zirconocene $Cp_2Zr$ have been playing a vital role in synthetic organometallic chemistry,[1] olefin polymerization, [2] organometallic chemical vapour deposition[3] and C-C coupling and cleavage reactions.[4,5] The carbene-type frontier orbitals of $Cp_2M$ (M = Ti, Zr) help in the reaction with unsaturated compounds such as 1,3-butadiynes and 1,2,3-butatrienes to form several mono and dinuclear metallacycles (Scheme 4.1).[4j,4k,6]

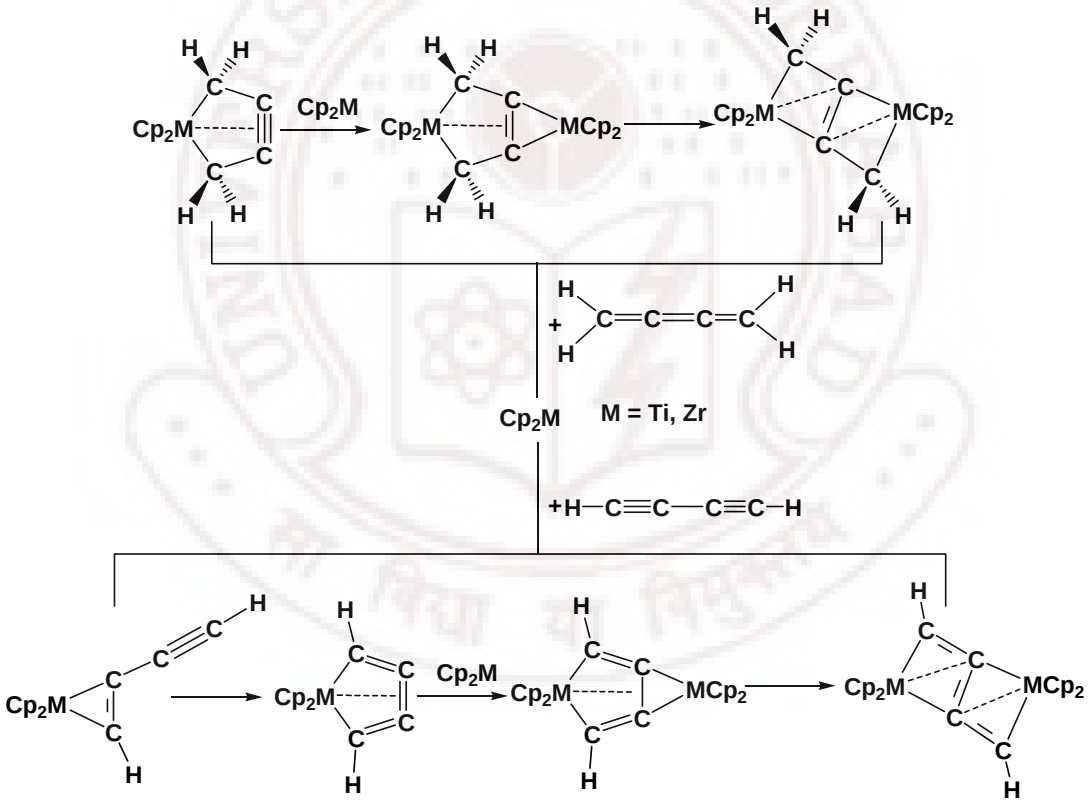


**Scheme 4.1**: Schematic representations of the reactivity of $Cp_2M$ (M = Ti, Zr) with 1,2,3-butatriene and 1,3-butadiyne.

The stability of these metallacycles as compared to their organic counterpart is attributed to the interaction of in-plane π molecular orbitals of unsaturated carbon

skeleton with the vacant d-orbital of the metallocene fragments.[7] The structure, bonding and reactivity of these complexes are well studied both experimentally and theoretically. However, as per our knowledge similar three and five membered 2,5-dihetero-substituted metallacycles are not reported. Rosenthal and coworkers suggested involvement of 1-zircona-2,5-diazacyclopent-3-yne as an intermediate in the reaction of isocyanide ligands with 1-zirconacyclopent-3-yne, which leads to a substituted 1-zircona-2,5-diazacyclopent-3-ene, anellated with a cyclobutene ring having two exocyclic double bonds.[8]

On the other hand, dinuclear complexes of 2,5-dihetero substituted metallacycles have been reported in the literature (Scheme 4.2). Hessen and co-workers reported the formation of $Cp_2Ti$-(Cl)[$\mu$-($\eta^3$:$\eta^3$-RNCCNR)]Ti(Cl)$Cp_2$ (R = *t*-Bu) containing NCCN skeleton in a trans geometry.[9] The complexes of Mo,[10] Nb[11,12] and Ta[12] are reported with the NCCN skeleton in a cis geometry. Structurally similar dinuclear complex of ruthenium and tungsten[13] with SCCS skeleton in a cis geometry and uranium complex[14] of cyclic-$C_3O_3^{2-}$ having a planar skeletal arrangement have also been reported. This intrigue the study of structure, nature of bonding and stability of 2,5-dihetero-substituted metallacycles. Here, we present a comprehensive structural and bonding analysis of three and five membered mono-metallacycles as well as cis and trans dinuclearmetallabicycles of $Cp_2M$ with ethenedione (OCCO) and ethenediimine (HNCCNH) ligands. The structure, bonding and stability of these metallacycles are also compared with the metallacycles of 1,2,3-butatriene and 1,3-butadiyne.

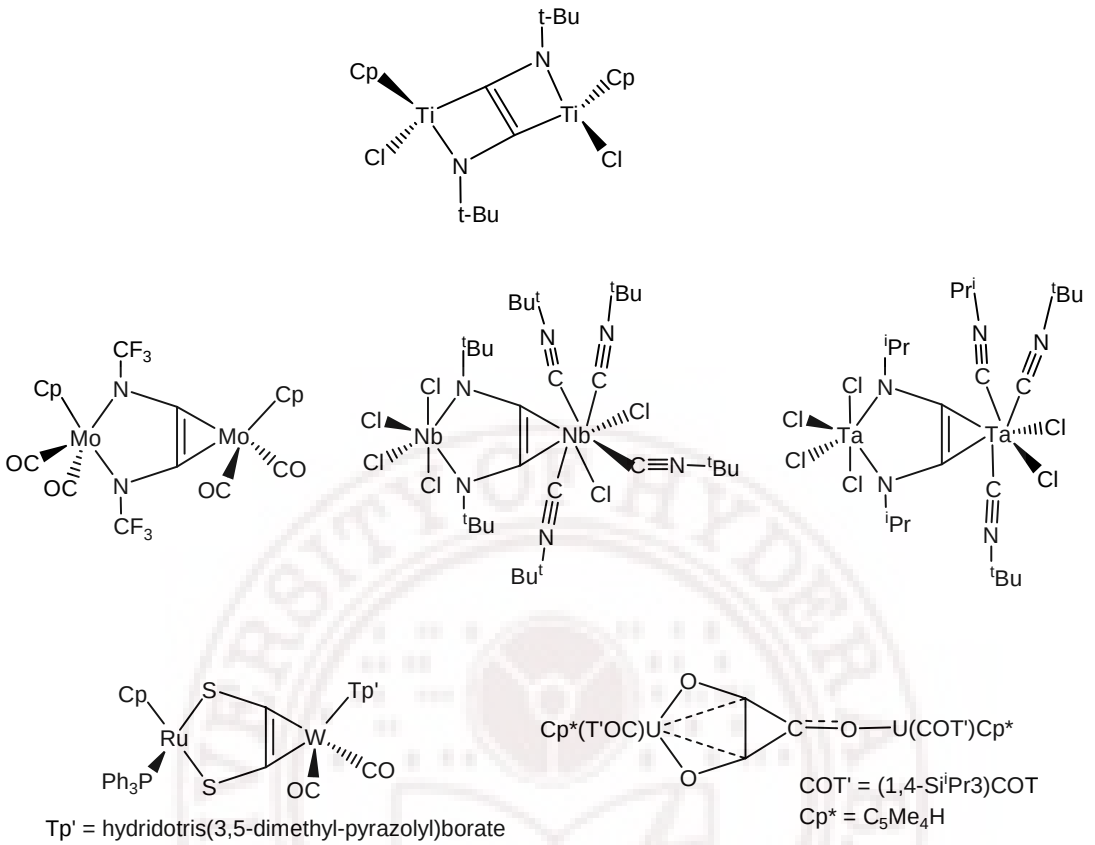


**Scheme 4.2:** Experimentally known dinuclear complexes of 2,5-dihetero metallacycles.

## [4.2] Computational Details

All structures were optimized using the hybrid HF-DFT method, B3LYP/LANL2DZ, based on Becke's three-parameter functional including Hartree-Fock exchange contribution with a non-local correction for the exchange potential proposed by Becke[15,16a-b] together with the non-local correction for the correlation energy suggested by Lee et al.[15,16c] The LANL2DZ basis set uses the effective core potential (ECP) of Hay and Wadt.[15,17] The nature of the stationary points were characterized by vibrational frequency calculations. The Gaussian 03 program package was used in this study.[18] We used fragment molecular orbital approach[19] to

understand the geometrical and bonding patterns in mono and dinuclear metallacycles of $Cp_2M$ (M = Ti, Zr) with C2-cumulenic ligands XCCX (X = O, NH).

## [4.3] Results and Discussion

These metallacycles can be best described by the interaction of the bent metallocene fragments $Cp_2Ti$ and $Cp_2Zr$ with ligands XCCX (X = O, NH, CH, $CH_2$). The structure, bonding and stability of these metallacycles were studied. The discussion starts with metallocene fragments and the ligands fragments separately. This is followed by the analysis on three- and five membered metallacycles. Lastly, the structure and bonding in cis- and trans-dinuclearmetallabicycles are described.

### [4.3.1] Bent Metallocenes, $Cp_2M$ (M = Ti, Zr)

The titanocene and zirconocene are highly reactive and generated in the reaction medium for immediate reaction.[20] The high reactivity of these 14-electron metallocences arises due to their electron deficiency, which forces them to accept electrons from other ligands. Unlike ferrocene, they have bent geometry. These bent metallocenes $Cp_2M$ (M = Ti, Zr) have three in-plane valence molecular orbitals and two electrons ($d^2$ system) available for bonding with other ligands (Figure 4.1). This is similar to the frontier orbitals of carbene,[4b] where carbene has two in-plane molecular orbitals in contrast to three in-plane molecular orbitals of the $Cp_2M$ fragment. These three frontier molecular orbitals of $Cp_2M$ fragment can rehybridize to form suitably oriented molecular orbitals for the interaction with the ligand.

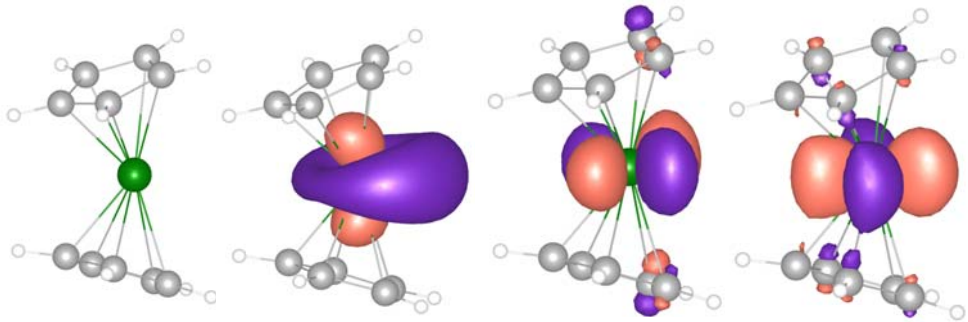

$Cp_2M$
M = Ti, Zr

**Figure 4.1:** Frontier molecular orbitals of $Cp_2M$ (M = Ti, Zr).

### [4.3.2] C2-Cumulenic Ligands, XCCX (X = O, NH)

The C2-cumulenic organic ligands considered for this study are ethenedione (OCCO),[21] ethenediimine (HNCCNH).[22] The reactivity of these ligands is attributed to the π electrons in their unsaturated backbone. Despite their highly reactive nature, the linear or quasi-linear hetero cumulenes have been characterized by neutralization-reionization and collisional activation mass spectrometry.[21c,22a] The geometrical and bonding patterns of the two hetero-cumulenic ligands as compared to 1,3-butadiyne (HCCCCH)[23] and 1,2,3-butatriene ($H_2CCCCH_2$)[24] are given below.

The linear OCCO ligand has one imaginary frequency (i424 $cm^{-1}$) in its singlet electronic state. The imaginary frequency vector corresponds to the dissociation into two CO molecules.[21d] However, the linear OCCO ligand is minimum in the triplet electronic ground state.[21d] The C-C bond length in this ligand is (1.288Å) closer to the central C-C bond length of 1,2,3-butatriene (1.266Å) (Scheme 4.3).

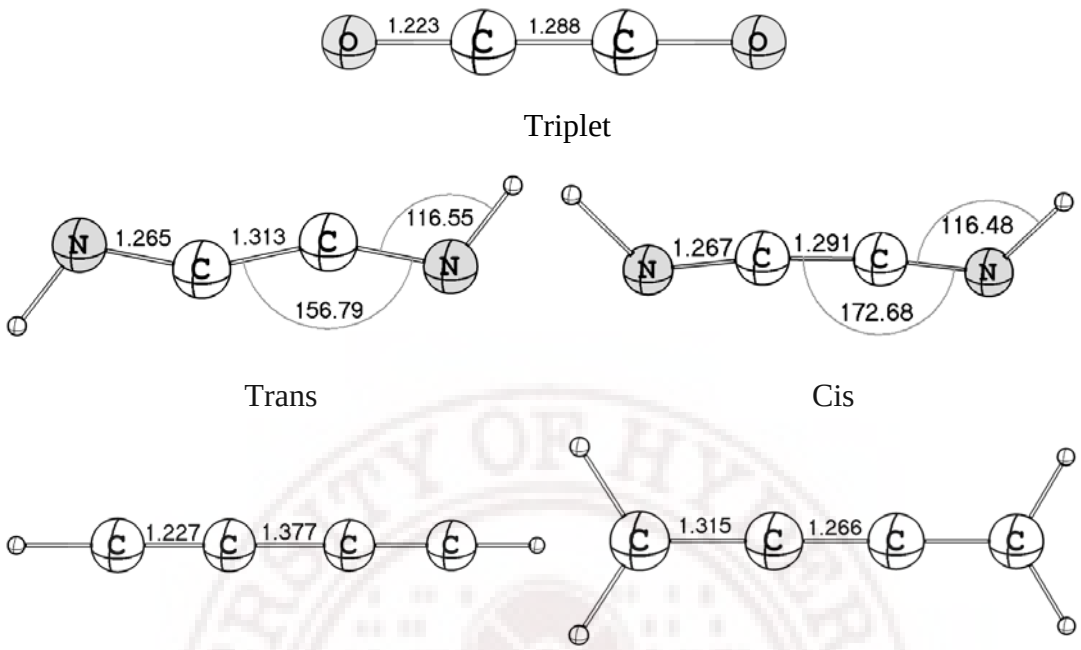


**Scheme 4.3**: Optimized geometries and important geometrical parameters of the ligands XCCX (X = O, NH, CH, $CH_2$) at the B3LYP/LANL2DZ level of theory. Distances are in Å and bond angles are in degree.

On the other hand, the MO description shows that the in-plane and perpendicular π-type frontier orbitals form four linear combinations, much the same in symmetry as the π orbitals of 1,3-butadiyne. The highest occupied molecular orbitals (HOMO) of OCCO are degenerate singly occupied $\Psi_{\parallel}^{3}$ and $\Psi_{\perp}^{3}$, which correspond to the degenerate lowest unoccupied molecular orbitals (LUMO) of 1,3-butadiyne in symmetry (Scheme 4.4). These molecular orbitals (MO) have bonding interaction between the central carbon atoms, which in turn shortens the C-C bond length in OCCO molecule with respect to the central C-C bond distance (1.377Å) in 1,3-butadiyne. Hence, the bonding of OCCO can be better described by considering this ligand as dianion of 1,3-butadiyne.

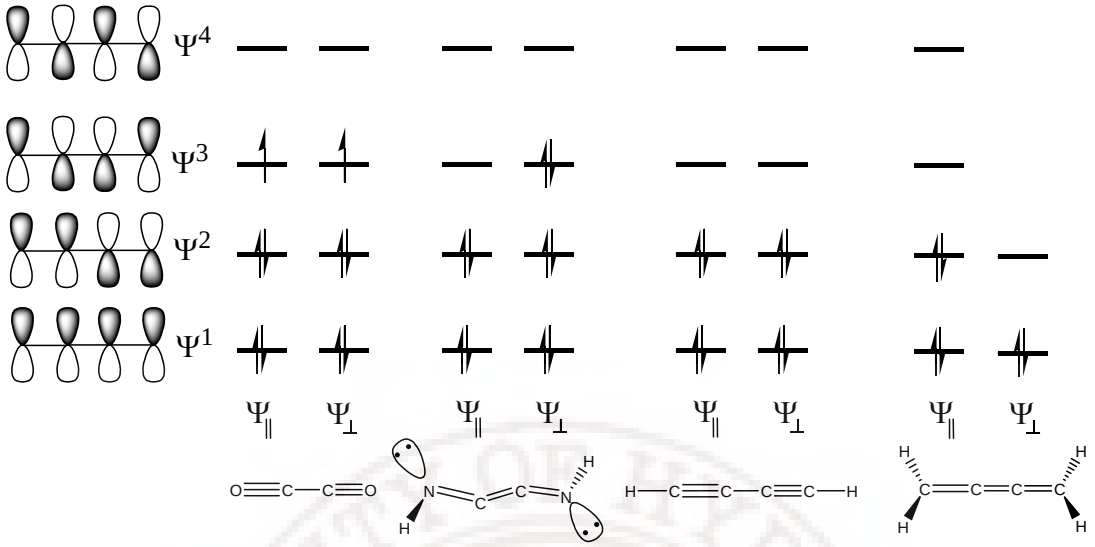


**Scheme 4.4:** Schematic representation of the in-plane ($\Psi_{\parallel}$) and perpendicular ($\Psi_{\perp}$) π MOs of the ligand XCCX (X = O, NH, CH, $CH_2$).

The ligand HNCCNH is non-linear and the trans isomeric form is slightly (1.6 kcal/mol) more stable than the cis-form. The C-C bond length of cis-isomer (1.291Å) is more close to the central C-C bond length of the 1,2,3-butatriene (1.266Å), whereas the C-C bond length in the trans-isomer (1.313Å) is amidst of the central C-C bond length of the 1,2,3-butatriene (1.266Å) and 1,3-butadiyne (1.377Å) (Scheme 4.3). However, the perpendicular π MOs $\Psi^2_{\perp}$ and $\Psi^3_{\perp}$ of HNCCNH correspond to the interaction of lone pair on N atoms with the C-C π MO (Scheme 4.4). It is to be noted that the perpendicular central C-C π MO ($\Psi^1_{\perp}$) in 1,2,3-butatriene is localized. Hence one can consider the bonding of HNCCNH ligand as similar to 1,2,3-butatriene, where terminal $CH_2$ groups are replaced by isolobal NH groups having lone pair. It is interesting to note that the number of filled in plane π MOs are same in all these four ligands (for bent OCCO), but the

two hetero-cumulenic ligands have two additional electrons in the perpendicular π MO.

**[4.3.3] Three-Membered Metallacycles, 1MX and 2MX**

The terminal C-X as well as the central C-C bond of ligand XCCX (X = O, NH, CH, $CH_2$) can coordinate with $Cp_2M$ fragment to form three membered metallacycles **1MX** and **2MX** respectively. Rosenthal and coworkers reported the metallacycle similar to **1MCH** with titanocene and (t-Bu)CCCC(t-Bu) ligand.[27] They had also characterized by NMR technique the three membered metallacycle of titanocene with terminal C-C bond of hexatriyne.[29] The complexes **1MO** and **1MCH** can be described as formed by the interaction of one of the formal C-X triple bond with $Cp_2M$ fragment. On the other hand, the complexes **1MNH** and **1MCH$_2$** can be viewed as formed by the interaction of one of the formal C-X double bond with the $Cp_2M$ fragment.

The bonding in **1MX** can be described as similar to Dewar-Chatt-Duncanson[25] description of π donation from the C-X bond and back-donation from $Cp_2M$ fragment to the C-X π* molecular orbital. The MOs in XCCX corresponding to these interactions are $\Psi^2_{\|}$ and $\Psi^3_{\|}$. The $Cp_2M$ fragment does not have proper symmetrical metal d-orbitals to interact with the perpendicular π MOs of the ligands. Thus, the LUMO of the complex **1MX** is an unoccupied in-plane metal d-orbital.[7g,h] This bonding description explains elongation of the coordinated C-X bond in the complex **1MX** as compared to the free ligands (Schemes 4.3 and 4.5). The more

elongated C-X bond of **1ZrX** as compared to **1TiX** is attributed to the bigger size of Zr.[7]

Owing to the similar bonding description for the **1MX** for all X, we have calculated the dissociation energy (Eq. 4.1, Table 4.1) to understand the relative stability as X changes from O to $CH_2$. The order of the dissociation energy of **1MX** is **1MO** > **1MNH** > **1MCH** > **1MCH$_2$**. This indicates that OCCO ligand forms the most stable three membered metallacycle than the other ligands. The dissociation energy of Zr complexes is higher than Ti complexes (Table 4.1). The free ligands OCCO and HNCCNH are highly reactive due to the presence of two additional π elelctrons as compared to HCCCCH and $H_2CCCCH_2$ ligands (Scheme 4.4). This results in high dissociation energies for **1MO** and **1MNH**.

According to earlier discussion, the central C-C bond of $H_2CCCCH_2$ is a localized double bond. The ligand HNCCNH can be considered as isolobal to $H_2CCCCH_2$ where the $CH_2$ group is replaced by NH having lone pair. Hence, these ligands can interact with the $Cp_2M$ fragment through the central C-C π bond to form three membered metallacycle **2MX**. This is not possible for the ligands HCCCCH and OCCO. However, the structure **2ZrNH** is not a stationary point on the potential energy surface. The complex similar to **2MCH$_2$** has been recently reported by Suzuki and coworkers by the interaction of $Cp_2Zr$ with 1,3,5-hexatriyne.[26]

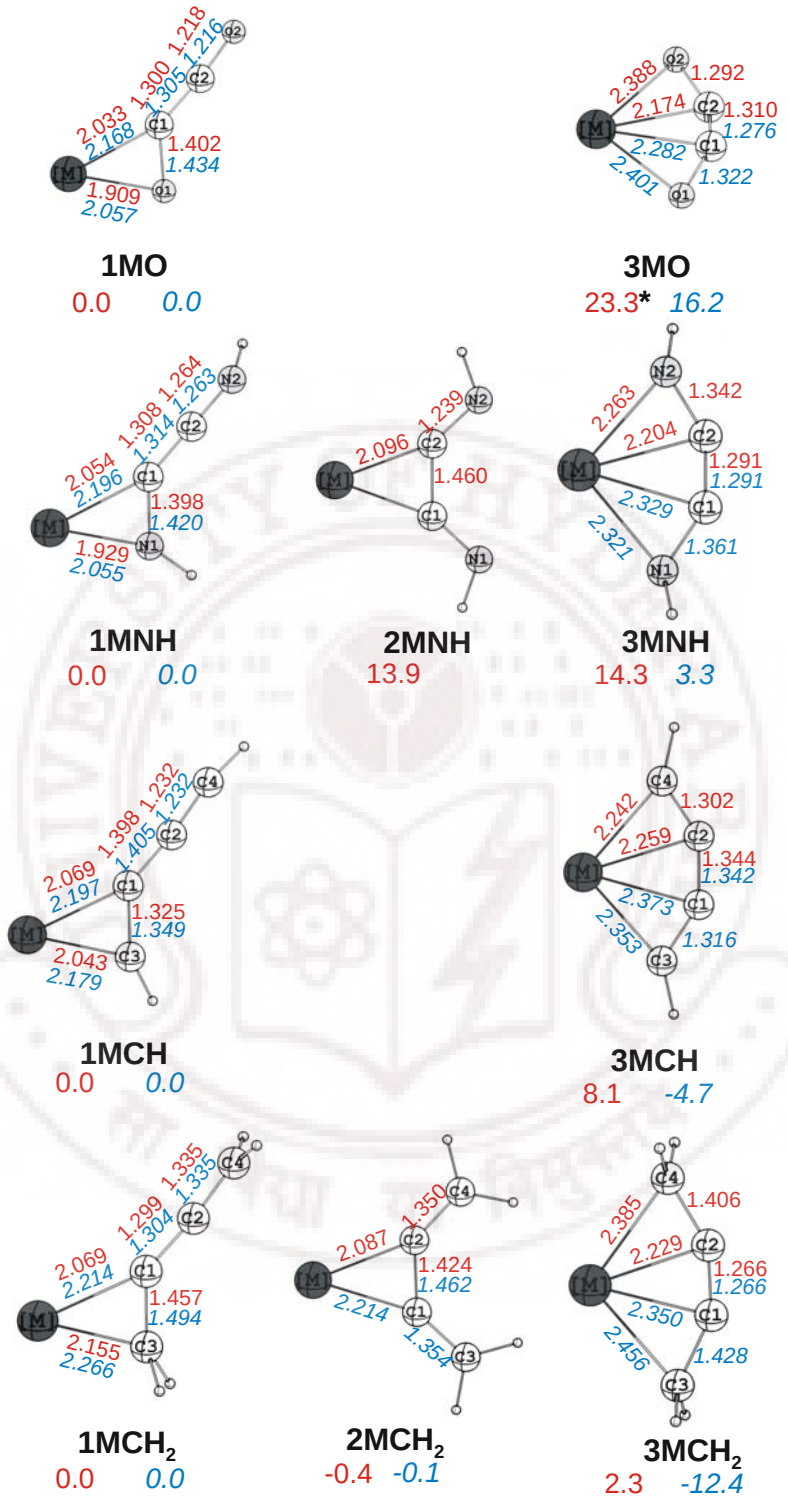


**Scheme 4.5:** Schematic representation of various three- and five membered metallacycles $Cp_2M(XCCX)$ (X = O, NH, CH, $CH_2$; M = Ti, Zr). Important bond lengths (Å) and relative energies (kcal/mol) at B3LYP/LANL2DZ level of theory are given. The values in normal font corresponds to M = Ti and that in italics corresponds to M = Zr. *The structure **3TiO** is a first order saddle point on the potential energy surface.

The complex **1TiNH** is more stable than **2TiNH** by 13.9 kcal/mol, while the relative energies of **1MCH$_2$** and 2**MCH$_2$** are comparable (Scheme 4.5). This trend in the energy difference can be explained by considering the more susceptible π MO at the C-N bond as compared to C-C bond in HNCCNH ligand. It is to be noted that the $Cp_2M$ fragment is coordinated to C-C π bond in both **1MCH$_2$** and 2**MCH$_2$**, whereas it is coordinated to the C-N π bond in **1TiNH** and C-C π bond in **2MNH**. This is reflected in the higher dissociation energy of **1TiNH**.

**1MX** → $Cp_2M$ + XCCX ΔE1 (4.1)

**2MX** → $Cp_2M$ + XCCX ΔE2 (4.2)

**3MX** → $Cp_2M$ + XCCX ΔE3 (4.3)

**Table 4.1:** Dissociation energy (kcal/mol) of metallacycles **1MX**, **2MX** and **3MX** into $Cp_2M$ (M = Ti, Zr) fragments and XCCX ligands (X = O, NH, CH, $CH_2$).

| X | **1MX** (ΔE1) | | **2MX** (ΔE2) | | **3MX** (ΔE3) | |
|---|---|---|---|---|---|---|
| | Ti | Zr | Ti | Zr | Ti | Zr |
| O | 53.9 | 81.9 | - | - | - | 65.6 |
| NH | 46.0 | 73.1 | 32.1 | - | 31.7 | 69.8 |
| CH | 28.6 | 52.8 | - | - | 20.5 | 57.5 |
| $CH_2$ | 25.9 | 47.3 | 26.3 | 47.4 | 23.6 | 59.7 |

### [4.3.4] Five-Membered Metallacycles, 3MX

The three membered metallacycle **1MX** has in-plane vacant metal d-orbital (LUMO) and hence is electron deficient.[7g,h] The electron deficiency can be overcome by accepting electrons from the electron donating ligands such as $PMe_3$[6b] or by coordinating with the other unsaturated C-X π bond of the same ligand. One such possibility is the rearrangement to five membered metallacycle **3MX**. It has been reported that the five membered metallacyclocumulenes (**3MCH**) exist in a dynamic equilibrium with their respective three membered isomers (**1MCH**).[27,7d]

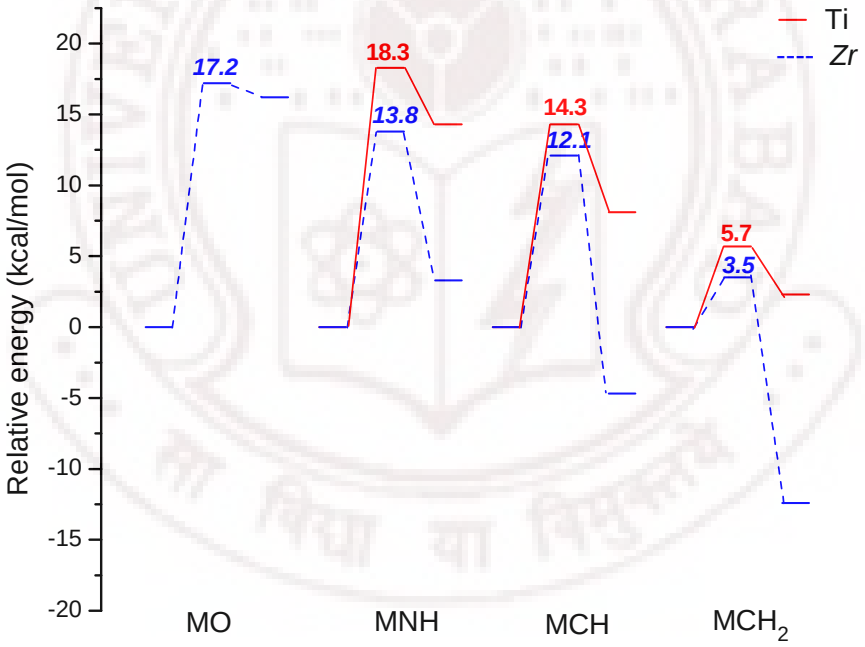


**Figure 4.2:** Reaction energy profile for the conversion of **1MX** to **3MX** (**X** = **O**, **NH**, **CH**, **$CH_2$**) at B3LYP/LANL2DZ level of theory.

The energetic for the transformation of the three membered metallacycle **1MX** to five membered metallacycle **3MX** is shown in figure 4.2. It is interesting to note that as X changes from O to $CH_2$, the relative stability of the five membered metallacycle **3MX** increases. The gradual decrease in the energy barrier for this

rearrangement supports the trend in the relative energy. This trend is more pronounced for $Cp_2Zr$ complexes. All the five membered metallacycles of $Cp_2Ti$ are less stable than the corresponding three membered metallacycles. This can be attributed to less preference of smaller Ti to form five membered metallacycles.[7] However, the complexes **3ZrO** and **3ZrNH** are less stable while the complexes **3ZrCH** and **3ZrCH$_2$** are more stable than the corresponding three membered metallacycles.

It is to be noted that **3TiO** is a transition state for the sliding of the $Cp_2M$ fragment along OCCO ligand for the conversion of **1TiO** to its degenerate alternative. The energy barrier for this transformation is 23.3 kcal/mol. The three membered metallacycle **1ZrO** is more stable than **3ZrO** by 16.2 kcal/mol and the energy barrier for the transformation is 17.2 kcal/mol. The closer energies and geometrical parameters of **3ZrO** and the transition state indicate more feasibility for the rearrangement of **3ZrO** to **1ZrO**. However, the relative energy difference between the complexes **1ZrNH** and **3ZrNH** is 3.3 kcal/mol while the complex **1TiNH** is more stable than **3TiNH** by 14.3 kcal/mol.

The above-mentioned relative energies can be rationalized based on the FMO approach. As we have described in Scheme 4.4, the ligands differ in the number of perpendicular $\pi$ electrons. Thus, one can expect the in-plane interaction in all these **3MX** to be similar. Earlier studies show that the interaction between the in-plane $\pi$ MOs of the ligands and the metal fragment is similar for both **3MCH** and **3MCH$_2$**.[7d,e] The bonding in these complexes can be described by the donation of two filled in-plane $\pi$ MOs ($\Psi_{\|}^1$ and $\Psi_{\|}^2$) to the metal fragment and back donation of

metal d-electrons to third in-plane π MO ($\Psi^3_{\parallel}$). However, these two metallacycles differs in the perpendicular π MOs. The metallacycle **3MCH$_2$** has a localized perpendicular π MO $\Psi^1_{\perp}$ at C1-C2 bond whereas **3MCH** has delocalized perpendicular π MOs $\Psi^1_{\perp}$ and $\Psi^2_{\perp}$. As a result, the C1-C2 bond distance in **3MCH$_2$** is shorter (1.266Å for both **3TiCH$_2$** and **3ZrCH$_2$**) than **3MCH** (1.344Å for **3TiCH** and 1.342Å for **3ZrCH**). The comparable dissociation energy of **3MCH$_2$** and **3MCH** also supports this bonding description (Eq. 4.3, Table 4.1). On the contrary, **1MCH** has higher dissociation energy than **1MCH$_2$** (Eq. 4.1, Table 4.1). It has to be noted that **1MCH$_2$** is formed by the interaction of formal double bond of 1,2,3-butatriene with $Cp_2M$ fragment whereas, the complex **1MCH** is formed by the interaction of one of the formal triple bond of 1,3-butadiyne.

Even though the linear OCCO ligand is stable in triplet electronic state, the cis-OCCO fragment in **3ZrO** can be considered as similar to HNCCNH ligand. The interaction of the in-plane π MOs in **3ZrO** and **3MNH** is similar to that of the metallacyclocumulene and metallacyclopentyne (Figure 4.3). The third filled perpendicular π MO ($\Psi^3_{\perp}$) has anti-bonding interaction between the terminal C-N and C-O bonds (Scheme 4.4). This anti-bonding interaction results in the distortion of the five membered ring in **3ZrO** and **3MNH**. The similarity in the bonding is adequately reflected in similar dissociation energy of **3ZrO** (65.6 kcal/mol) and **3ZrNH** (69.8 kcal/mol). On the other hand, the dissociation energy of **1ZrO** (81.9 kcal/mol) is higher than **1ZrNH** (73.1 kcal/mol). This indicates that the interaction of $Cp_2Zr$ fragment with the terminal C-O bond in OCCO ligand is stronger as

compared to the interaction of the terminal C-N bond in HNCCNH ligand in **1ZrNH**. Hence, the relative energy difference between three membered and five membered metallacycles is higher in **MO** as compared to **MNH**. The higher stability of the three membered metallacycles **1MO** and **1MNH** can be ascribed to stronger in-plane interaction between the metal and terminal C-O and C-N π bond as compared to the interaction between the metal and non-planar OCCO and NHCCNH ligands in five membered metallacycle. This indicates that the relative energy difference between the three membered (**1MX**) and five membered (**3MX**) metallacycles is mainly governed by the relative stability of the metallacycle **1MX**.

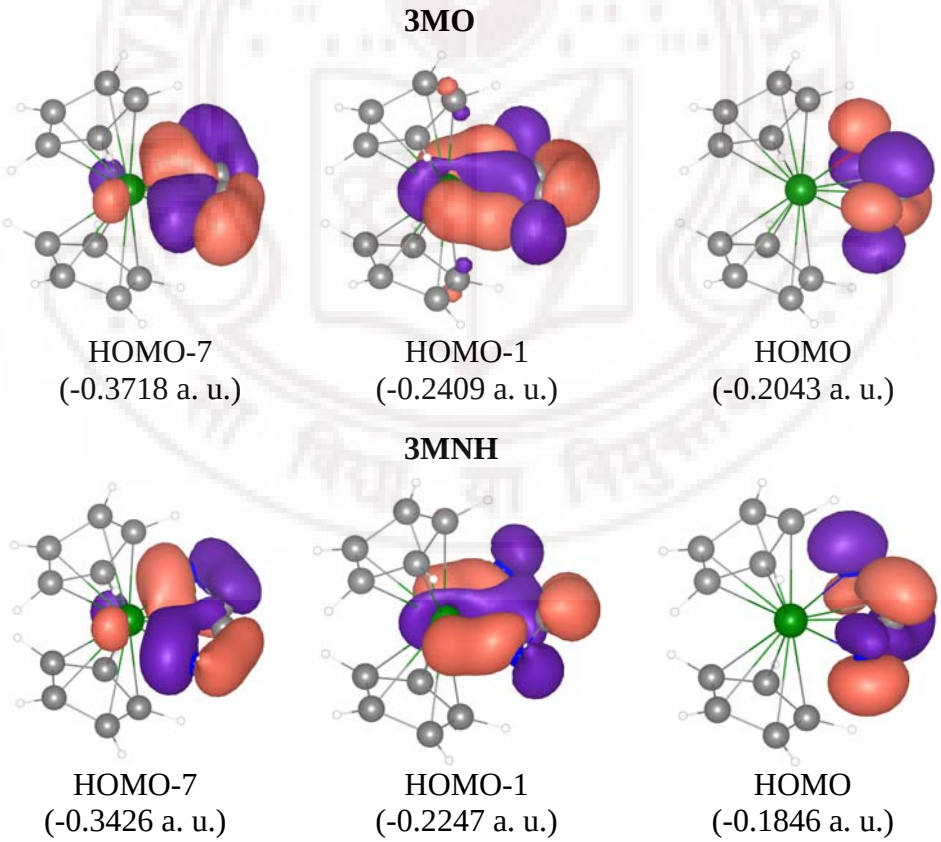


**Figure 4.3:** Important MOs of **3MO** and **3MNH** showing in-plane interaction with the $Cp_2M$ fragment and non-interacting perpendicular π MO of the ligands.

**[4.3.5] Dimetallabicycles, 4MX and 5MX**

The interaction of another $Cp_2M$ fragment with the central C-C bond of the five membered metallacycle **3MX** can lead to the dinuclear metallacycle **4MX**, where XCCX fragment is in cis orientation. The M1-C1 (M1-C2) distance is longer and M1-X1 (M1-X2) distance is shorter in **4MX** as compared to the corresponding distances in **3MX** (Schemes 4.5 and 4.6). This variation in bond length is more predominant in **4MO** and **4MNH**. It is to note that the five membered ring (MXCCX) in **3MCH** and **3MCH$_2$** are planar whereas it is non-planar in **3MO** and **3MNH**. The XCCX fragment in **3MO** and **3MNH** are in out-of-plane trans orientation with respect to the central C1-C2 bond whereas it is in cis orientation in **4MX**. All the cis dinuclear complexes except **4MCH** are non-planar. The non planarity of these complexes can be measured by the bending angles θ1 and θ2, which are the deviations of M1 and M2 from the XCCX plane respectively (Figure 4.4).

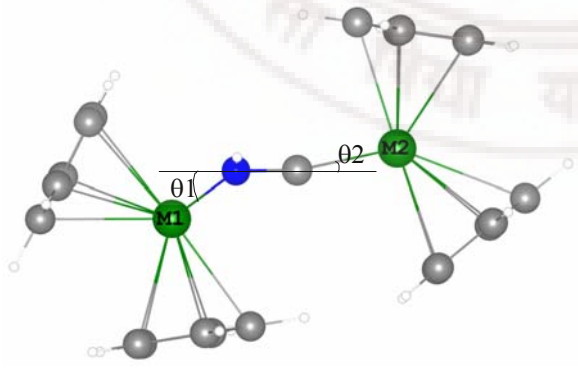


| X | Ti | | Zr | |
|---|---|---|---|---|
| | θ1 | θ2 | θ1 | θ2 |
| O | 20.2 | 9.6 | 14.5 | 3.4 |
| NH | 23.7 | 13.7 | 26.4 | 11.8 |
| CH | 0.0 | 0.0 | 0.0 | 0.0 |
| $CH_2$ | 6.0 | -2.1 | 15.9 | -0.8 |

**Figure 4.4:** Schematic representation of **4MX**. The bending angles θ1 and θ2 are the deviations of M1 and M2 from the XCCX plane respectively.

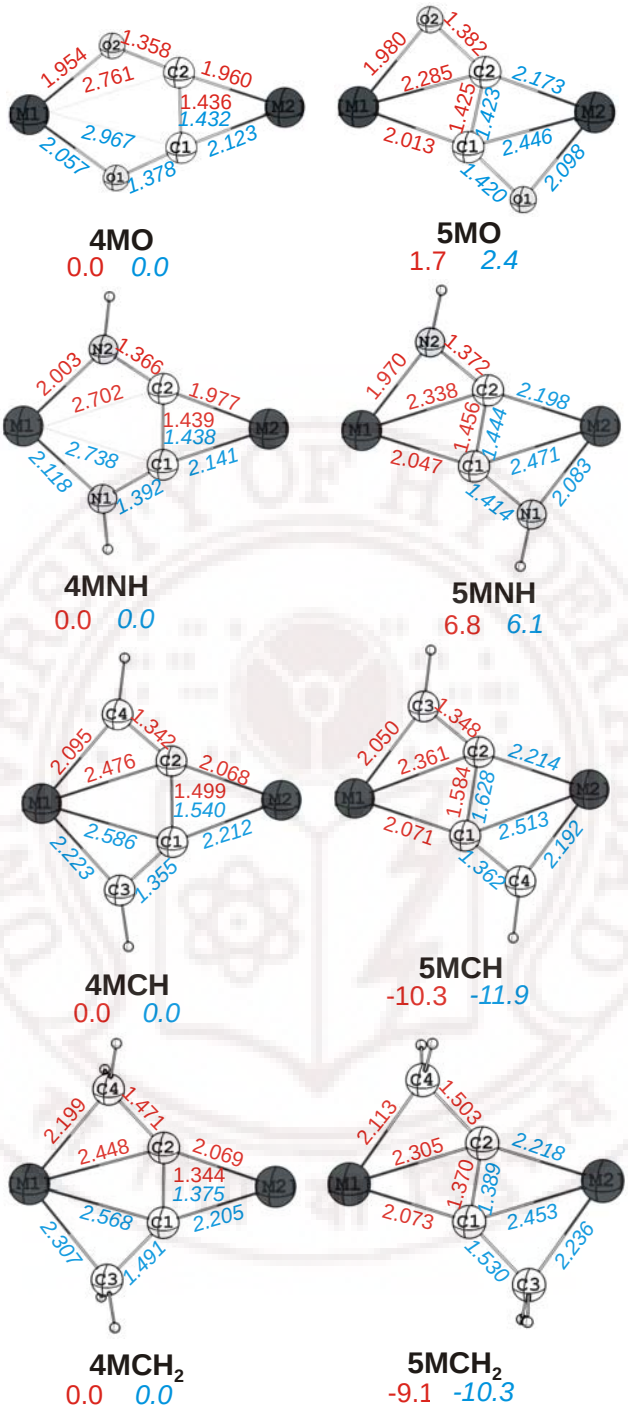


**Scheme 4.6:** Schematic representation of dinuclearbimetallacycles $Cp_2M(XCCX)MCp_2$, (X = O, NH, CH and $CH_2$). Important bond lengths (Å) and relative energies (kcal/mol) at B3LYP/LANL2DZ level of theory are given. The values in normal font corresponds to M = Ti and that in italics corresponds to M = Zr.

These bending angles are larger when X = NH and O. The nitrogen atoms in **4MNH** are planar whereas pyramidal in **3MNH**. The non-planarity of **4MX** can be understood from the fragment molecular orbital approach by considering the out-of-plane cis-**3MX** interacting with second metallocene fragment. However, the metallacycles similar to **3MO** and **3MNH** in which XCCX in out-of-plane cis-orientation are not stationary points on the potential energy surface whereas, cis- and trans- metallacyclopentenes of $Cp_2M$ (Ti, Zr) are reported.[28] Earlier studies on the structural and bonding analysis showed that the five membered ring in the cis- as well as trans-isomer is pocked due to the large interaction between C=C double bond and metal center.[7e]

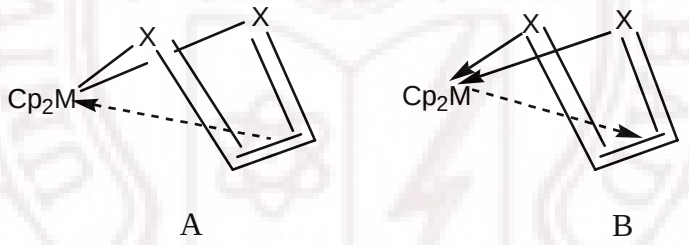


**Scheme 4.7:** Schematic representation of the bonding in cis five-membered metallacycle $Cp_2M(XCCX)$.

The bonding in cis-**3MO** and cis-**3MNH** can be explained by two fragmentation models (Scheme 4.7). Model A represents electron-sharing bond between X and $Cp_2M$ fragment whereas model B represents donor-acceptor interaction. According to bonding model A the ligand possesses two electrons in the third perpendicular $\pi$ MO $\Psi_{\perp}^{3}$. This MO can be stabilized by the interaction with the vacant d-orbital of the metallocene fragment. This can be effectively done by the out-of-plane distortion of the metallocene fragment. Earlier reports show similar bending of the metal fragment to reduce the antibonding interaction in the dinuclear

complex of 1,2,3-butatriene.[6b,7h] The similar distortion of the $Cp_2M$ fragment can also be explained from the fragmentation model B, where the metal electrons are donated to $\Psi^3_\perp$. On the contrary, the five membered metallacycles **3MCH** and **3MCH$_2$** have two electrons less in the π molecular orbitals, which in turn makes it planar. These frontier π MOs of cis-**3MX** interact with the second metallocene fragment to form cis-dimetallabicycles.

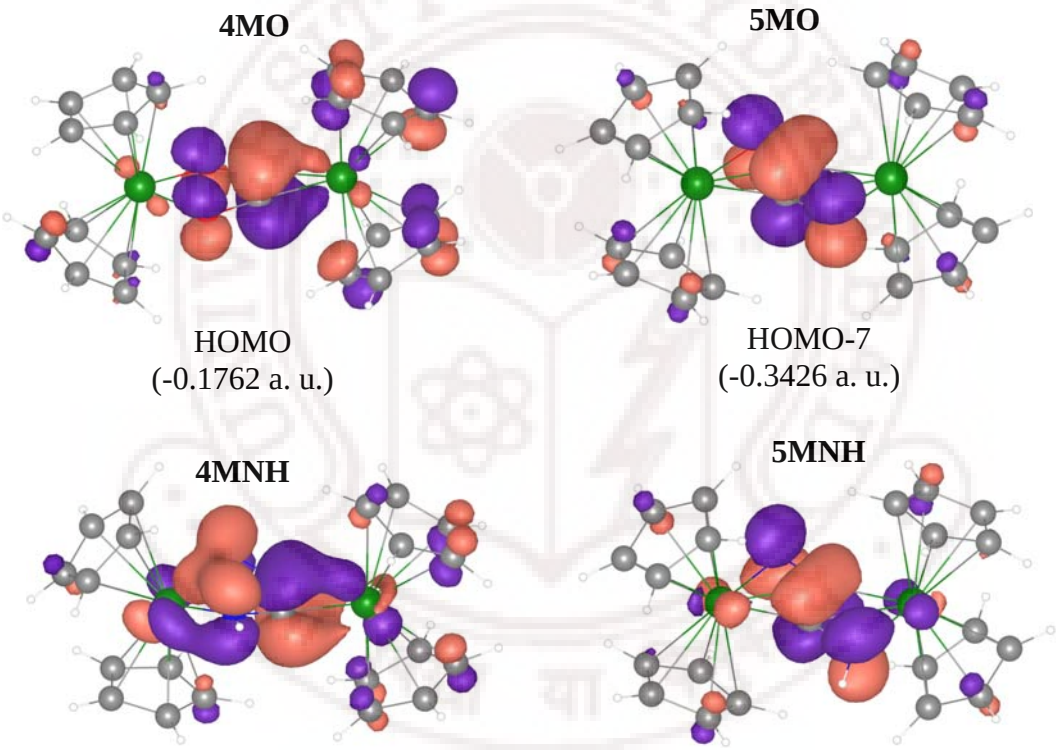


**Figure 4.5:** Important frontier MOs of (a) showing interaction of the metal fragments with the perpendicular π MO in **4MO** and **4MNH** and (b) non-interacting perpendicular π MO for **5MO** and **5MNH**.

This interaction of cis-**3MX** with second $Cp_2M$ fragment is similar to familiar DCD model.[25] The perpendicular ($\Psi^3_\perp$) and the in-plane ($\Psi^3_\parallel$) π MOs in

**3MO** and **3MNH** have same symmetry and can possibly interact with the vacant d-orbital of the second $Cp_2M$ fragment to form **4MX**. Likewise, the localized perpendicular π orbital ($\Psi^1_\perp$) in **3MCH$_2$** has the same symmetry as that of $\Psi^3_\parallel$. This leads to the rehybridization of the in-plane and perpendicular π MO and results in the bending of the two metallocene fragments with respect to XCCX plane (Figure 4.5). In contrast to that, the highest occupied in-plane ($\Psi^3_\parallel$) and perpendicular ($\Psi^2_\perp$) π MO of **3MCH** have different symmetry. This leads to planar geometry for **4MCH**.

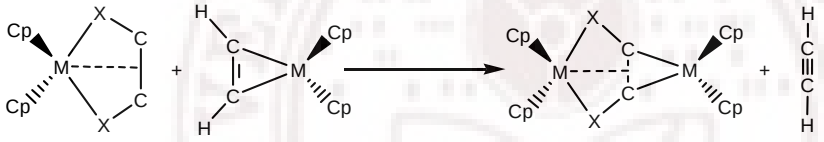


**3MX** **4MX** ΔE4 (4.4)

| X | O | NH | CH | $CH_2$ |
|---|---|---|---|---|
| Ti | - | -35.0 | -6.0 | 7.9 |
| Zr | -39.0 | -34.0 | -1.8 | 10.7 |

The reaction energy obtained from the isodesmic equation (Eq. 4.4) shows that the cis-dimetallabicycles **4MX** are more stable than the five membered metallacycles **3MX**. The reaction energy decreases when X changes from O to $CH_2$. The filled perpendicular π MO ($\Psi^3_\perp$) having anti bonding interaction at C-X bond in **3MO** and **3MNH** leads to their higher reactivity. As shown earlier, the stability of the cis-dinuclear metallacycle **4MX** will be greater when the C-C-H bond angle in the metal-acetylene complex is closer to the C1-C2-C3 angle of **3MX**.[7g,h] Therefore, the reaction energy ΔE4 is higher for **4MCH** as compared to **4MCH$_2$**.

The metal atom M2 in **4MX** has vacant d-orbital as similar to three membered metallacycle **1MX**. The electron deficiency due to this vacant metal d-orbital can be overcome by rearranging the XCCX skeleton to the trans orientation (**5MX**) or by accepting electrons from Lewis bases such as $PMe_3$.[6b] Unlike the cis-dimetallabicycles, the two $Cp_2M$ fragments in **5MX** are in the same plane with respect to XCCX ligand. The M1-C2 (M2-C1) distances are shorter as compared to M1-C1 (M1-C2) distances in **4MX** and longer as compared to M2-C1 (M2-C2) distance in **4MX** (Scheme 4.6). This indicates the better interaction of the metal fragments with in-plane π MO of the XCCX ligand in trans geometry. The energetic for the cis to trans transformation is exothermic when X = CH and $CH_2$ and is endothermic for other two complexes. However, the respective energy barriers for the transformation are very high (Figure 4.6).

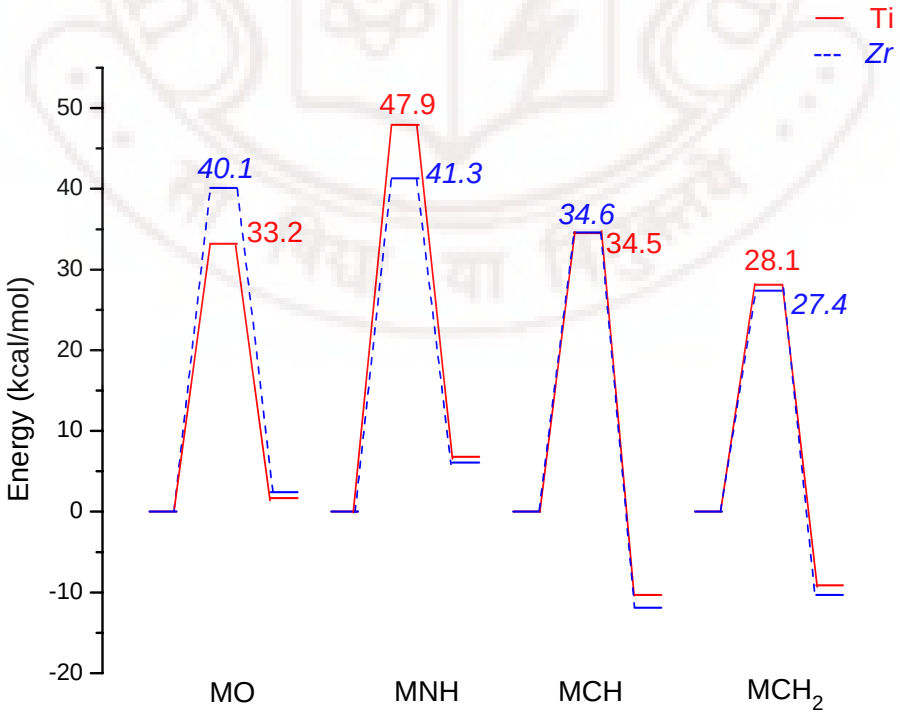


**Figure 4.6:** Reaction energy profile for the conversion of **4MX** to **5MX** (X = O, NH, CH, $CH_2$) at B3LYP/LANL2DZ level of theory.

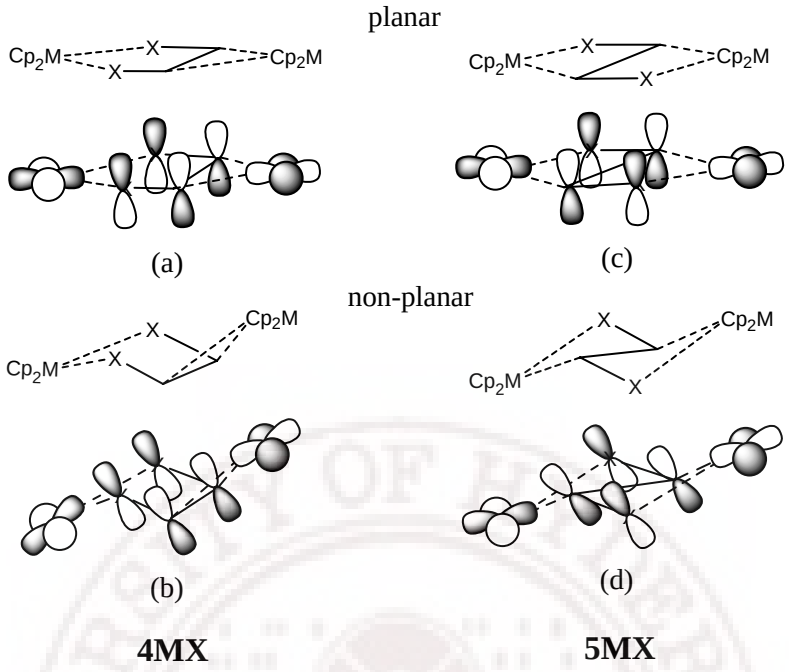


**Scheme 4.8**: Schematic representation of the orbital interaction in planar and non-planar geometry of **4MX** and **5MX**.

The perpendicular π MO $\Psi_{\perp}^{3}$ in planar cis-**4MX** (X = NH and O) does not have proper symmetry to interact with the in plane metal d-orbitals (Scheme 4.8a). However, it is stabilized by the interaction with $Cp_2M$ fragments in non-planar geometry (Scheme 4.8b). On the other hand, the $Cp_2M$ fragments do not have appropriate symmetric metal d-orbital to interact with $\Psi_{\perp}^{3}$ in both planar and non-planar geometry of trans-**5MX** (X = NH and O) (Schemes 4.8c and 4.8d). As a result, **5MNH** and **5MO** are planar unlike their cis isomers. This results in the destabilization of trans isomers **5MNH**, **5MO.**

## [4.4] Conclusions

The structure and bonding in mono- and dinuclear metallacycles of C2-cumulenic ligands OCCO and HNCCNH are studied in this chapter and compared

with the similar metallacycles of 1,2,3-butatriene and 1,3-butadiyne. The ligand OCCO can be described by considering it as dianion of 1,3-butadiyne and the ligand HNCCNH as similar to 1,2,3-butatriene, where terminal $CH_2$ groups are replaced by isolobal NH groups having lone pair. The number of filled in plane π MOs are same in all these four C2-cumulenic ligands, but the two hetero-cumulenic ligands have two additional electrons in the perpendicular π MO. The ligands $H_2CCCCH_2$ and HNCCNH can interact with the $Cp_2M$ fragment through the terminal C-X (X = $CH_2$, NH) as well as central C-C π bond to form three membered metallacycles **1MX** and **2MX**. On the other hand, three membered metallacycle **2MX** are not the stationary points on the potential energy surface for the ligands OCCO and HCCCCH. The interaction of the in-plane π MOs in **3ZrO** and **3MNH** is similar to that of the metallacyclocumulene and metallacyclopentyne. However, the anti-bonding interaction in the third filled perpendicular π MO results in distortion of the five membered ring of **3ZrO** and **3MNH**. The relative stability of the five membered metallacycle **3MX** as compared to three membered metallacycle **1MX** increases when X changes from O to $CH_2$. This trend is more pronounced in Zr complexes due to the bigger size of Zr. All the cis-dinuclear complexes except **4MCH** are non-planar and the bending of the metallocene fragments from the plane of XCCX are larger for X = NH and O. The rehybridization of the in-plane and perpendicular π MO results in the bending of the two metallocene fragments in **4MX** with respect to XCCX plane. Unlike the cis-dimetallabicycles, the two $Cp_2M$ fragments in **5MX** are in the same plane with respect to XCCX ligand.

## [4.5] References


1. Togni, A., Halterman, R. L. (Eds.), Metallocenes: Synthesis, Reactivity, Applications, Wiley-VCH, Weinheim, 1998, Vols. 1 and 2 and references therein.
2. (a) Alt, H. G.; Köppl, A. *Chem. Rev.* **2000**, *100*, 1205. (b) Resconi, L.; Cavallo, L.; Fait, A.; Piemontesi, F. *Chem. Rev.* **2000**, *100*, 1253. (c) Kaminsky, W. J. *Chem. Soc., Dalton Trans.* **1998**, 1413. (d) Bochmann, M. *J. Chem. Soc., Dalton Trans.* **1996**, 255. (e) Brintzinger, H. H.; Fischer, D.; Mulhaupt, R.; Rieger, B.; Waymouth, R. M. *Angew. Chem., Int. Ed. Engl.* **1995**, *34*, 1143.
3. (a) Choukroun, R.; Donnadieu, B.; Zhao, J.-S.; Cassoux, P.; Lepetit, C.; Silvi, B. *Organometallics* **2000**, *19*, 1901. (b) Choukroun, R.; Cassoux, P. *Acc. Chem. Res.* **1999**, *32*, 494. (c) Choukroun, R.; Donnadieu, B.; Zhao, J.; Cassoux, P.; Lepetit, C.; Silvi, B. *Organometallics* **2002**, *19*, 1901. (d) Danjoy, C.; Zhao, J. S.; Donnadieu, B.; Legros, J.-P.; Valade, L.; Choukroun, R.; Zwick, A.; Cassoux, P. *Chem. Eur. J.* **1998**, *4*, 1100.
4. (a) Sato, F.; Urabe, H.; Okamoto, S. *Chem. Rev.* **2000**, *100*, 2835. (b) Rosenthal, U.; Pellny, P.-M.; Kirchbauer, F. G.; Burlakov, V. V. *Acc. Chem. Res.* **2000**, *33*, 119. (c) Ohff, A.; Pulst, S.; Peulecke, N.; Arndt, P.; Burlakov, V. V.; Rosenthal, U. *Synlett.* **1996**, 111. (d) Negishi, E.; Takahashi, T. *Acc. Chem. Res.* **1994**, *27*, 124. (e) Buchwald, S. L.; Nielsen, R. B. *Chem. Rev.* **1988**, *88*, 1047. (f) Miura, K.; Funatsu, M.; Saito, H.; Ito, H.; Hosomi, A. *Tetrahedron Lett.* **1996**, *37*, 9059. (g) Rosenthal, U.; Burlakov, V. V. In *Titanium and Zirconium in Organic Synthesis, Marek, I.*

(Ed.), Wiley-VCH, Weinheim, 2002, p. 355. (h) Rosenthal, U.; Burlakov, V. V.; Arndt, P.; Baumann, W.; Spannenberg, A. *Organometallics* **2003**, *22*, 884. (i) Rosenthal, U. *Angew. Chem., Int. Ed.* **2004**, *43*, 3882. (j) Pulst, S.; Arndt, P.; Heller, B.; Baumann, W.; Kempe, R.; Rosenthal, U. *Angew. Chem., Int. Ed. Engl.* **1996**, *35*, 1112. (k) Pellny, P.-M.; Peulecke, N.; Burlakov, V. V.; Tillack, A.; Baumann, W.; Spannenberg, A.; Kempe, R.; Rosenthal, U. *Angew. Chem., Int. Ed. Engl.* **1997**, *36*, 2615.

5. (a) Rosenthal, U.; Görls, H. *J. Organomet. Chem.* **1992**, *439*, C36. (b) Rosenthal, U.; Ohff, A.; Tillack, A.; Baumann, W.; Görls, H. *J. Organomet. Chem.* **1994**, *468*, C4. (c) Erker, G.; Frömberg, W.; Mynott, R.; Gabor, B.; Krüger, C. *Angew. Chem., Int. Ed. Engl.* **1986**, *25*, 463. (d) Erker, G. *Angew. Chem., Int. Ed. Engl.* **1989**, *28*, 397. (e) Erker, G.; Frömberg, W.; Benn, R.; Mynott, R.; Angermund, D.; Kruger, C. *Organometallics* **1989**, *8*, 911. (f) Teuben, J. H.; de Liefde Meijer, H. J. *J. Organomet. Chem.* **1969**, *17*, 87. (g) Sekutowski, D. G.; Stucky, G. D. *J. Am. Chem. Soc.* **1976**, *98*, 1376. (h) Wood, G. L.; Knobler, C. B.; Hawthorne, M. F. *Inorg. Chem.* **1989**, *28*, 382. (i) Cuenca, T.; Gómez, R.; Gómez-Sal, P.; Rodriguez, G. M.; Royo, P. *Organometallics* **1992**, *11*, 1229. (j) Varga, V.; Mach, K.; Hiller, J.; Thewalt, U.; Sedmera, P.; Polasek, M. *Organometallics* **1995**, *14*, 1410. (k) Metzler, N.; Nöth, H. *J. Organomet. Chem.* **1993**, *454*, C5. (l) Cano, A.; Cuenca, T.; Galakhov, M.; Rodríguez, G. M.; Royo, P.; Cardin, C. J.; Convery, M. A. *J. Organomet. Chem.* **1995**, *493*, 17. (m) Lang, H.; Blau, S.; Nuber, B.; Zsolnai, L. *Organometallics* **1995**, *14*, 3216. (n) Heshmatpour, F.; Wocadlo, S.; Massa, W.; Dehnicke, K. *Acta Crystallogr.* **1995**, *C51*,

2225. (o) Hsu, D. P.; Davis, W. M.; Buchwald, S. L. *J. Am. Chem. Soc.* **1993**, *115*, 10394.

6. (a) Rosenthal, U.; Burlakov, V. V.; Arndt, P.; Baumann, W.; Spannenberg, A. *Organometallics* **2005**, *24*, 456, and references therein. (b) Bach, M. A.; Burlakov, V. V.; Arndt, P.; Baumann, W.; Spannenberg, A.; Rosenthal, U. *Organometallics* **2005**, *24*, 3047. (c) Suzuki, N.; Aihara, N.; Takahara, H.; Watanabe, T.; Iwasaki, M.; Saburi, M.; Hashizume, D.; Chihara, T. *J. Am. Chem. Soc*. **2004**, *126*, 60. (d) Suzuki, N.; Watanabe, T.; Iwasaki, M.; Chihara, T. *Organometallics* **2005**, *24*, 2065. (e) Rosenthal, U.; Ohff, A.; Baumann, W.; Kempe, R.; Tillack, A.; Burlakov, V. V. *Organometallics* **1994**, *13*, 2903. (f) Rosenthal, U.; Pulst, S.; Ohff, A.; Tillack, A.; Baumann, W.; Kempe, R.; Burlakov, V. V. *Organometallics* **1995**, *14*, 2961. (g) Pulst, S.; Kirchbauer, F. G.; Heller, B.; Baumann, W.; Rosenthal, U. *Angew. Chem. Int. Ed. Engl.* **1998**, *37*, 1925. (h) Rosenthal, U.; Ohff, A.; Baumann, W.; Kempe, R.; Tillack, A.; Burlakov, V. V. *Angew. Chem. Int. Ed. Engl.* **1994**, *33*, 1605. (i) Rosenthal, U.; Burlakov, V. V.; Arndt, P.; Baumann, W.; Spannenberg, A.; Shur, V. B. *Eur. J. Inorg. Chem.* **2004**, 4739. (j) Erker, G.; Venne-Duncker, S.; Kehr, G.; Kleigrewe, N.; Fröhlich, R.; Mück-Lichtenfeld, C.; Grimme, S. *Organometallics* **2004**, *23*, 4391. (k) Pellny, P.-M.; Kirchbauer, F. G.; Burlakov, V. V.; Baumann, W.; Spannenberg, A.; Rosenthal, U. *J. Am. Chem. Soc.* **1999**, *121*, 8313.

7. (a) Pavan Kumar, P. N. V.; Jemmis, E. D. *J. Am. Chem. Soc.* **1988**, *110*, 125. (b) Jemmis, E. D.; Giju, K. T. *Angew. Chem., Int. Ed.* **1997**, *36*, 606. (c) Jemmis, E. D.; Giju, K. T. *J. Am. Chem. Soc.* **1998**, *120*, 6952. (d)

Jemmis, E. D.; Phukan, A. K.; Giju, K. T. *Organometallics* **2002**, *21*, 2254. (e) Jemmis, E. D.; Phukan, A. K.; Jiao, H.; Rosenthal, U. *Organometallics* **2003**, *22*, 4958. (f) Burlakov, V. V.; Arndt, P.; Baumann, W.; Spannenberg, A.; Rosenthal, U.; Parameswaran, P.; Jemmis, E. D. *Chem. Commun.* **2004**, 2074. (g) Jemmis, E. D.; Parameswaran, P.; Phukan, A. K. *Mol. Phys.* **2005**, *103*, 897. (h) Bach, M. A.; Parameswaran, P.; Jemmis, E. D.; Rosenthal, U. *Organometallics* **2007**, *26*, 2149. (i) De, S.; Jemmis, E. D. In *Chemical Reactivity Theory A Density Functional View*; Chattaraj, P. K. Ed.; Taylor & Francis, CRC Press: Boca Raton, FL, 2009; p 193.

8. Bach, M. A.; Beweries, T.; Burlakov, V. V.; Arndt, P.; Baumann, W.; Spannenberg, A.; Rosenthal, U. *Organometallics* **2007,** *26*, 4592-4597.
9. Hessen, B.; Blenkers, J.; Teuben, J. H.; Helgesson G.; Jagner, S. *Organometallics*, **1989**, *8*, 830.
10. Lentz, D.; Brüdgam, I.; Hartl, H. *Angew. Chem., Int. Ed. Engl.*, **1984**, *23*, 525 and references cited therein.
11. Cotton, F. A.; Roth, W. J. *J. Am. Chem. Soc.* **1983**, *105*, 3734.
12. Cotton, F. A.; Duraj, S. A.; Roth, W. J. *J. Am. Chem. Soc.* **1984**, *106*, 6987.
13. Seidel, W. W.; Schaffrath, M.; Pape, T. *Angew. Chem., Int. Ed.* **2005**, *44*, 7798.
14. (a) Summerscales, O. T.; Cloke, F. G. N.; Hitchcock, P. B.; Green, J. C.; Hazari, N. *Science* **2006**, *311*, 829. (b) Summerscales, O. T.; Cloke, F. G. N.; Hitchcock, P. B.; Green, J. C.; Hazari, N. *J. Am. Chem. Soc.* **2006**, *128*, 9602. (c) Frey, A. S.; Cloke, F. G. N.; Hitchcock, P. B.; Day, I. J.; Green, J. C.; Aitken, G. *J. Am. Chem. Soc.* **2008**, *130*, 13816-13817.

15. Hehre, W. J.; Radom, L.; Schleyer, P. v. R.; Pople, J. A. *Ab Initio Molecular Orbital Theory*; Wiley: New York, **1986**.
16. (a) Becke, A. D. *J. Chem. Phys.* **1993**, *98*, 5648. (b) Becke, A. D. *Phys. Rev. A* **1988**, *38*, 3098. (c) Lee, C.; Yang, W.; Parr, R. G. *Phys. Rev. B* **1988**, *37*, 785.
17. (a) Hay, P. J.; Wadt, W. R. *J. Chem. Phys.* **1985**, *82*, 270. (b) Wadt, W. R.; Hay, P. J. *J. Chem. Phys.* **1985**, *82*, 284. (c) Hay, P. J.; Wadt, W. R. *J. Chem. Phys.* **1985**, *82*, 299.
18. Gaussian 03, Revision E.01, Frisch, M. J.; Trucks, G. W.; Schlegel, H. B.; Scuseria, G. E.; Robb, M. A.; Cheeseman, J. R.; Montgomery, Jr., J. A.; Vreven, T.; Kudin, K. N.; Burant, J. C.; Millam, J. M.; Iyengar, S. S.; Tomasi, J.; Barone, V.; Mennucci, B.; Cossi, M.; Scalmani, G.; Rega, N.; Petersson, G. A.; Nakatsuji, H.; Hada, M.; Ehara, M.; Toyota, K.; Fukuda, R.; Hasegawa, J.; Ishida, M.; Nakajima, T.; Honda, Y.; Kitao, O.; Nakai, H.; Klene, M.; Li, X.; Knox, J. E.; Hratchian, H. P.; Cross, J. B.; Bakken, V.; Adamo, C.; Jaramillo, J.; Gomperts, R.; Stratmann, R. E.; Yazyev, O.; Austin, A. J.; Cammi, R.; Pomelli, C.; Ochterski, J. W.; Ayala, P. Y.; Morokuma, K.; Voth, G. A.; Salvador, P.; Dannenberg, J. J.; Zakrzewski, V. G.; Dapprich, S.; Daniels, A. D.; Strain, M. C.; Farkas, O.; Malick, D. K.; Rabuck, A. D.; Raghavachari, K.; Foresman, J. B.; Ortiz, J. V.; Cui, Q.; Baboul, A. G.; Clifford, S.; Cioslowski, J.; Stefanov, B. B.; Liu, G.; Liashenko, A.; Piskorz, P.; Komaromi, I.; Martin, R. L.; Fox, D. J.; Keith, T.; Laham, M. A.; Peng, C. Y.; Nanayakkara, A.; Challacombe, M.; Gill, P.

M. W.; Johnson, B.; Chen, W.; Wong, M. W.; Gonzalez, C.; and Pople, J. A. Gaussian, Inc., Wallingford CT, 2004.

19. (a) Hoffmann, R. J. *Chem. Phys.* **1963**, *39*, 1397. (b) Hoffmann, R.; Lipscomb, W. N. *J. Chem. Phys.* **1962**, *36*, 2179. (c) Fujimoto, H.; Hoffmann, R. *J. Phys. Chem.* **1974**, *78*, 1167.
20. Lauher, J. W.; Hoffmann, R. *J. Am. Chem. Soc.* **1976**, *98*, 1729.
21. (a) Raine, G. P.; Schaefer III, H. F. Haddont, R. C. *J. Am. Chem. Soc.* **1983,** *105***,** 194-198. (b) Korkin, A. A.; Balkova, A.; Bartlett, R. J.; Boyd, R. J.; Schleyer, P. V. R. *J. Phys. Chem.* **1996,** *100*, 5702-5714. (c) Chen, H.; Holmes, J. L. *Int. J. Mass Spec. and Ion Proc.* **1994**, *133*, 111–119. (d) (a) Talbi, D.; Chandler, G. S. *J. Phys. Chem. A* **2000**, *104*, 5872-5881. (b) Korkin, A. A.; Balkova, A.; Bartlett, R. J.; Boyd, R. J.; Schleyer, P. v. R. *J. Phys. Chem.* **1996,** *100*, 5702-5714.
22. (a) Wong, M. W. *J. Mass Spec.* **1995**, *30*, 1144-1148 (b) Jobst, K. J.; Ruzni Hanifa, M.; Terlouw, J. K. *Chemical Physics Letters* **2008**, *462*, 152–157.
23. (a) Rogers, D. W.; Matsunaga, N.; McLafferty, F. J.; Zavitsas, A. A.; Liebman, J. F. *J. Org. Chem.*, **2004**, *69*, 7143–7147. (b) Sabbe, M. K.; Saeys, M. Reyniers, M.-F.; Van Speybroeck, G. B. M.-V. Waroquier, M. *J. Phys. Chem. A*, **2005**, *109*, 7466-7480. (c ) Jarowski, P. D.; Wodrich, M. D.; Wannere, C. S.; Schleyer, P. v. R.; Houk, K. N. *J. Am. Chem. Soc.*, **2004**, *126*, 15036–15037.
24. Morris, V. R.; Pollack, S. K. *J. Phys. Chem. B* **1998,** *102*, 5042-5046.
25. (a) Dewar, M. J. S. *Bull. Soc. Chim. Fr.* **1951**, C71-C79. (b) Chatt, J.; Duncanson, L. A. *J. Chem. Soc.* **1953**, 2939.

26. Suzuki, N.; Hashizume, D.; Yoshida, H.; Tezuka, M.; Ida, K.; Nagashima, S.; Chihara T. *J. Am. Chem. Soc.* **2009**, *131*, 2050.

27. Pellny, P.-M.; Burlakov, V. V.; Arndt, P.; Baumann, W.; Spannenberg, A.; Rosenthal, U. *J. Am. Chem. Soc.* **2000**, *122*, 6317.

28. (a) Yasuda, H.; Kajihara, Y.; Mashima, K.; Lee, K.; Nakamura, A. *Chem. Lett.* **1981**, *226*, 519. (b) Erker, G.; Krüger, C.; Müller, G. *Adv. Organomet. Chem.* **1985**, *24*, 1. (c) Yasuda, H.; Nakamura, A. *Angew. Chem., Int. Ed. Engl.* **1987**, *26*, 723. (d) Erker, G.; Wicher, J.; Engel, K.; Rosenfeldt, F.; Dietrich, W.; Krüger, C. *J. Am. Chem. Soc.* **1980**, *102*, 6344. (e) Beckhaus, R. *Angew. Chem., Int. Ed. Engl.* **1997**, *36*, 686.

# CHAPTER 5

## *mno* RULE FOR CONDENSED BORANES VERSUS MINGOS' RULE FOR CONDENSED TRANSITION METAL CLUSTERS: THE MISSING LINK

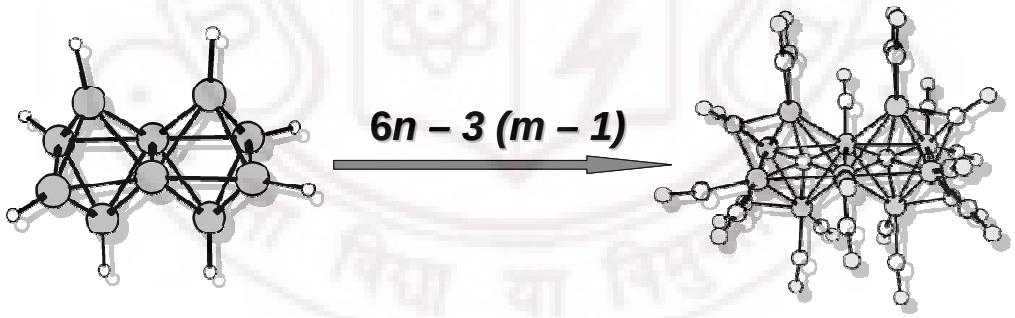


***mno* rule**
**SEP = *m* + *n* + *o***

**Mingos' rule**
**TEC = (*A*) + (*B*) - (*Δc*)**

# Abstract

The correlation between the electron count for the polyhedral boranes (Wade's $n$ + 1 rule) and for the transition metal clusters (PSEPT, 7$n$ + 1 rule) can be understood from the isolobal analogy between BH and transition metal fragments. The relationship between the electron count of poly-condensed polyhedral boranes (*mno* rule) and poly-condensed transition metal clusters (Mingos' rule) is not straightforward. Here, a total valence electron count for the condensed transition metal clusters was proposed, which establishes the missing link between the electron count for condensed boranes (*mno* rule) and transition metal clusters (Mingos' rule). According to this rule, $m + n + o + 6n - 3(m - 1) = 7n - 2m + o + 3$ ($n$ = number of vertices, $m$ = number of polyhedra, $o$ = number of single vertex sharing) number of electron pairs are necessary for the stability of *closo* polycondensed transition metal clusters. The additional electron pairs required for *nido* and *arachno* polyhedra, one and two respectively, are to be added separately. Comparison of this electron count with Mingos' rule gives a relation between $n_s$ (number of shared vertices), $y$ (number of bonds between the shared atoms) and $m$ (number of polyhedra) as $y = 2n_s - 3(m - 1) + o$. Two possible ways of dividing the total electron count into skeletal and non-skeletal bonding electron pairs were discussed. The rule is also extended as $m + n + o + p + 6x - x_s/n_s\{3(m - 1)\}$, (where $x$ = number of transition metals, $x_s$ = number of shared transition metals and $n_s$ = number of shared atoms) to incorporate the electron counts of the metallaboranes. This rule gives *mno* rule ($x = x_s = 0$) for

condensed boranes and $7n - 2m + o + 3$ rule ($x = n$, $x_s = n_s$) for condensed transition metal clusters.

## [5.1] Introduction

Electron-counting rules[1-11] are efficient tools to predict qualitatively the structure, stability and bonding of molecules and clusters. The octet rule[1] for main group molecules, the 18-electron rule[2] for transition metal complexes, Hückel $4n + 2$ rule[3] for aromatic planar cyclic systems, Lipscomb's styx rule[4] for boranes and CVMO[8,9] for transition metal clusters are some of the well known examples. Electron counts based on graph theoretical approaches[10] are occasionally used for boranes and transition metal clusters. Contributions of Wade[5] and Mingos'[11] in formulating the electronic requirement for boranes and transition metal clusters especially stand out. Wade's $n + 1$ rule[5] is not only helpful in rationalizing the known cage structures of polyhedral boranes, but also in suggesting the probable structures of unknown polyhedral boranes. Wade[5a] and Mingos[11a] recognized a common structural and electronic relationship between main group and transition metal polyhedral clusters in the early 1970's. This lead to the development of PSEPT,[11b] according to which stable *closo* boranes require $n + 1$ skeletal electron pairs respectively, ($n$ is the number of vertices) whereas, the electronic requirement for isostructural *closo* polyhedral transition metal clusters is $7n + 1$ total valence electron pairs. One and two additional electron pairs are required for *nido* and *arachno* polyhedra.

The difference between the skeletal electron pairs in boranes and total valence electron pairs in transition metal clusters is therefore $6n$, which corresponds to metal-ligand exohedral bonding electrons and non-bonding metal electrons (Figure 5.1, top). This can be rationalized by isolobal analogy,[12] according to which

BH fragments in boranes and $d^8ML_3$ fragments [e.g. $Ru(CO)_3$, CoCp] in transition metal clusters contribute three orbitals and two electrons for the skeletal bonding. For example the two '$e_g$' electrons of $Ru(CO)_3$ would correspond to two valence electrons in the BH group. The '$t_{2g}$' (6 electrons) and 3 CO groups (6 electrons) contribute 6 additional electron pairs for $Ru(CO)_3$ fragment. Accordingly, the skeletal electron pairs for octahedral $B_6H_6^{-2}$ is 7 ($n$ = 6) and the total valence electron pairs for octahedral $Ru_6(CO)_{18}^{-2}$ is 43 ($n$ = 6). The difference between the two electron counts is 36 (= 6$n$) electron pairs (Figure 5.1, top).

Mingos' proposed another rule to explain the condensation of polyhedral transition metal complexes.[11c,d] This rule states that "the total electron count in a condensed cluster is equal to the sum of the electron counts for the parent polyhedra (A) and (B) minus the electron count (Δc) characteristic of the shared unit (atom, pair of atoms etc.)". If polyhedron (A) is characterized by 'a' number of valence electrons and polyhedron (B) by 'b' number of valence electrons, then the condensed cluster (C) will have a total of 'a + b - Δc' valence electrons. The characteristic electron count (Δc) for vertex sharing is 18, edge sharing is 34 and triangular face sharing is 48 (or 50, when (A) and (B) are deltahedra with number of vertices ≥ 6).[11c,d] A generalized skeletal electron counting rule, the *mno* rule,[6] for polycondensed polyhedral boranes has been introduced by Jemmis and coworkers. According to this rule, $m + n + o$ skeletal electron pairs are necessary for a closed macro-polyhedral system to be stable. Here, $m$ is the number of condensed polyhedra; $n$ is the number of vertices and $o$ is the number of single-atom sharing between two polyhedra. Wade's $n + 1$ rule is a special case of $m + n + o$ rule, where

*m* = 1 and *o* = 0.[6] However, unlike Wade's *n* + 1 rule for boranes and 7*n* + 1 rule for non-condensed transition metal clusters, the relation between *mno* rule and Mingos' rule for poly-condensed systems is not obvious.

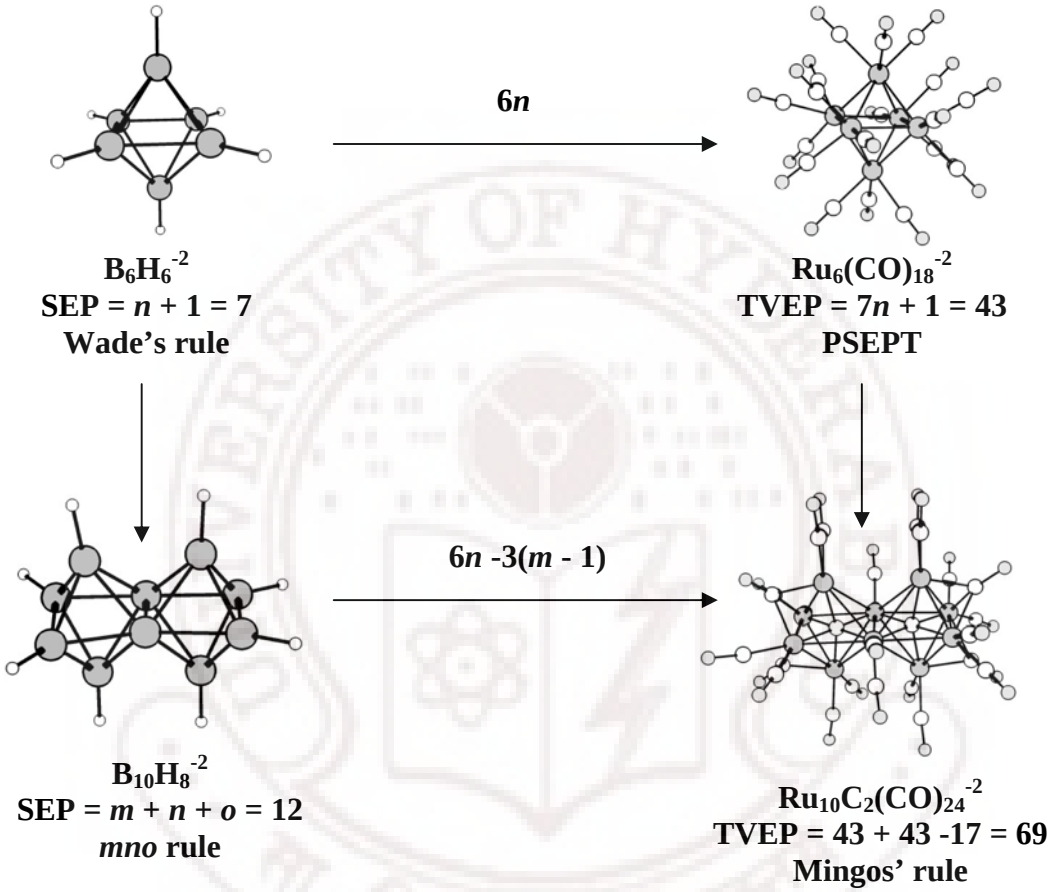


**Figure 5.1**: Schematic representation of the correlation among the electron count rules for mono cage and condensed polyhedral boranes and transition metal clusters. SEP is number of skeletal electron pairs and TVEP is number of total valence electron pairs.

For example, the skeletal electron pairs for edge shared bioctahedral $B_{10}H_8^{-2}$ is 12 (by *mno* rule, where *m* = 2, *n* = 10 and *o* = 0) (Figure 5.1, bottom). The total valence electron pairs (TVEP) for isostructural edge shared metal cluster $Ru_{10}C_2(CO)_{24}^{-2}$ is 69 (by Mingos' rule, where 'a' = 'b' = 43 electron pairs, Δc = 17

electron pairs). For mono-cage polyhedra, the difference between the electron count of boranes and transition metal cluster is 6*n* (Figure 5.1, top). However, the difference between the electron counts of isostructural condensed transition metal cluster $Ru_{10}C_2(CO)_{24}^{-2}$ and borane $B_{10}H_8^{-2}$ is 57 electron pairs (= 69 - 12, Figure 5.1, bottom), which is less than 6*n* = 60 electron pairs (*n* = 10). Analysis of a large number of experimentally known condensed transition metal clusters (Table 5.1) shows that addition of 6*n* to the skeletal electron pair of isostructural condensed boranes (*mno* rule) does not give TVEP for isostructural transition metal clusters (Mingos' rule), as it does for Wade's *n* + 1 and 7*n* + 1 rules (PSEPT). In that scenario, what is the relationship between *mno* rule and Mingos' rule for poly-condensed clusters? The *mno* rule for condensed boranes and Mingos' rule for transition metal clusters are based on two entirely different sets of parameters and thus one to one correspondence between these two rules is missing. In our attempt to determine this missing link between these two electron counting rules, the electron count for the condensed transition metal clusters is revised in terms of parameters *m*, *n* and *o*. This has been done by analyzing a series of the crystal structures of the condensed polyhedral transition metal clusters (Table 5.1).

## [5.2] Total Valence Electron Pair (TVEP) Count for Transition Metal Clusters: 7*n* - 2*m* + *o* + 3

The total valence electron pairs for the *closo* condensed transition metal clusters can be expressed in terms of the number of vertices (*n*), the number of polyhedra (*m*) and the number of single vertex sharing (*o*) as *m* + *n* + *o* + 6*n* - 3(*m* - 1) = 7*n* - 2*m* + *o* + 3. For *nido* and *arachno* metal clusters, one and two additional

pairs of electrons are required ($7n - 2m + o + 3 + p$; $p = 1$ for *nido* and $p = 2$ for *arachno*). According to this electron count, the number of TVEP required for the stability of edge sharing octahedral cluster $Ru_{10}C_2(CO)_{24}^{-2}$ (Figure 5.1, bottom) is $7n - 2m + o + 3 + p = 69$ ($m = 2$, $n = 10$, $o = 0$ and $p = 0$). This number is same as predicted by Mingos' rule (Figure 5.1, bottom). When number of polyhedra ($m$) is one, the TVEP count $7n - 2m + o + 3$ becomes $7n + 1$ ($o = 0$) electron pairs, which is equal to the total valence electron pairs obtained by the PSEPT for *closo* systems. Therefore, our revised rule gives a generic electron count for condensed and non-condensed transition metal clusters. Applications of this electron count rule for a large number of condensed clusters are discussed in section 5.5.

The difference between the *mno* count in boranes and total valence electron count in condensed transition metal clusters is $6n - 3(m - 1)$. What does this difference '$6n - 3(m - 1)$' signify? In the condensed boranes, assignment of the skeletal and exohedral electron pairs is straightforward. The terminal BH fragment donates two electrons and shared boron atom, which does not have any exohedral bond, donates three electrons to the cluster bonding. However, this kind of assignment of the total electron count for condensed transition metal clusters is not practical due to the presence of closely spaced d orbitals. Thus, the simple argument of one to one mapping using isolobal analogy of BH and transition metal fragment is not sufficient to classify the TVEP of transition metal clusters into skeletal and non-skeletal electron pairs. On the other hand, the number of electrons donated by the shared metal fragment to the cluster bonding depends on the number of ligands attached to the metal. Since the connectivity of the terminal vertices does not change upon condensation, they would contribute equal numbers of electrons in

non-condensed as well as in condensed clusters. Therefore, it is apparent that the variable numbers of orbitals donated by shared metals are responsible for this difference in the electron count.

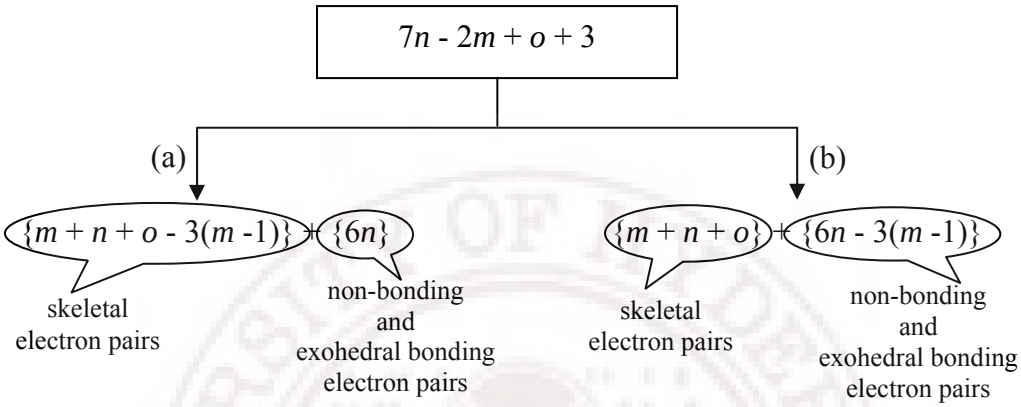


Chart 5.1

The TVEP count $7n - 2m + o + 3$ can be empirically divided into two ways – (a) $\{m + n + o - 3(m - 1)\} + \{6n\}$ and (b) $\{m + n + o\} + \{6n - 3(m - 1)\}$– to account for the skeletal and non-skeletal electron pairs for the condensed transition metal clusters. In chart 5.1a, it is assumed that the skeletal electron count for the condensed transition metal clusters is $m + n + o - 3(m - 1)$. It is observed that the number of ligands attached to the shared metals in condensed transition metal clusters commonly vary from one to three, which is less than the number of ligands attached to terminal vertices. The number of electrons contributed by these metal fragments for cluster bonding can be understood from secondary isolobal analogy.[12] The analysis of the frontier orbitals of the $ML_3$ fragment indicates presence of three orbitals in the frontier region (Figure 5.2a). The prime consequence of removing two ligands along the z-axis from a $ML_4$ fragment is the stabilization of the metal

$dz^2$ orbital (Figure 5.2b).[12] Similarly, when four ligands from the $ML_5$ fragment is removed, $dz^2$ and $dx^2$-$y^2$ orbitals become stabilized (Figure 5.2c).

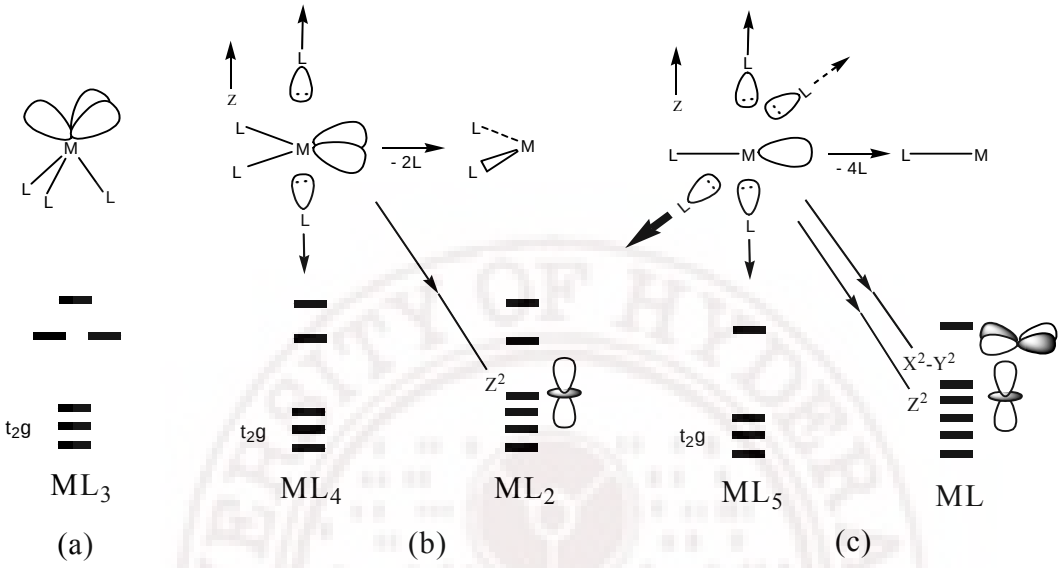


**Figure 5.2**: Frontier orbitals of metal ligand fragments (a) $ML_3$ (b) $ML_2$ obtained by removing two ligands from $ML_4$ and (c) ML obtained by removing four ligands from $ML_5$.

According to the above-mentioned argument, the $d^8ML_2$ and $d^{10}ML$ fragments would not contribute any electron to the cluster bonding and $d^8ML_3$ (isolobal to BH fragment) would donate two electrons. This also holds true for other metal fragments as well. Therefore, in contrast to the shared B atoms in the condensed boranes, which donate three electrons as compared to terminal BH groups, all the transition metal fragments in the shared positions would donate less number of electrons for the skeletal bonding as compared to the terminal metal fragments. This accounts for the decrease in the number of skeletal electron pairs for the condensed transition metal clusters.

However, one can argue that a constant number of skeletal electrons are necessary for the stability of any particular topology. Therefore, division of the TVEP in the above-mentioned fashion implies different skeletal electrons for similar topology of boranes and transition metal clusters. This contradiction suggests the second way of dividing the TVEP into skeletal and non-skeletal components i.e. $\{m + n + o\} + \{6n - 3(m - 1)\}$ (Chart 5.1b). In this case, it is assumed that the skeletal electron pairs remain invariant for both condensed transition metal clusters and boranes of identical topology. It implies additional participation of $3(m - 1)$ number of non-bonding electron pairs by the shared metal fragments as compared to non shared metal fragments.

The electronic requirement of transition metal clusters depends upon the types of condensation as well as the nature of the shared metal fragments and number of ligands attached to it. Therefore, the TVEP count is considered the best way to describe condensed transition metal clusters rather than skeletal electron count.

## [5.3] Correlation between Mingos' Rule and TVEP Count for Poly-Condensed Transition Metal Clusters

In most of the cases, the TVEP count ($7n - 2m + o + 3$) gives the same electrons as predicted by Mingos' rule (Table 5.1, section 5.5). This indicates the existence of a one to one relationship between these two rules. The difference $\Delta c$ in Mingos' rule can be expressed as $9n_s - y$ number of electron pairs, where $n_s$ = number of shared atoms and $y$ = number of bonds between the shared atoms.

Chart 5.2

**Mingos' Rule:**

$a + b - (9n_s - y)$ electron pairs

For condensation of <u>two</u> polyhedra, the required number of electron pairs

$= a + b - (9n_s - y)$

$= (7n_a + 1) + (7n_b + 1) - (9n_s - y)$

$= (1 + 1) + 7(n_a + n_b - n_s) - (2n_s - y)$

$= 2 + 7n - (2n_s - y)$

$= m + 7n - (2n_s - y)$

For condensation of <u>three</u> polyhedra, the required number of electron pairs

$= a + b + c - (9n_s - y)$

$= (7n_a + 1) + (7n_b + 1) + (7n_c + 1) - (9n_s - y)$

$= (1 + 1 + 1) + 7(n_a + n_b + n_c - n_s) - (2n_s - y)$

$= 3 + 7n - (2n_s - y)$

$= m + 7n - (2n_s - y)$

Hence, in general Mingos' electron count can be expressed as

$= m + 7n - (2n_s - y)$ electron pairs (5.1)

$n_s$ = number of shared vertices

$y$ = number of bonds between the shared atoms

$n_a$ = number of vertices in polyhedra A

$n_b$ = number of vertices in polyhedra B

$n$ = number of vertices in the condensed polyhedra

$m$ = number of polyhedra

**TVEP Count:**

$m + 7n + o - 3(m - 1)$ electron pairs (5.2)

Comparing Mingos' Rule (5.1) and TVEP count (5.2) we get,

$2n_s - y = 3(m - 1) - o$

OR, $y = 2n_s - 3(m - 1) + o$ (5.3)

This transforms the electron count by Mingos' rule as $a + b - (9n_s - y)$ electron pairs, where 'a' and 'b' are number of total valence electron pairs of the parent polyhedra. According to the PSEPT theory, $7n + 1$ ($n$ = number of vertices of the polyhedra) number of electron pairs are required for *closo* non-condensed polyhedra.[11a,b] Applying the PSEPT theory to the Mingos' rule, we get the TVEP count for the poly-condensed transition metal clusters as $(7n_a + 1) + (7n_b + 1) - (9n_s -$

*y*), where $n_a$ and $n_b$ are the number of vertices of the polyhedra A and B (Chart 5.2). From chart 5.2, it is clear that Mingos' rule for the condensed transition metal clusters can be written as $m + 7n - (2n_s - y)$, and the number of bonds formed between the shared atoms ($y$) depend upon the number of shared atoms ($n_s$), the number of polyhedra ($m$) and number of single vertex sharing. For *nido* and *arachno* polyhedra one and two additional electron pairs is to be added in both eq. 5.1 and 5.2 (Chart 5.2).

## [5.4] Extension of TVEP Count for Condensed Metallaboranes and Metallacarboranes

The electronic requirement for the condensed metallaboranes and metallacarboranes can be explained by the *mno* rule,[6] where the exohedral electrons are not involved in the skeletal bonding. However, sometimes it is difficult to understand the number of electrons donated by the metal fragments for skeletal bonding in a metallaboranes. This difficulty is more predominant for the poly-condensed transition metal clusters due to great influence of the exohedral ligands on the number of electrons participating in the skeletal bonding. Therefore, the skeletal electrons for the main group elements and total valence electrons for the transition metal fragments are considered for metallaboranes.

As discussed earlier, the difference in the electron counts for boranes by *mno* rule and transition metal clusters by TVEP count arises from the atoms in the shared positions. Therefore, the terminal transition metal fragment would donate $6x$ ($x$ = number of metal atom) number of electron pairs, in comparison with 1 electron pair

donated by terminal B-H. Hence, the TVEP count for the condensed metallaboranes, where the metal occupies the terminal position, will be $m + n + o + 6x$.

A similar argument can be invoked when the transition metal fragments occupy the shared positions. The shared transition metal fragments in transition metal clusters contain less number of ligands and as a result donate less number of electrons as compared to the terminal transition metal fragments. These difference is manifested by "$3(m - 1)$" in our electron count for the condensed transition metal clusters. This implies that all the metal fragments in the shared position together will contribute "$3(m - 1)$" electron pairs less in comparison with the terminal transition metal fragments irrespective of the mode of condensation. Thus, "$3(m - 1)$" electron pairs is to be subtracted from the total valence electron pairs if all the shared positions are occupied by transition metal fragments. This gives an electron count of $m + n + o + 6x - 3(m - 1)$ electron pairs for this type of condensed metallaboranes.

The metallaboranes where both boron and transition metal fragment are present in the shared position are also reported. For these metallaboranes, the aforementioned electron count cannot be used. Here, "$x_s/n_s\{3(m - 1)\}$" number of electron pairs is to be subtracted from the total valence electron pairs, $m + n + o + 6x$, where $n_s$ is the total number of shared atoms and $x_s$ is the number of shared metal atoms. For example, if one of the shared position of an edge shared metallaborane is occupied by a transition metal fragment, then the subtraction parameter in electron count will be "$1/2\{3(m - 1)\}$". Similarly, for a face shared metallaborane, where one

shared position is occupied by a transition metal fragment, the reduction in the electron count will be "1/3{3(*m* - 1)}". Thus, in order to incorporate all these factors we propose one electron count that can explain the electronic requirement of the condensed boranes, metallaboranes as well as transition metal clusters; $m + n + o + 6x - x_s/n_s\{3(m - 1)\}$. Here $m$ is the number of polyhedra, $n$ is the total number of vertices, $o$ is the number of single atom sharing, $x$ is the number of metal atoms, $n_s$ is the number of shared vertices and $x_s$ is the number of shared metal atoms. One additional electron pair is to be added for each missing vertex in terms of the variable $p$. For condensed boranes, $x$ and $x_s$ is 0; then, the electron count $m + n + o + 6x - x_s/n_s\{3(m - 1)\}$ is equivalent to $m + n + o$. If three is no metal atom in the shared position of metallaboranes, then, $x_s = 0$ and the electron count becomes $m + n + o + 6x - 0/n_s\{3(m - 1)\} = m + n + o + 6x$. For transition metal clusters, $x = n$ and $x_s = n_s$ then the electron count becomes, $m + n + o + 6n - n_s/n_s\{3(m - 1)\} = m + n + o + 6n - 3(m - 1)$. Thus, this electron count can be in principle applicable to the condensed boranes, metallaboranes and transition metal clusters. In case of boranes, this electron count reduces to *mno* rule and in case of transition metal clusters it equals $m + n + o + 6n - 3(m - 1)$. It has to be noted that for those condensed metallaboranes, where isolobal analogy can be used for the transition metal fragments, *mno* rule can be applied directly. For metallaboranes, where *mno* rule is difficult to apply, this rule for the mixed cluster might be useful (Table 5.2, Figure 5.4, Section 5.5).

## [5.5] Illustrations of TVEP Count

Table 5.1 illustrates the application of TVEP count on experimentally known transition metal clusters.[13-15] The Mingos' electron count (TVEC) for all the structures is also given. The detailed description of some selected structures is presented in figure 5.3. The description of structures starts with the planar clusters followed by clusters having tetrahedral, and octahedral skeletal units. Unless specified, all the clusters obey Mingos' electron count rule. The extension of the TVEP count for the polycondensed metallaboranes are illustrated in table 5.2 and figure 5.4. Nevertheless, there are other structures which obey this TVEP count.[13]

### [5.5.1] Application to Transition Metal Clusters

#### [5.5.1.1] Clusters Based on Planar Skeleton (Structures 1-3)

The structures of this class of cluster are based on triangular units. The smallest triangular cluster $Os_3(CO)_{12}$ (**1**) has three $Os(CO)_4$ metal fragments. The metal fragment $Os(CO)_4$ ($d^8ML_4$) utilizes one electron pair for the skeletal bonding (Figure 5.2) and the corresponding isolobal main group fragment is $CH_2$. Apparently this molecule can be viewed as an *arachno* system derived from a trigonal bipyramid, where two of the apical vertices are removed. Hence, number of polyhedra, $m = 1$, number of vertices, $n = 3$, number of single atom sharing, $o = 0$ and number of missing vertices, $p = 2$. Therefore, according to the rule total valence electron pairs required for the molecule is $(7\times3 - 2\times1 + 0 + 3 + 2) = 24$. The 3 Os atoms contribute 12 electron pairs and 12 CO groups together also contribute 12 electron pairs.

**Table 5.1**: TVEP count for transition metal clusters by $7n - 2m + o + 3 + p$ rule[16] and Mingos' rule are given. It is compared with the number of electron pairs provided by the constituent metal fragments.

| St. No. | Molecular formula | *m* | *n* | *o* | *p* | calc. TVEP[16] | obs. TVEP | *c* | Mingos' Count | Ref |
|---|---|---|---|---|---|---|---|---|---|---|
| 1. | $Os_3(CO)_{12}$ | 1 | 3 | 0 | 2 | 24 | 24 | 0 | 24 | 8 |
| 2. | $Os_5(CO)_{19}$ | 2 | 5 | 1 | 4 | 39 | 39 | 0 | 39 | 8 |
| 3. | $Os_6(CO)_{21}$ | 4 | 6 | 0 | 8 | 45 | 45 | 0 | 45 | 8 |
| 4. | $Ir_4(CO)_{11}CN(^tbu)$ | 1 | 4 | 0 | 1 | 30 | 30 | 0 | 30 | 15g |
| 5. | $Os_6Pt(CO)_{18}H_8$ | 2 | 7 | 1 | 2 | 51 | 51 | 0 | 51 | 15h |
| 6. | $Os_6(CO)_{18}H_2$ | 1 | 6 | 0 | 0 | 43 | 43 | 0 | 43 | 15d |
| 7. | $Os_7(CO)_{21}$ | 2 | 7 | 0 | 1 | 49 | 49 | 0 | 49 | 15d |
| 8. | $Ru_{10}C_2(CO)_{24}^{-2}$ | 2 | 10 | 0 | 0 | 69 | 68 | -2 | 69 | 14r,s |
| 9.[b] | $Ru_6Pt_3(CO)_{21}H_4$ | 2 | 9 | 0 | 0 | 62 | 62 | 0 | 61 | 14k,n |
| 10.[b] | $Ru_6Pt_3(CO)_{21}[Au(PEt_3)]_2H_2$ | 2 | 9 | 0 | 0 | 62 | 62 | 0 | 61 | 14m |
| 11.[b] | $[Ir_9(\mu\text{-}CO)_7(CO)_{13}]^{-3}$ | 2 | 9 | 0 | 0 | 62 | 60.5 | -3 | 61 | 14i |
| 12.[b] | $[Ir_{12}(\mu\text{-}CO)_8(CO)_{18}]^{-2}$ | 3 | 12 | 0 | 0 | 81 | 80 | -2 | 79 | 14j |
| 13.[a,b] | $[Rh_8Pt(CO)_7(\mu_3\text{-}CO)_3(\mu\text{-}CO)_9]^{-2}$ | 2 | 9 | 0 | 0 | 62 | 60 | -4(-2) | 61 | 14g |
| 14. | $Rh_{11}(CO)_{23}^{-3}$ | 3 | 11 | 0 | 0 | 74 | 72.5 | -3 | 72.5 | 15c |
| 15.[a] | $Os_6Pt_2(CO)_{16}(COD)_2$ | 3 | 8 | 0 | 2 | 55 | 54 | -2(0) | 55 | 15e,f |
| 16. | $Os_7(CO)_{19}Au_2(dppm)$ | 4 | 9 | 0 | 2 | 60 | 60 | 0 | 60 | 15b |
| 17.[a,b] | $Ru_8Pt_2(CO)_{23}H_2$ | 4 | 10 | 0 | 2 | 67 | 66 | -2(0) | 50 | 14o |
| 18.[b] | $[Ir_9(\mu\text{-}CO)_7(CO)_{12}H]^{-4}$ | 2 | 9 | 0 | 0 | 62 | 60 | -4 | 60 | 14b |
| 19.[b] | $Os_6Pt_4(CO)_{21}(COD)H_2$ | 2 | 9 | 0 | 0 | 62 | 62 | 0 | 62 | 14d |
| 20. | $Ru_5Pt_5(CO)_{18}(COD)_2H_2$ | 3 | 10 | 0 | 1 | 68 | 68 | 0 | 68 | 14f |
| 21.[b] | $Ru_6Pt_3(CO)_{20}(\mu_3\text{-}Ph_2C_2)H_2$ | 2 | 9 | 0 | 0 | 62 | 62 | 0 | 61 | 14k,n |
| 22.[b] | $Ru_6Pt_3(CO)_{21}[Au(PEt_3)]H_3$ | 2 | 9 | 0 | 0 | 62 | 62 | 0 | 61 | 14m |
| 23.[b] | $Ru_6Pt_3(CO)_{21}(\mu_3\text{-}IrCp^*)H_2$ | 2 | 9 | 0 | 0 | 62 | 62 | 0 | 61 | 14p |
| 24.[b] | $[Ru_6Pt_3(CO)_{21}(\mu_3\text{-}HgI)H_2]^-$ | 2 | 9 | 0 | 0 | 62 | 61.5 | -1 | 61 | 14p |
| 25.[b] | $Os_6Pt_4(CO)_{21}(COD)_2$ | 2 | 9 | 0 | 0 | 62 | 62 | 0 | 61 | 14d |
| 26. | $[Os_{10}C(CO)_{24}]^{-2}$ | 5 | 10 | 0 | 4 | 67 | 66 | -2 | 67 | 14a |
| 27. | $[Ru_6Pt_3(CO)_{21}H_3]^-$ | 2 | 9 | 0 | 0 | 62 | 61.5 | -1 | 62 | 14n |
| 28.[a,b] | $Ru_7Pt_3(CO)_{22}H_2$ | 4 | 10 | 0 | 2 | 67 | 66 | -2(0) | 50 | 14o |
| 29. | $Ru_6Pt_3(CO)_{19}(SMe_2)(\mu_3\text{-}Ph_2C_2)H_2$ | 2 | 9 | 0 | 0 | 62 | 62 | 0 | 62 | 14q |
| 30. | $Os_6Pt_4(CO)_{22}(COD)$ | 2 | 9 | 0 | 0 | 62 | 62 | 0 | 62 | 14d,e |
| 31.[a,b] | $[Rh_9(CO)_7(\mu_3\text{-}CO)_3(\mu\text{-}CO)_9]^{-3}$ | 2 | 9 | 0 | 0 | 62 | 59.5 | -5(-3) | 61 | 14c |
| 32. | $[Rh_{10}(CO)_{21}]^{2-}$ | 3 | 10 | 0 | 0 | 67 | 66 | -2 | 67 | 14h |
| 33. | $Ru_6Pt_3(CO)_{18}(\mu_3\text{-}\eta^6\text{-}PhC_2H_4Ph)H_4$ | 2 | 9 | 0 | 0 | 62 | 62 | 0 | 62 | 14l |
| 34. | $Ru_6Pt_3(CO)_{18}(\eta^6\text{-}TolC_2H_4Tol)H_4$ | 2 | 9 | 0 | 0 | 62 | 62 | 0 | 62 | 14l |
| 35. | $Ru_6Pt_3(CO)_{21}[\mu\text{-}PhCC(H)Ph]H$ | 2 | 9 | 0 | 0 | 62 | 62 | 0 | 62 | 14n |
| 36. | $Os_6Pt_2(CO)_{17}(COD)_2$ | 3 | 8 | 0 | 2 | 55 | 55 | 0 | 55 | 15e,f |
| 37. | $Os_8(CO)_{22}^{-2}$ | 3 | 8 | 0 | 2 | 55 | 54 | -2 | 55 | 15d |

*m* = number of polyhedra; *n* = number of vertices; *o* = number of single vertex bridge; *p* = number of missing vertices; *c* = charge of the molecule obtained by TVEP count and actual charge is given in parenthesis. Last column gives the references to experimental structures.

[a] indicates structures that do not obey the electron count $7n - 2m + o + 3 + p$ and [b] indicates structures where Mingos' count does not match the electron count.

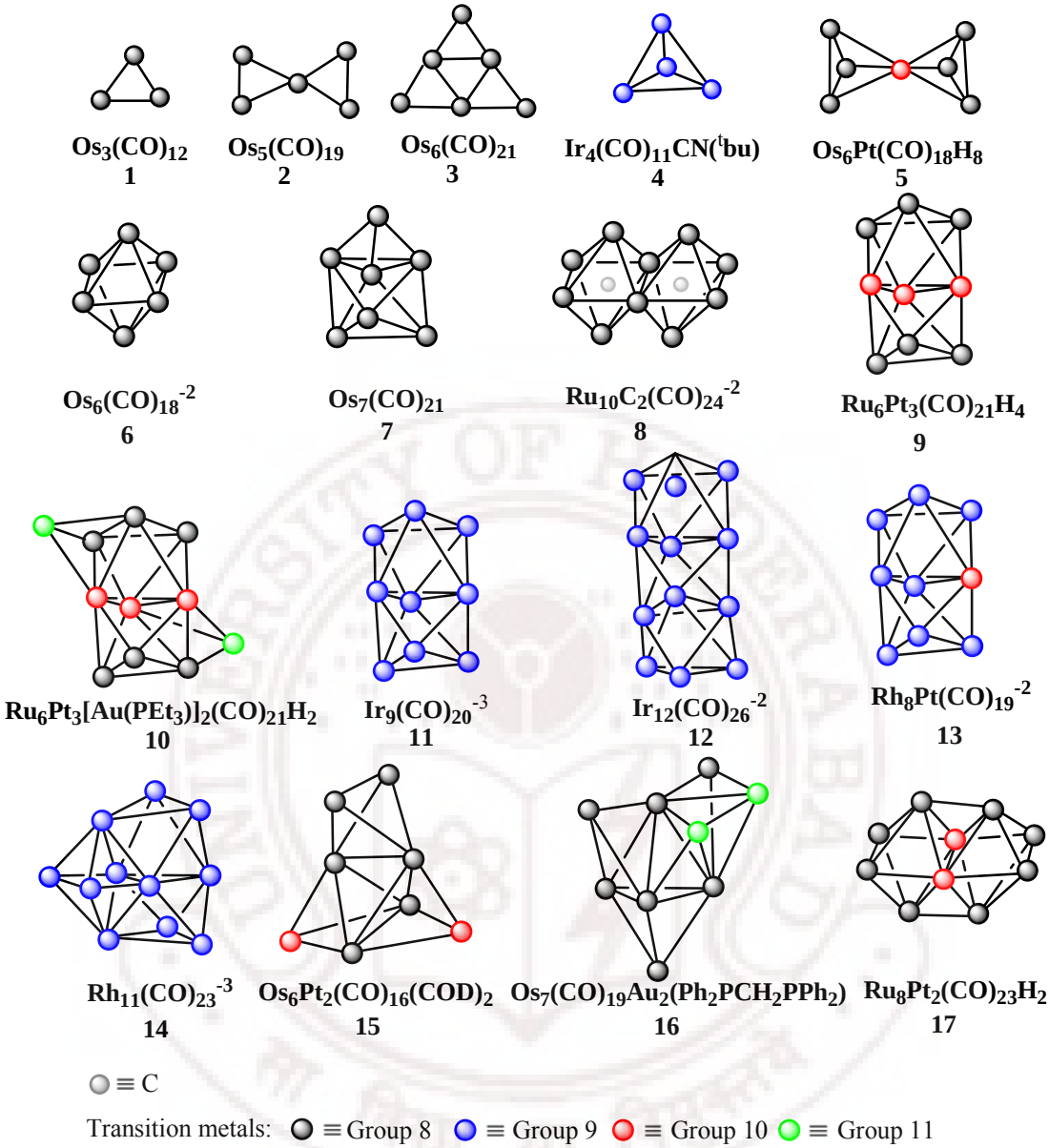


**Figure 5.3**: Schematic representation of some experimentally known metal clusters. The ligands are omitted for clarity.

Thus, the charge of the molecule is zero. PSEPT ($7n + 1 + p$) also gives the same electron count. On the other hand, $Os_3(CO)_{12}$ is considered equivalent to saturated cyclic hydrocarbon (cyclo-propane).[11] Hence, it cannot be considered as an arachno fragment of trigonal bipyramid geometry. The ideal arachno fragment of a trigonal bipyramid geometry of borane is $B_3H_3^{-6}$. Hence, the corresponding metal cluster is

$Os_3(CO)_9^{-6}$, where each vertex $Os(CO)_3$ is isolobal to BH. These three additional electron pairs are provided by three CO ligands in $Os_3(CO)_{12}$.

The molecule $Os_5(CO)_{19}$ (**2**) shows a vertex sharing between two triangular metal clusters. The total electron count for this cluster is 39 [$m$ = 2, $n$ = 5, $o$ = 1, $p$ = 4]. The electron pairs contributed by 5 Os atoms and 19 CO groups are 20 and 19 respectively and thus it is neutral. This cluster can also be considered as an equivalent to the saturated hydrocarbon system. The molecule $Os_6(CO)_{21}$ (**3**) exhibits face sharing among four triangular metal clusters, where all the three edges of the central triangle is shared. According to $7n - 2m + o + 3 + p$ electron count, it should have 45 total valence electron pairs [$m$ = 4, $n$ = 6, $p$ = 8]. The 6 Os atoms and 21 CO groups donate the 24 and 21 electron pairs respectively and this makes the molecule neutral. As mentioned above, this molecule can be considered equivalent to the saturated cyclic hydrocarbon rather than fragment of polyhedral clusters. According to Mingos' rule, the electronic requirement of planar $Os_3(CO)_{12}$, $Os_5(CO)_{19}$ and $Os_6(CO)_{21}$ are 24, 39 and 45 electron pairs respectively, which is same as obtained from $7n - 2m + o + 3 + p$ electron count.[11]

**[5.5.1.2] Clusters Based on Tetrahedral Skeleton (Structures 4-5)**

This class of structures can be considered as a *nido* fragment of trigonal bipyramidal cluster. The number of total valence electron count for the non-condensed tetrahedral cluster $Ir_4(CO)_{11}CN(tbu)$ (**4**) is $7n - 2m + o + 3 + p = 30$ electron pairs ($m$ = 1, $n$ = 4, $p$ = 1). Each Ir atom contributes 4.5 electron pairs, 11

CO groups and one CN(tbu) group contribute 12 electron pairs. Hence this cluster is neutral.

The vertex shared cluster $Os_6Pt(CO)_{18}H_8$ (**5**) has number of polyhedra, $m$ = 2, number of vertices, $n$ = 7, number of single vertex sharing, $o$ = 1 and number of missing vertices, $p$ = 2. Thus according to the total electron count ($7n - 2m + o + 3 + p$ ) the number of electron pairs required for its stability is 51. The six $Os(CO)_3$ vertices donate 42 electron pairs, Pt atom donates 5 electron pairs and 8 hydrogen atoms give 4 electron pairs. This results a neutral cluster.

**[5.5.1.3] Clusters Based on Octahedral Skeleton (Structures 6-13)**

$Os_6(CO)_{18}H_2$ (**6**) is an example for non-condensed clusters based on octahedral skeleton . In this cluster $m$ = 1, $n$ = 6, and $o$ = 0. Hence, the number of total valence electron pairs is 43 [$7n - 2m + o + 3 + p = 43$]. The six Os atoms donate 48 electrons, each CO group contributes 2 electrons to the valence electron count and two hydrogen atoms donate 2 electrons. Hence, the cluster is neutral according to this electron count rule.

The simplest extension of octahedral cluster is $Os_7(CO)_{21}$ (**7**), where one of the triangular face of the octahedra is capped by $Os(CO)_3$ fragment. This structure demonstrates the validity of the electron count in the capped polyhedra. Here the number of polyhedron $m$ = 2, the number of vertices $n$ = 7, the number of single vertex sharing $o$ = 0, and number of missing vertex $p$ = 1 (considering the capped vertex as a *nido* fragment derived from trigonal bipyramid). The number of total electron pairs is 49 ($7n - 2m + o + 3 + p = 49$). The seven Os atoms and 21 CO

groups contribute 49 total valence electron pairs and hence the cluster is neutral. If the $Os(CO)_3$ is considered as a capped vertex, it would donate two valence electrons to the octahedral $Os_6(CO)_{18}^{-2}$ and form a neutral cluster $Os_7(CO)_{21}$.

As per our knowledge, there is no example, until date, of the vertex shared octahedral metal cluster in the literature. The non-existence of these clusters is probably due to the non-bonded repulsive interaction between the ligands on the vertices adjacent to the shared atoms. An example of edge sharing between two octahedra is demonstrated by the molecule $Ru_{10}C_2(CO)_{24}^{-2}$ (**8**). The electron count ($7n - 2m + o + 3 + p$) gives 69 total valence electron pairs ($m = 2$, $n = 10$, $o = 0$). The 10 Ru atoms donate 40 electron pairs, two carbon atoms donate 4 electron pairs and 24 CO groups contribute 24 electron pairs. Therefore, the metal cluster requires two negative charges to be stable and it is predicted to be a dianion.

Next example describes the validity of the electron count in a cluster $Ru_6Pt_3(CO)_{21}H_4$ (**9**), where two octahedra are fused by a face. Here, $m = 2$, $n = 9$, $o = 0$ and hence, this structure requires 62 valence electron pairs. The molecule has 6 Ru atoms contributing 24 electron pairs and 3 shared Pt atoms that contribute 15 electron pairs. The 21 CO groups and 4 bridging H atoms contribute 21 and 2 electron pairs respectively. This makes the molecule neutral. On the other hand, Mingos' electron count gives different electron counts for the cluster (Table 5.1).[11c,d] According to Mingos' the characteristic electron count ($\Delta c$) for the triangular face sharing is 50 when number of vertices of one or both deltahedral $\geq 6$. Therefore, it predicts 61 valence electron pairs as the required number of electron pairs for a stable face shared bioctahedral cluster. The structures **10-13, 18-19, 21-25** have

similar skeleton where two or more octahedra are fused by face. In these structures CO ligands are replaced by other ligands like COD, $Ph_2C_2$, $Tol_2C_2$ etc. They also obey the electron count and have appropriate charges and bridging H atoms to satisfy the electron count. The principle of capping is valid in this class of clusters also, as demonstrated by $Ru_6Pt_3(CO)_{21}[Au(PEt_3)]_2H_2$ (**10**). This molecule has two capping vertices. Since $m$ = 4, $n$ = 11, $o$ = 0 and $p$ = 2, the structure requires 74 electron pairs for stability. The 6 Ru atoms, 3 Pt atoms, 21 CO groups and 2 bridging H atoms contribute 61 electron pairs for skeletal bonding. The 2 $Au(PEt_3)$ groups contribute 13 electron pairs and thus the molecule is neutral. Similar structure (St. **22**, Table 5.1) with one capping $Au(PEt_3)$ group also obeys the total valence electron couunt. The cluster $[Rh_8Pt(CO)_{19}]^{-2}$ (**13**) is another example of face shared bioctahedra which requires 62 electron pairs [$m$ = 2, $n$ = 9, $o$ = 0]. The 8 Rh atoms, 1 Pt atom and 19 CO groups contribute 60 electron pairs. The molecule needs 4 more electrons to satisfy the electron count and hence it is electron deficient. However, this molecule is observed as dianion and hence does not obey electron count rule. On the other hand, Mingos' electron count predicts this cluster to be dianion (Table 5.1). Interestingly, it is found to decompose to smaller fragments under CO atmosphere.[13g] The isoelectronic structure $Rh_9(CO)_{19}^{-3}$ (St. **31**, Table 5.1) also undergo decomposition in CO atmosphere,[14c] which is also electron deficient by two electrons according to our electron count rule.

### [5.5.1.4] Some Special Cases

$[Ru_{11}(CO)_{23}]^{-3}$ (**14**) : This structure can be described as the condensation of three octahedra by four atoms. Here, $m$ = 3, $n$ = 11, $o$ = 0 and hence it require 74

electron pairs to be stable. The 11 Rh atoms and 23 CO groups donate 49.5 and 23 electron pairs respectively. Hence, the cluster requires 1.5 electron pairs and thus exists as trianion. This structure also obeys Mingos' electron count. The Mingos considered this cluster as a condensation of a butterfly unit between an octahedra and a component polyhedra which is formed by face sharing between two octahedron.[11] The St. **32** (Table 5.1) also shows condensation between three polyhedra by four atoms and obeys the total valence electron count.

$Os_6Pt_2(CO)_{16}(COD)_2$ (**15**) : This molecule shows a relatively rare condensation of three polyhedra in which one trigonal bipyramid and one tetrahedron are fused by face and that fused polyhedra shares an edge with another tetrahedron. According to our electron count it requires 55 valence electron pairs [$m$ = 3, $n$ = 8, $p$ = 2]. There are 6 Os atoms, 2 Pt atoms, 16 CO groups and 2 COD groups and together contribute 54 skeletal electron pairs. Thus, it is electron deficient by 2 electrons and also found to be converted to stable structure (St. **36**, Table 5.1) in CO atmosphere.[14e,f] According to Mingos' approach, it can be considered as an edge sharing between, a tetrahedron, and a bicapped tetrahedron. The Mingos' electron count for this cluster is 55 total valence electron pairs, same as predicted by our rule.

$Os_7(CO)_{19}Au_2(Ph_2PCH_2PPh_2)$ (**16**) : This complex is essentially a face fused system between two trigonal bipyramid having two capping vertices. Application of our total electron count to this system predicts an electron count of 60 skeletal electron pairs ($m$ = 4, $n$ = 9, $p$ = 2). The 28 electron pairs are provided by 7 Os atoms, 11 electron pairs by 2 Au atoms, 19 electron pairs by 19 CO groups and 2

electron pairs by $Ph_2PCH_2PPh_2$ ligand. As a result, the molecule is stable as a neutral species. Mingos' electron count for this cluster is also the same.

### [5.5.2] Application to Metallaboranes

#### [5.5.2.1] Clusters where *mno* Rule can be Applied

The structures **38** is a triple decker sandwich compound and thus the number of polyhedra, $m = 3$. In this structure, the number of vertices ($n$) is 17 and there are two metal atoms in the vertex-shared position. Hence, $x$, $x_s$, $n_s$ and $o$ equals to 2. The Cp* ligand on Ru and Co can be considered as *nido* fragments derived from pentagonal bipyramid, which gives $p = 2$. Therefore, the electron count for this cluster according to $m + n + o + p + 6x - x_s/n_s\{3(m - 1)\}$ is $3 + 17 + 2 + 2 + 6\times2 - 2/2\{3(3 - 1)\} = 30$ electron pairs. This structure contains 3 BH groups, 10 CMe groups and 2 CR groups. They contribute 21 electron pairs. The number of electron pairs contributed by Ru and Co are 4 and 4.5 electron pairs respectively. The H attached to Ru contributes 1 electron. Therefore, the total number of electron pairs in this metallaborane is $21 + 4 + 4.5 + 0.5 = 30$. The electron count for this cluster can also be obtained by applying *mno* rule ($m + n + o + p$; the $m$, $n$, $o$ and $p$ represents the same variables as described earlier), which predicts an electron count of $3 + 17 + 2 + 2 = 24$ electron pairs ($m = 3$, $n = 17$, $o = 2$ and $p = 2$). In this case, the skeletal electron pairs contributed by Ru and Co are 1 and 1.5 electron pairs respectively. It is also considered that the H attached to Ru will donate its electron for the cluster bonding. This makes the electron count by *mno* rule as 24 electron pairs (21 electron pairs contributed by CMe, CR and BH groups and 3 electron pairs contributed by Ru, Co and one negative charge).

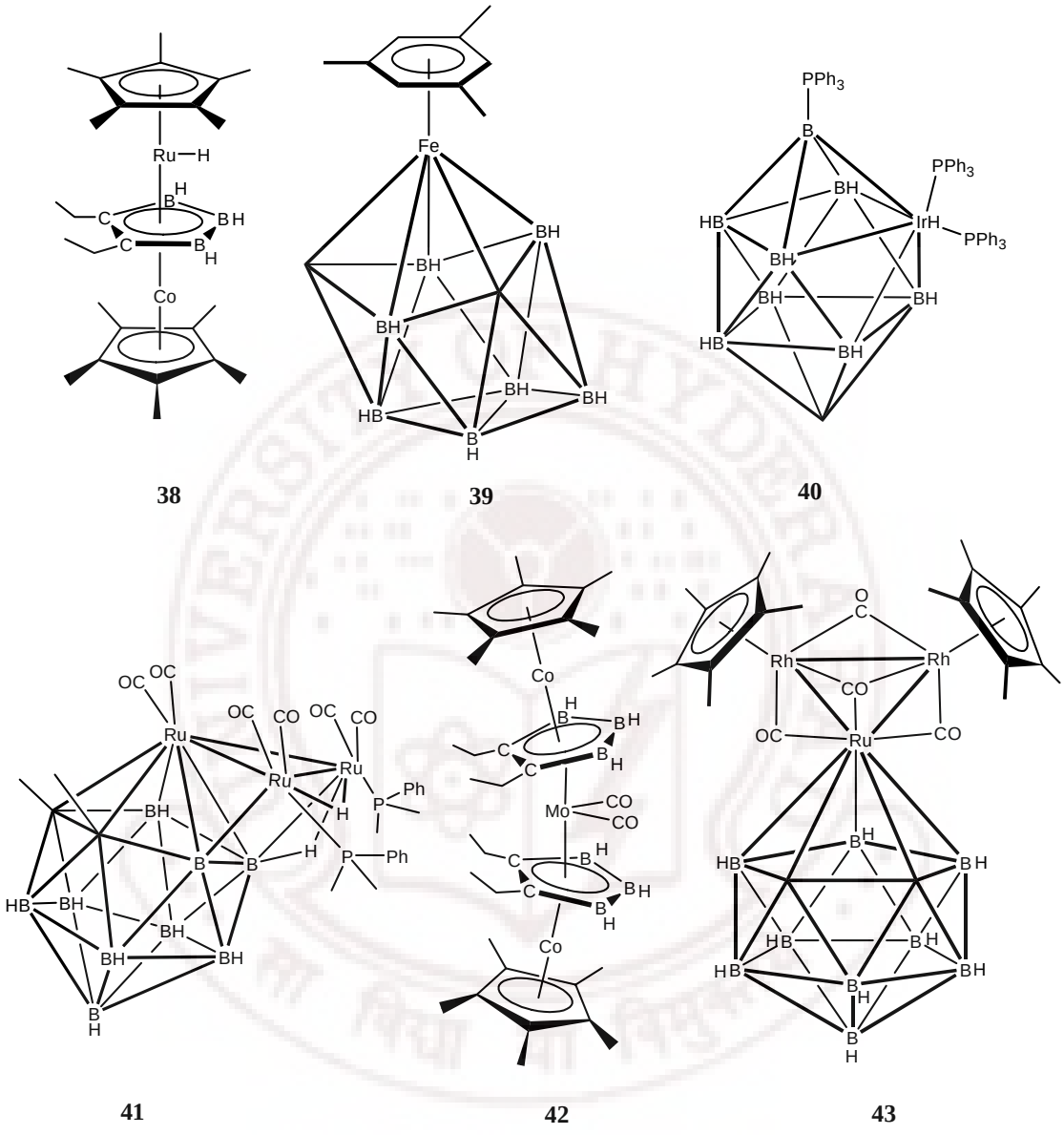


**Figure 5.4**: Schematic representation of some experimentally known metallaboranes and metallacarboranes. A point at the vertex and a line drawn from the vertex represents the CH group and the CMe group respectively.

**Table 5.2**: The electron count of metallaboranes and carboranes according to *mno* ($m + n + o + p$) and $m + n + o + p + 6x - x_s/n_s\{3(m - 1)\}$ rules. It is compared with the number of electron pairs provided by the constituent fragments.

| St. No.* | *m* | *n* | *O* | *p* | *x* | $x_s$ | $n_s$ | electron pairs | | | | Ref |
|---|---|---|---|---|---|---|---|---|---|---|---|---|
| | | | | | | | | *mno* | obs. | new rule | obs. | |
| **38** | 3 | 17 | 2 | 2 | 2 | 2 | 2 | 24 | 24 | 30 | 30 | 18a |
| **39** | 2 | 16 | 1 | 1 | 1 | 1 | 1 | 20 | 20 | 23 | 23 | 18b |
| **40** | 1 | 10 | 0 | 0 | 1 | 1 | 1 | 11 | 11 | 17 | 17 | 18c |
| **41**[a] | 2 | 14 | 0 | 1 | 3 | 1 | 3 | 17 | 16 | 34 | 34 | 18d |
| **42**[a] | 4 | 23 | 3 | 2 | 3 | 3 | 3 | 32 | 30 | 41 | 41 | 18e |
| **43**[a] | 4 | 24 | 3 | 4 | 3 | 3 | 3 | 34 | 30 | 44 | 44 | 18f |
| **44** | 1 | 12 | 0 | 0 | 1 | 0 | 0 | 13 | 13 | 19 | 19 | 18g |
| **45** | 2 | 13 | 1 | 0 | 1 | 1 | 1 | 16 | 16 | 19 | 19 | 18h |
| **46**[b] | 1 | 10 | 0 | 0 | 1 | 0 | 0 | 11 | 10 | 17 | 16 | 18i |
| **47**[b] | 2 | 15 | 1 | 3 | 1 | 1 | 1 | 21 | 18.5 | 24 | 23.5 | 18j |
| **48** | 3 | 22 | 2 | 1 | 2 | 2 | 2 | 28 | 28 | 34 | 34 | 18k |
| **49**[a] | 2 | 14 | 0 | 1 | 3 | 1 | 3 | 17 | 16 | 34 | 34 | 18l |
| **50** | 4 | 21 | 3 | 4 | 3 | 3 | 3 | 32 | 32 | 41 | 41 | 18m |

*m* = number of polyhedra; *n* = number of vertices; *o* = number of single vertex bridge; *p* = number of missing vertices. Last column gives the references to experimental structures.
[a] indicates the structures whose electron count does not obey *mno* rule but obey rule A and [b] indicates where both the rule fails. *Molecular Formula of the structures are given below
**38 :** $RuCo(Cp^*)_2B_3H_4C_2Et_2$; **39 :** $FeMe_3C_5B_7H_{12}$; **40 :** $Ir(PPh_3)_3CB_8H_9$;
**41 :**$Ru_3(CO)_6(PPhMe_2)_2C_2B_9H_9Me_2$; **42 :** $Co_2(Cp^*)_2Mo(CO)_2B_6H_6C_4Et_4$
**43 :** $Rh_2(Cp^*_2)Ru(CO)_4C_2B_9H_{11}$; **44 :** $[C_8H_{20}N_1]^+[Ru(PPh_3)_2C_2B_9H_{12}]^-$
**45 :** $FeH_2C_4B_8(Et)_{12}$; **46 :** $Os(PPh_3)_2B_7H_8B(OMe)C(Ph)$; **47 :** $CpRu(PPh_3)CB_8H_{12}$
**48 :** $Cp^*RuRhB_9C_6(Me_6)H_9$; **49 :**$Os_3(CO)_8B_8H_8C(NMe_3)$; **50 :** $Ru_3(Cp^*)_2B_8H_{20}$

The complex **39** can be considered as a sandwich structure, where the Fe atom is shared between a carboranes unit and an arene ring. Here, number of polyhedra $m = 2$, number of vertices $n = 16$ and number of single atom sharing $o = 1$. The arene ring can be considered as a *nido* fragment and thus $p = 1$. Since, this structure has only one metal atom, which occupies the shared position, the value of $x$, $x_s$ and $n_s$ is 1. Thus, according to $m + n + o + p + 6x - x_s/n_s\{3(m - 1)\}$ the total valence electron count of this transition metal cluster is $2 + 16 + 1 + 1 + 6 - 2/2\{3(2 - 1)\} = 23$ electron pairs. There are 5 CH groups and 3 CMe groups, contributing 12 electron pairs and 7 BH groups contributing 7 electron pairs. The Fe atom

contributes 4 electron pairs. As a result, the total electron count for this cluster becomes 12 + 7 + 4 = 23 electron pairs. The electronic requirement of this structure can be determined from *mno* rule in a similar fashion as described for the structure **38** (Table 5.2).

The structure **40** is a 10-vertex *closo* structure ($m$ = 1, $n$ = 10, $o$ = 0 and $p$ = 0), where one vertex is a transition metal fragment. Therefore, the electron count according to *mno* rule will be $m + n + o + p = 1 + 10 = 11$ electron pairs. According to the electron count for mixed cluster, the electronic requirement is $m + n + o + p + 6x = 1 + 10 + 6\times1 = 17$ electron pairs. This structure contains 7 BH groups, one CH and one $BPh_3$ groups. They will together contribute 10 electron pairs. The secondary isolobal analogy (Figure 5.2) predicts that the $Ir(PPh_3)_2$ group donates 1 electron for skeletal bonding. In addition, H also donates 1 electron to the cluster bonding. Therefore, the total skeletal electron pairs for this cluster are 11 electron pairs. Hence, this cluster obeys *mno* rule. The $Ir(PPh_3)_2$ fragment would contribute 6.5 electron pairs (4.5 by Ir atom and 2 by two $PPh_3$ groups) if we consider the electron count rule for the mixed cluster. As a result, the total number of electron will be equal to 17 electron pairs (10 electron pairs from 7 BH, 1 CH and 1 $BPh_3$; 6.5 electron pairs from $Ir(PPh_3)_2$ and 0.5 electron pair from H atom). Thus, this structure obeys both *mno* and the electron count for the mixed metallaboranes and carboranes.

**[5.5.2.2] Clusters where *mno* Rule cannot be Applied**

The structure **41** is a face shared polyhedra, where one icosahedron and one *nido* square pyramid are condensed. One of the vertex of the shared face is metal atom and remaining two are B atoms. Here, $m$ = 2, $n$ = 14, $o$ = 0 and $p$ = 1. Therefore, the electron count according to *mno* rule ($m + n + o + p$) will be 2 + 14 + 0 + 1 = 17 electron pairs. The 7 BH, 2 CH groups and 2 B atoms of this cluster will contribute 7, 3 and 3 electron pairs respectively. The two $Ru(CO)_2(PPhMe_2)$ groups also contributes 2 electron pairs and 2 H atoms will give 1 electron pair. According to the secondary isolobal analogy discussed earlier (Figure 5.2) the $Ru(CO)_2$ fragment will not donate any electron pair to the skeletal bonding. Hence, the total electron pairs for the skeletal bonding by *mno* rule are 7 + 3 + 3 + 2 + 1 = 16 electron pairs. It implies that the cluster is electron deficient by 2 electrons, but, this cluster is neutral. If we apply the $m + n + o + p + 6x - x_s/n_s\{3(m - 1)\}$ electron count for this cluster, the electron count becomes $2 + 14 + 0 + 1 + 1 + 6\times3 - 1/3\{3(2 - 1)\}$ = 34 electron pairs ($x$ = 1, $x_s$ = 1 and $n_s$ = 3). The electron pairs donated by 7 BH groups, 2 CH groups, 2 B atoms and 2 H atoms will remain the same, but the total electron pairs donated by 3 Ru atoms, 5 CO groups and 2 ($PPhMe_2$) groups will be 12, 5 and 2 respectively. Thus, the total valence electron count for this cluster is 7 + 3 + 3 +1 + 12 + 8 = 34. This matches the electronic requirement for this cluster.

The structure **42** exemplifies a tetra-decker mixed cluster of transition metal and carborane. The electron count for this cluster following the *mno* rule ($m + n + o + p$) is 4 + 23 + 3 + 2 = 32 ($m$ = 4, $n$ = 23, $o$ = 3 and $p$ = 2). It includes 6 BH, 10 CMe and 4 CEt groups. They contribute 6, 15 and 6 electron pairs to the cluster

bonding respectively. The 2 Co atoms will contribute 3 electron pairs. The $Mo(CO)_2$ group will not contribute any electron pairs to the cluster bonding according to the secondary isolobal analogy (Figure 5.2). Thus, the total valence electron count is 6 + 15 + 6 +3 = 30, which is less by 2 electron pairs than the electronic requirement provided by *mno* rule. However, this cluster is neutral and therefore does not obey *mno* rule. The values for $x = x_s = n_s = 3$, since his cluster has 3 transition metal fragments and all are in the vertex shared position. Therefore, the total valence electron pairs required for this cluster are $4 + 23 + 3 + 2 + 6\times3 - 3/3\{3(4 - 1) = 41$ electron pairs. The 27 electron pairs are contributed by 6 BH, 10 CMe and 4 CEt groups. The total electron pairs donated by two Co atoms and one Mo atom are 9 and 3 electron pairs respectively. The 2 CO groups attached to the Mo donate 2 electron pairs. Thus, the total valence electron pairs for this cluster are 6 + 15 + 6 + 9 + 3 + 2 = 41, same as predicted by the electron count for the mixed cluster.

The last example (**43**) depicts condensation of 4 polyhedra ($m = 4$) and it has 24 vertices ($n = 24$). The triangular metal skeleton (2Rh and 1Ru) is considered as bis-*nido* trigonal bipyramid. The 2 Rh are shared by the Cp* ligand (*nido* pentagonal bipyramid) and the Ru atom is shared by *closo* icosahedral carboranes. Therefore, the number of missing vertices $p = 4$ and the number of single vertex sharing $o = 3$. The *mno* rule ($m + n + o + p$) predicts 4 + 24 + 3 + 4 = 35 skeletal electron pairs for this cluster. There are 9 BH groups, which contributes 9 electron pairs. The 10 CMe and 2 CH groups contribute 18 electron pairs. The 2 Rh atoms, 1 Ru atom and 4 bridging CO groups can be divided into 2 $Rh(CO)_2$ groups and one

Ru atom so that the electron pairs contributed by the transition metal fragments become 2 (1 by Ru and 1 by 2 $Rh(CO)_2$, following the secondary isolobal analogy discussed in Figure 5.2). Thus, the skeletal electron pairs for this cluster are 9 + 15 + 3 + 1 + 1 = 29. This suggests that this cluster is electron deficient by 6 electron pairs, whereas the cluster is neutral. Application of the electron count for the mixed cluster to this structure gives the total electron count as $m + n + o + p + 6x - x_s/n_s\{3(m - 1)\} = 4 + 24 + 3 + 4 + 6\times3 - 3/3\{3(4 - 1)\} = 44$ electron pairs ($x = x_s = n_s = 3$). The number of electron pairs donated by 9 BH, 10 CMe and 2 CH groups will remain the same. The total electron pairs donated by 2 Rh atoms, 1 Ru atom and 2 CO groups are 9, 4 and 4 respectively. Thus, the total valence electron pairs for this cluster are 9 + 15 + 3 + 9 + 4 + 4 = 44 electron pairs.

This new rule, however, has its limitations. Some of the exceptions to this are illustrated in the Table 5.2. This rule is useful for those metallaboranes, where the number of skeletal electron pairs donated by the transition metal fragments cannot be assigned appropriately.

## [5.6] Concluding Remarks

The connection between the skeletal electron count in polycondensed boranes by *mno* rule and total valence electron pairs in polycondensed transition metal clusters by Mingos' rule is established. The total electron count of the transition metal clusters can be expressed as $m + n + o + 6n - 3(m - 1)$, where $m$ = number of polyhedra, $n$ = number of vertices and $o$ = number of single vertex sharing. One and two additional pairs of electrons have to be added to the total

electron count for *nido* and *arachno* systems respectively. This rule indicates the difference between the electron count for condensed boranes (*mno* rule) and transition metal clusters as $6n - 3(m-1)$ and establishes the missing link between the electron count in boranes and transition metal clusters. According to this rule, $6n - 3(m - 1)$ numbers of electron pairs have to be added to the *mno* count of boranes to achieve the total valence electron pairs of an isostructural transition metal clusters. This rule gives a unifying electron count for the electron count of both condensed and non-condensed transition metal clusters. The $7n + 1$ rule for non-condensed transition metal cluster becomes a special case of this generalized rule, when $m = 1$. This can successfully explain the stability and charge of a large number of transition metal clusters. The variables in the Mingos' rule is correlated with the variables in the mno rule by the relation $y = 2n_s - 3(m - 1) + o$, where $n_s$ = number of shared vertices, $y$ = number of bonds between the shared atoms and $m$ = number of polyhedra. It is not possible to identify the skeletal and non-skeletal electron pairs for the condensed transition metal clusters unambiguously. This is due to the difficulty in defining a sharp boundary for the skeletal electrons in case of condensed transition metal clusters. In the attempt to bridge the gap between the electron count rule in condensed boranes (*mno* rule) and transition metal clusters (Mingos' rule) we have also formulated a counting rule to incorporate all the clusters ranging from boranes to metallaboranes to transition metal clusters under the same umbrella. This rule gives the total valence electron pairs of the condensed polyhedra as $m + n + o + p + 6x - x_s/n_s\{3(m - 1)\}$, where $x$ = number of transition metals, $x_s$ = number of shared transition metals and $n_s$ = number of shared atoms.

## [5.7] References


1. (a) Lewis, G. N. *J. Am. Chem. Soc.* **1916**, *38*, 762. (b) Abegg, R. *Z. Anorg. Chem.* **1904**, *39*, 330.
2. Sidgwick, N. V. *The electronic theory of valency*; Cornell University Press: Ithaca, NY, 1927.
3. Hückel, E. *Z. Phys.* **1931**, *70*, 204.
4. Lipscomb, W. N. *Boron Hydrides*, Benjamin, New York, 1963.
5. (a) Wade, K. *Chem. Commun*. **1971**, 792. (b) Wade, K. *Adv. Inorg. Chem. Radiochem.* **1976**, *18*, 1.
6. Jemmis, E. D.; Balakrishnarajan, M. M.; Pancharatna, P. D. *J. Am. Chem. Soc.* **2001**, *123*, 4313.
7. Mingos, D. M. P. *Nature (London), Phys. Sci.* **1972**, *236*, 99.
8. (a) Ciani, G.; Sironi, A. *J. Organomet. Chem.* **1980**, *197*, 233-248. (b) Lauher, J. W. *J. Am. Chem. Soc*. **1978**, *100*, 5305. (c) Teo, B. K. *Inorg. Chem.* **1985**, *24*, 115-116.
9. (g) Mingos, D. M. P. *Inorg. Chem.* **1985**, *24*,114-115.
10. (a) King, R. B.; Rouvary, D. H. *J. Am. Chem. Soc.* **1977**, *99*, 7834. (b) King, R. B. *Inorg. Chem. Acta.* **1993**, *212*, 57.
11. (a) Mingos, D. M. P. *Nature Phys. Sci.* **1972**, *236*, 99. (a) Mingos, D. M. P. *Acc. Chem. Res*. **1984**, *17*, 311. (b) Mason, R.; Thomas, K. M.; Mingos, D. M. P. *J. Am. Chem. Soc.* **1973**, *95*, 3802. (c) Mingos, D. M. P. *J. Chem. Soc., Chem. Commun.* **1983**, 706. (d) Mingos, D. M. P.; Welch, A. J. *J.*

*Chem. Soc., Dalton Trans*. **1980**, 1674. (e) Mingos, D. M. P. *J. Chem. Soc., Dalton Trans*. **1974**, 133.

12. (a) Hoffmann, R. Nobel Lecture, Science **1981**, *211*, 995. (b) Hoffmann, R. *Angew. Chem. Int. Ed. Engl*. **1982**, *21*, 711.
13. (a) Mingos, D. M. P *Structure and bonding*, Springer-Verlag, 1997, Vol 87. (b) Michael, D.; Mingos, P.; Johnston, R. L. In *Theoretical models of cluster bonding* Springer Berlin /Heidelberg, 1987, Vol.68. (c) Dyson, P. J.; McIndoe, J. S. In *Transition Metal Carbonyl Cluster Chemistry* CRC; 2000.
14. (a) Jackson, P. F.; Johnson, B. F. G.; Lewis J.; McPartlin M.; Nelson W. J. H. *J. Chem. Soc., Chem. Commun.* **1980,** 224**.** (b) Pergola, R. D.; Cea, F.; Garlaschelli, L.; Masciocchi, N.; Sansoni, M. *J. Chem. Soc., Dalton Trans.* **1994,** 1501**.** (c) Martinengo, S.; Fumagalli, A.; Bonfichi, R.; Ciani, G.; Sironi, A. *J. Chem. Soc., Chem. Commun.* **1982**, 825. (d) Adam, R. D.; Lii, J.-C.; Wu, W. *Inorg. Chem*. **1991**, *30*, 2257. (e) Adam, R. D.; Lii, J.-C.; Wu, W. *Inorg. Chem*. **1991**, *30*, 3613. (f) Adam, R. D.; LI, Z.; Lii, J.-C.; Wu, W. *Inorg. Chem*. **1992**, *31*, 3445**.** (g) Fumagalli, A.; Martinengo, S.; Ciani, G.; Marturano, G. *Inorg. Chem.* **1986**, *25*, 592. (h) Martinengo, S.; Ciani, G.; Sironib, A. *J. Chem. Soc., Chem. Commun.***1986**, 1282. (i) Pergola, R. D.; Demartin, F.; Garlaschelli, L.; Manassero, M.; Martincngo, S.; Masciocchi, N.; Strumolo, D.; *Inorg. Chem.* **199**1, *30*, 846. (j) Pergola, R. D.; Demartin, F.; Garlaschelli, L.; Manassero, M.; Martinengo, S.; Sansoni, M. *Inorg. Chem.* **1987**, *26*, 3487. (k) Adams, R. D.; Li, Z.; Swepston, P.; Wu, W.; Yamamotoia, J. *J. Am. Chem. Soc.* **1992**, *114*, 10657**.** (l) Adams, R. D.; Bamard, T. S.; Li, Z.; Wu, W.; Yamamoto, J. H. *J. Am. Chem. Soc.* **1994**,

*116*, 9103. (m) Adams, R. D.; Barnard, Cortopassi, J. E. *Organometallics* **1996,** *14,* 2232. (n) Adams, R. D.; Barnard, T. S.; Li, Z.; Wu, W.; Yamamoto, J. *Organometallics* **1994**, *13*, 2357. (o) Adams, R. D.; Li, Z.; Lii, J.-C.; Wu, W.; *Organometallics* **1992,** *11,* 4001**.** (p) Adams, R. D.; Barnard, T. S.; Cortopassi, J. E.; Zhang, L. *Organometallics* **1996,** *15,* 2664. (q) Adams, R. D.; Barnard, T. S. *Organometallics* **1998,** *17,* 2885. (r) Hayward, C.-M. T.; Shapley, J. R.; Churchill, M. R.; Bueno, C.; Rheingold, A. L. *J. Am. Chem. Soc*. **1982**, *104*, 7347. (s) Churchill, M. R.; Bueno, C.; Rheingold, A. L. *J. Organomet. Chem*. **1990**, *395*, 85.

15. (a) Couture, C.; Farrar, D. H. *J. Chem. Soc., Chem. Commun.*, **1985**, 197. (b) Ahkter, Z.; Edwards, A. J.; Ingham, S. L.; Lewis, J.; Castro, A. M. M.; Raithby, P. R.; Shields, G. P. *J. Cluster Sci.* **2000**, *11*, 217. (c) Fumagalli, A.; Martinengo, S.; Ciani, G.; Sironi, A. *J. Chem. Soc., Chem. Commun.* **1983**, 453. (d) McPartlin, M. *Polyhedron* **1984**, 3, 1279-1288. (e) Couture, C.; Farrar, D. H. *J. Chem. Soc., Chem. Commun.* **1985**, 197. (f) Couture, C.; Farrar, D. H. *J. Chem. Soc., Dalton Trans.* **1986**, 1395. (g) Churchill, M. R.; Hutchinson, J. P. *Inorg. Chem.* **1979**, *18*, 2451. (h) Adams, R. D.; Pompeo, M. P.; Wu, W. *Inorg. Chem.* **1991**, *30*, 2425.
16. While distributing the bridging ligands between the shared and terminal vertices, the shared vertices are assigned with less number of ligands.
17. Dobrott, R. D.; Friedman, L. B.; Lipscomb, W. N. *J. Chem. Phys.* **1964**, *40*, 866.
18. (a) Davis Junior, J. H.; Sinn, E., Grimes, R. N. *J. Am. Chem. Soc.* **1989**, *111*, 4776. (b) Briguglio, J. J.; Sneddon, L. G. *Organometallics* **1986**, *5*, 327. (c)

Alcock, N. W.; Taylor, J. G.; Wallbridge, M. G. H. *Chem. Commun.* **1983**, 1168. (d) Liao, Y.-H.; Mullica, D. F.; Sappernfield, E. L.; Stone, F. G. A. *Organometallics* **1996**, *15*, 5102. (e) Curtis, M. A.; Houser, E. J. ;Sabat, M. ; Grimes, N *Inorg. Chem.* **1998**, *37*, 102. (f) Jeffery, J. C.; Jelliss, P. A.; Rudd, G. E. A.; Sakanishi, S.; Stone, F. G. A.; Whitehead, J. *J. Organomet. Chem.* **1999**, *582*, 90. (g) Chizhevsky, I. T.; Lobanova, I. A.; Petrovskii, P. V.; Bregadze, V. I.; Dolgushin, F. M.; Yanovsky, A. I.; Struchkov, Y. T.; Chistyakov, A. L.; Stankevich, I. V.; Knobler, C. B.; Hawthorne, M. F. *Organometallics* **1999**, *18*, 726. (h) Wrackmeyer, B.; Schanz, H.-J.; Milius, W.; McCammon, C. *Collect. Czech. Chem. Commun.* **1999**, *64*, 977. (i) Konoplev, V. E.; Pisareva, I. V.; Vorontsov, E. V.; Dolgushin, F. M.; Franken, A.; Kennedy, J. D.; Chizhevsky, I. T. *Inorg. Chem. Commun.* **2003**, *6*, 1454. (j) Alcock, N. W.; Jasztal, M. J.; Wallbridge, M. G. H. *J. Chem. Soc., Dalton Trans.*, **1987**, 2793. (k) Muller, T.; Kadlecek, D. E.; Carroll, P. J.; Sneddon, L. G.; Siebert, W. *J. Organomet. Chem.* **2000**, *614,* 125. (l) Lebedev, V. N.; Mullica, D. F.; Sappenfield, E. L.; Stone, F. G. A. *J.Organomet.Chem.* **1997**, *536*, 537. (m) Lei, X.; Shang, M.; Fehlner, T. P.; *Angew. Chem., Int. Ed.* **1999** , *38,* 1986.

## *List of Publications*

- "*Reactivity of Cationic Terminal Borylene Complexes: Novel Mechanisms for Insertion and Metathesis Chemistry Involving Strongly Lewis Acidic Ligand Systems*"; Susmita De, Glesni A. Pierce, Dragoslav Vidovic, Deborah L. Kays, Natalie D. Coombs, Eluvathingal D. Jemmis and Simon Aldridge **Organometallics 2009**, *28* (10), pp 2961–2975.

- "*Half-Sandwich Group 8 Borylene Complexes: Synthetic and Structural Studies and Oxygen Atom Abstraction Chemistry*"; Glesni A. Pierce, Dragoslav Vidovic, Deborah L. Kays, Natalie D. Coombs, Amber L. Thompson, Eluvathingal D. Jemmis, Susmita De and Simon Aldridge **Organometallics 2009**, *28* (10), pp 2947–2960.

- "*Application of Density Functional Theory in Organometallic Complexes: A Case Study of $Cp_2M$ Fragment (M = Ti, Zr) in C-C Coupling and Decoupling Reactions*"; Susmita De and Eluvathingal D. Jemmis In **Chemical Reactivity Theory A Density Functional View**; Chattaraj, P. K. Ed.; Taylor & Francis, CRC Press: Boca Raton, FL, **2009**; pp 193-214.

- "*Design, Synthesis, and DNA Binding Properties of Photoisomerizable Azobenzene−Distamycin Conjugates: An Experimental and Computational Study*"; Sumana Ghosh, Dandamudi Usharani, Ananya Paul, Susmita De, Eluvathingal D. Jemmis and Santanu Bhattacharya **Bioconjugate Chem. 2008**, *19* (12), pp 2332–2345.

- "*Photophysical and Duplex-DNA-Binding Properties of Distamycin Dimers Based on 4,4prime- and 2,2prime-Dialkoxyazobenzenes as the Core*"; Sumana Ghosh, Dandamudi Usharani, Susmita De, Eluvathingal D. Jemmis and Santanu Bhattacharya **Chem. Asian J. 2008**, *3* (11), pp 1949-1961 (with Cover Picture).

- "*Differing Reactivities of Zirconium and Titanium Alkoxides with Phenyl Isocyanate: An Experimental and Computational Study*"; Akshai Kumar, Susmita De, Ashoka G. Samuelson and Eluvathingal D. Jemmis **Organometallics 2008**, *27* (5), pp 955–960.

- "*A Theoretical Study on the Mechanism of Boron Metathesis*"; Susmita De, Pattiyil Parameswaran and Eluvathingal D. Jemmis **Inorg. Chem. 2007**, *46* (15), pp 6091–6098.

- "*Structure and Bonding in Mono and Dinuclear Metallacycles of $Cp_2M$ (M = Ti, Zr) with C2-Cumulenic Ligands XCCX (X = O, NH): A Comparison with Metallacycles of 1,2,3-Butatriene and 1,3-Butadiyne*"; Susmita De and Eluvathingal D. Jemmis (manuscript under preparation)

- "*mno Rule for Condensed Boranes versus Mingos' Rule for Condensed Transition Metal Clusters: The Missing Link*"; Susmita De and Eluvathingal D. Jemmis (manuscript under preparation)